UNIVERSITÀ
degli STUDI
di CATANIA

Dipartimento
di Fisica
e Astronomia
"Ettore Majorana"

PhD programme in Physics

Farmesk Jalil Abubaker

Development of a new portable instrument for in-situ activity measurement of Radionuclides in Nuclear Medicine

PhD thesis

Supervisors:
Chiar.mo Dr. Marco Capogni
Dr. Concetta Sutera
Prof. Cristina Tuvè

---

academic year 2019/2022

This thesis is submitted to the University of Catania in fulfillment of the requirement for the
Degree of Doctor of Philosophy.

The work presented in this thesis is original except as acknowledged in the text. I hereby declare that I have not submitted this material, either in full or in part, for a degree at this or any other institution.

Signature: Date: July 30, 2022

I dedicate this thesis to
My parents, my brother and sisters
For their unconditional love and
unending support.
You are all very precious to me
and love you all.

Preface

This thesis is submitted to the Department of Physics and Astronomy "Ettore Majorana", Catania University, Italy in partial fulfilment of the PhD degree in Physics. The work presented in this thesis was carried out from 31^{st} March 2019 to 30^{th} June 2022, at the Department of Physics and Astronomy "Ettore Majorana", Catania University, Italy in collaboration with the Italian National Institute of Ionizing Radiation Metrology (ENEA-INMRI)- Italy, Istituto Nazionale di Fisica Nucleare (INFN) - Catania section in Italy, Costruzioni Apparecchiature Elettroniche Nucleari (CAEN), Viareggio-Italy and Centro de Investigaciones Energéticas, Medioambientales y Tecnológicas (CIEMAT)-Madrid (Spain).

The work consisted of development of the new in-situ $4\pi\beta(LS) - \gamma$ detection system for activity measurements of short half-lived radionuclides, or α and $\beta - \gamma$ emitter radionuclides used in nuclear medicine.

This project was funded by the University of Catania in the framework of the National Operational Program (PON) on Research and Innovation 2014-2020.

This research project was supervised by Dr. Marco Capogni (main supervisor, senior scientist at ENEA-INMRI), Dr. Concetta Sutera (main supervisor, research scientist at INFN-Catania section), Prof. Vincenzo Bellini (Former PhD program director at Catania University), and Prof. Cristina Tuvè (main supervisor, research scientist at Catania University).

Abstract

The motivation of this research study is user demand, from radiopharmaceutical nuclear engineering and industries, for accurate and precise activity measurement of radionuclides used in nuclear medicine.

The first chapter of this thesis is the general information regarding the radionuclides used in nuclear medicine especially β, electron capture and $\beta - \gamma$ emitter radionuclides. The techniques of radionuclide production, physical properties and their applications are described briefly. As a 1^{st} year PhD student I participated in a training program at nuclear medicine laboratory in Cannizzaro hospital, Sicily region, Italy. The aim of my training program at Cannizzaro hospital, was essentially to obtain a general understanding of an operational cyclotron site, radionuclides production in nuclear medicine laboratories and to observe on-site cyclotron-PET radiopharmaceuticals operations in Italy.

The objectives of this training program were; learning about a cyclotron-PET facility's design and available equipments and tools in nuclear medicine facility, responsibilities, training and the qualification of the personnel, site-planning and operation of a cyclotron: liquid and gas targets, daily operational techniques, transferring radionuclides safely to the other PET center, PET radiopharmaceuticals such as $[^{18}F]$FDG and ^{11}C (^{11}C-methionine, ^{11}C-choline) productions and their quality controls for clinical PET in oncology, general understanding of how often the equipments need to be maintained, calibrated, and cleaned, and general knowledge about the maintenance of the cyclotron.

In the chapter two the history of radioactive measurement techniques

are explained in short. Later we focused on the techniques used for activity measurement techniques of pure β, electron capture, $\beta - \gamma$ emitting radionuclides. Afterword, we focused on the techniques in liquid scintillation counting, Triple-to-Double Coincidence Ratio (TDCR) and $4\pi\beta - \gamma$ coincidence methods. The activity measurement and standardization of pure β, pure electron capture (EC), $EC - \gamma$ or $\beta - \gamma$ emitters radionuclides are illustrated.

Furthermore, in the chapter three, the experimental setup of the portable TDCR system at Italian National Institute of Ionizing Radiation Metrology (INMRI) belonging to ENEA has been described. The experimental studies on the influence of the single photoelectron peak are carried out on pure β-emitters and the detection efficiency of the ENEA portable TDCR were measured for low energy pure β-emitter radionuclides ^{3}H, ^{63}Ni, and ^{14}C, medium and high energy pure β-emitter radionuclides such as ^{18}F and $^{90}Sr/^{90}Y$ respectively.

Next, Monte Carlo Simulation GEANT4 code was implemented to calculate the detection efficiency of the TDCR counter. For that reason the geometry of the TDCR counter and the complicated physical processes in particular the electron's attenuation and absorption processes and gamma ray interactions with the surrounding materials were simulated using GEANT4 code. Hereafter, Monte Carlo Simulation GEANT4 code was used to determine the detection efficiency of the portable TDCR counter. The simulated TDCR parameter for different kind of pure β-emitters such as ^{3}H,^{63} Ni,^{14} C,^{18} F and $^{90}Sr/^{90}Y$ radionuclides was computed then compared their results with experimental measurements in the chapter four.

In the chapter five the liquid scintillation counting such as customer-built TDCR and commercial HIDEX 300-SL at CIEMAT-Madrid (Spain) are then applied to standardize some important diagnostic radionuclides used in nuclear medicine such as ^{99m}Tc and ^{68}Ga during my stage at CIEMAT-Madrid (Spain).

This thesis presents my contributions as a PhD student with the staff of the Radionuclide Metrology Laboratory at the CIEMAT-Madrid (Spain) in the International comparison standardization of ^{109}Cd radionuclide project. The CCRI (II) decided to repeat this comparison and the Bureau International des Poids et Mesures (BIPM) volunteered to be the pilot laboratory, with the support of the Laboratoire National de Métrologie et

d'Essais Laboratoire National Henri Becquerel, France (LNE-LNHB).

The main part of this thesis is the chapter six, the hardware of the new in-situ $4\pi\beta(LS)-\gamma$ coincidence detection system is developed at ENEA in collaboration with Catania University and INFN-Catania section, for activity measurement of short half-lived radionuclides used in nuclear medicine. Whereas, the data analysis software of the ENEA portable $4\pi\beta(LS)-\gamma$ coincidence detection system is updated and modified in Electronic Nuclear Equipment Construction (CAEN) in Italy. The $4\pi\beta-\gamma$ coincidence counting technique is the most powerful technique for the absolute activity measurements of $\beta-\gamma$ or $EC-\gamma$ emitting radionuclides.

Short half-lived radionuclides such as ^{11}C which has half-life about 20 min, it needs to be standardized in-situ. It is difficult to send the ^{11}C source to nuclear metrology institute for example it is laborious to standardize ^{11}C radiopharmaceutical solution by sending this solution form Cannizzaro hospital in Catania to ENEA-INMRI in Rome. For that reason, it is important to have a portable instrument to standardize short half-live radionuclide inside radiopharmaceuticals centers. Furthermore, this portable detection system can be used to calibrate other radioactive measurement instruments such as activimeter in the nuclear medicine laboratory. The new ENEA portable $4\pi\beta(LS)-\gamma$ detection system can be used in all other regions in Italy or in other countries to measure and standardize short half-lived radionuclides.

Another important point is that we took this new detection system to the hospital. For the first time the $4\pi\beta(LS)-\gamma$ coincidence technique is used as in-situ detection system in the Ospedale Pediatrico Bambino Gesu (OPBG) hospital in Rome near ENEA, to measure the activity of an important therapeutic radiopharmaceutical radionuclides (^{131}I), which is used to diagnose and treat cancers of the thyroid gland.

Acknowledgements

I am very pleased to finish this thesis. Up until now, 2022 has been the most significant year for me. In retrospect, I am filled with all sorts of feelings and memories during my study. This work was a great experience for me, it gives me possibility to work in two public research institutes such as ENEA in Italy and CIEMAT in Spain, using several methods and techniques for measurement and standardization of different radionuclides. During my PhD program I had a golden chance to work and upgrade my knowledge in nuclear medicine field, especially in radionuclide production using cyclotron machine at Cannizzaro hospital in Sicily. In addition, working in the industrial company CAEN in Italy was an important experience for me. This PhD program is the key to my future work in the field of radionuclides production and radionuclides measurements and standardization. Without the assistance of many nice people around me, I would not be able to complete my thesis. I would like to express my appreciation and gratefully acknowledge to all those who helped me with this thesis and encouraged me during my PhD study.

It is my great pleasure to acknowledge European Union-funded investment program, the Programma Operativo Nazionale (PON) 2014-2020 funding this PhD project in collaboration with the Catania University.

First and foremost, I would like to give my deepest gratitude to my supervisors, Dr. Marco Capogni, Dr. Concetta Sutera, and Prof. Cristina Tuvè who gave me the opportunity to conduct PhD study and work on such an interesting topic in the motivating environment at the Catania

University. Dr. Marco Capogni was always around and available, providing support in the days when the study did not work, and encouraging me to continue. His dynamism, vision, sincerity and motivation have deeply inspired me. He has taught me the effective techniques for conducting research and various methodology to carry out the research during my study. I have learned from him to present the research works as clearly as possible. Working and studying under his direction was a tremendous honour and privilege. I am incredibly appreciative of what he has provided for me. I would like to express my gratitude for his friendship, compassion, and great sense of humour. Additionally, I have been fortunate to have the opportunity to work with and learn from Dr. Concetta Sutera, who shared a part of her immense knowledge and wisdom. During those difficult times especially COVID-19 pandemic, her organising and managerial skills were crucial. Her extensive knowledge, creative ideas, and excitement for scientific inquiry taught me a lot. Their in-depth knowledge of broad range of experimental techniques provided a good guidance in choosing the way where to direct and how to apply the development of new methods. I would also wish to express my gratitude to Professor Cristina Tuvè for in-depth conversations and insightful ideas that significantly improved the quality of my thesis.

Also, I take this opportunity to thank the current and the former PhD program directors at physics department Prof Albergo Sabastiano and Prof Vincenzo Bellini. Thanks in advance to Prof Vincenzo Bellini, I can still feel the excitement I had when I received the offer letter from you. I gained a lot from our conversation at your office. Where you always kindly started explaining the concepts and mechanics to me. You were continuously helped me in many occasions when I arrived to Catania.

I would like to express my special appreciation and thanks to Dr. Francesco Tortorici, you have been a tremendous mentor for me. I greatly benefited from his keen scientific insight, his knack for solving seemingly intractable practical difficulties, and his ability to put complex ideas into simple terms. You have a crucial role in my scientific life and my knowledge in the coding without your help, my work especially the Monte Carlo simulation GEANT4 coding cannot go so smoothly. And you are so efficient and enthusiastic. Every time I asked you about any question I had, you always gave me positive answers! Without you, the studies

could not be performed, and we could not have such a nice result.

I would like to express my thanks to Dr. Francesco Noto, Dr. Pablo Cirrone, and Dr. Giorgio Russo at INFN-Catania section. Dr. Francesco Noto helped us in the design and constructing the mechanical part of gamma detector of the new $4\pi\beta - \gamma$ detection system at ENEA. And Dr. Pablo Cirrone always gives his hand in many occasions for solving some problems in GEANT4 code. Dr. Giorgio Russo helped me to improve my knowledge in medical physics subjects especially in medical imaging. I really appreciate Dr. Giorgio Russo hard works to give me opportunity to be a trainer at the Cannizzaro hospital in Sicily (Italy) working on the cyclotron for production of the short half-lived radionuclides.

I would like to thank all my friends Dr. Massimo Ippolito, Dr. Marco Pometti, Dr. Gabriella Petralia, Dr. Giuseppe Benefatto, Dr. Marcella Sciortino, Piero Ingargiola, and Anna Munzone at the nuclear medicine laboratory at Cannizzaro hospital, most sincerely, for all of the help you have given me since my attendance at Cannizzaro hospital. From the very beginning you have made me feel welcome in your lab. Thank you for caring and supporting me wholeheartedly.

I would like to thank other collaborators involved in my projects. Special thanks go to Jacopo Givoletti the President of CAEN S.p.A for giving me this opportunity to spend eight months at CAEN in a positive and motivating atmosphere of his Company. It was very important for my professional development. I would like to thank Dr. Matteo Corbo especially appreciate all of the time you have taken away from your own work to" show me the ropes" and to ensure that I have the process knowledge and tools I need to do a great job each day, and also thank his wife Dr. Paola Cortopassi for your warm hospitality during my stay at CAEN and your continues help in many occasions during COVID-19 Pandemic. In addition, I would like to thank Dr. Massimo Morichi, Dr. Erica Fanchini, Giovanni Cerretani, Giacomo Mangiagalli, and Andrea Pepperosa. I really appreciate all of your informative comments on my projects, which have greatly enhanced my scientific research. I am also indebted to Francesco Pepe when I was lost and had no idea about writing the code of the my data analysis software, you aided me in getting my ideas straight and determining the best approach. You gave so much help thanks again.

I am deeply grateful to all the colleagues from the CIEMAT (Spain)

are sincerely thanked for making supportive and pleasant working atmosphere, in particularly to Dr. Miguel Roteta Ibarra, Dr. Nuria Gemma Navarro Ortega, Dr. Virginia Peyres Medina, and Marcos Meiuto Mendieta. I consider myself very fortune for having a chance to work with you. It is a great learning experience for me. I really value the knowledge and insight you have. I had a lovely experience and great collaboration with your group. I appreciate your patience and dedicated time on the experimental design and data analysis for the detection system available at your laboratory. You all assisted me with my work, and I learned a lot of knowledge from working with you. At the meantime, I would like to thank Prof. Eduardo García-Toraño for giving me his time to talk about the CIEMAT/NIST and TDCR methods and sent me the data regarding to the beta spectrum of some radionuclides.

I would especially like to thank Dr. Salvatore Libertini and Maria Sanfilippo. I appreciate your unwavering support in everything. I really would like to express my gratitude to you for your encouragement during this experience. I am extremely thankful to Maria Sanfilippo for her constant encouragement, love and care. She always gives me her hand for any problem I faced during my study, with her supports and kindness, she made my life goes smoothly.

I would like to thanks Dr. Pierino De Felice the director of ENEA-INMRI, he has a crucial role for my stage at ENEA.

I am extending my thanks to the nuclear medicine laboratory at OPBG hospital for providing and calibrating the standard solution of ^{131}I. Special thanks for Dr. Vittorio Cannatà, Dr. Slavatore Donatiello at OPBG hospital and Dr. Mauro Capone from ENEA-INMRI of preparing the liquid scintillation solution for ^{131}I radionuclide.

I would like to thanks my friends Rezan Shkur and Maria Luisa Margaria. I appreciate the positive influence you both have had on my life. Thank you for your concern and love, you have filled my life with pleasure and amusement and had spread so many color around it.

My great thanks go to one of the best person in my life Dr. Fabrizio Scopelliti for all your warm help during my life in Italy. In every moment in Italy, sharing immense love and care, I have found you like my family. Whenever I meet a problem, you are the first person I prefer to ask for help because I know I will get detailed suggestions and comfort from

you. You are one of the major parts of my happiness and successes. Our countless memories mean so much to me. Thank you so much for being there for me through thick and thin.

I am lucky to have met my best friend and my Matter Dr. Ruhani Khanna in Italy, and I thank her for her friendship, love, caring and unyielding support. Our shared memories are so precious to me. Words cannot express how grateful I am for your kindness and generosity. Thanks for adding loads of happiness to my life.

I am extremely grateful to my parents (Jalil Abubaker and Zhian Gharib), my sisters (Danaz, Khanda, Mzhda, Lana, and Payam), my brother (Mohemmad), and Payaman Sabah for their love, prayers, caring and sacrifices for educating and preparing me for my future. You have been supreme, and you have nurtured my learning, supported my dream. I love them so much, and I would not have made it this far without them. I know I always have my family to count on when times are rough. You taught me how to choose battles wisely. You showed me how to deal with life. Knowing that your family is proud of you, truly proud of you, that you have achieved what they have always believed that you could, is a sublime thing.

Finally, I would like to acknowledge friends and family who supported me during the studying of my PhD. Special thanks go to those relatives who believed in me thanks for your constant love and support.

To the ones I missed mentioning, I hope there will be an opportunity to thank in person.

Farmesk Abubaker

Publications

1. Abubaker F., Scopelliti F., Pometti M.A. et al. *Cyclotron for PET: System Upgrade after 13 Years of Service*. Radiochemistry 63, 77–86 (2021).

2. F. Abubaker, F. Tortorici, M. Capogni, C. Sutera, V. Bellini. *Effect of Birks Constant and Defocusing Parameter on Triple-to-Double Coincidence Ratio Parameter in Monte Carlo Simulation-GEANT4*. World Academy of Science, Engineering and Technology: International Journal of Nuclear and Quantum Engineering Vol: 15, No: 8, (2021).

3. F. Tortorici, F. Abubaker, M. Capogni, C. Sutera, V. Bellini, and G. Guarnieri. *Monte Carlo Simulation for TDCR method used in nuclear medicine applications*. High performance computing on CRESCO infrastructure: Research activities and results 2022 (Annual report of ENEA, 2021).

4. Abubaker F., Capogni M., Capone M., Cannatà V., Donatiello S., Tortorici F., Sutera C., Pepe F., Corbo M., De Felice P., and Bellini V. *Standardization of ^{131}I using portable $4\pi\beta(LS) - \gamma$ coincidence detection system in OPBG hospital*. Abstract is accepted for 108^{th} International Congress-Società Italiana di Fisica (SIF), 2022.

5. Abubaker F., Tortorici F., Pepe F., Capogni M., Sutera C., Bellini V., Corbo M., De Feliced P. *New analysis software for $\beta - \gamma$ coincidence technique to be applied for activity measurements of short-lived radionu-*

clides used in nuclear medicine. Invited Speaker in 107^{th} International Congress-Società Italiana di Fisica (SIF), 2021.

6. Abubaker F., Capogni M., Sutera C. Tortorici F., Noto F., Bellini V., De Feliced P. *Development of a new portable instrument for in situ activity measurement of Radionuclides in Nuclear Medicine*. Speaker in 106^{th} International Congress-Società Italiana di Fisica (SIF), 2020.

LIST OF ABBREVIATIONS

AC	Alternating Current
ADC	Analog-to-Digital Converter
AMC	Annual Maintenance Contract
ASCII	American Standard Code for Information Interchange
BIPM	Bureau International des Poids et Mesures (International Bureau of Weights and Measures)
CAEN	Costruzioni Apparecchiature Elettroniche Nucleari (Electronic Nuclear Equipment Construction)
CCL4	Carbon tetrachloride
CCRI (II):	Consultative Committee for Ionizing Radiation 'Section II (Radionuclide)'
CEA	Commissariat à l'énergie atomique et aux énergies Alternatives (The French Alternative Energies and Atomic Energy Commission)
CERN	Conseil Européen pour la Recherche Nucléaire (European Council for Nuclear Research)
CI	Charge Integration
CIEMAT	Centro para Investigaciones Energéticas, Medioambientales y Tecnológicas (Centre for Energy, Environment and Technology Research)
CMC	National calibration and measurement capability
CT	Computed Tomography
DAQ	Data acquisition
DC	Direct Current
DPP	Digital Pulse Processing

DSP	Digital Signal Processing
EC	Electron Capture
EDXRF	Energy Dispersion *X*-ray Fluorescence
EGS4	Electron Gamma shower 4
ENEA	Agenzia nazionale per le nuove tecnologie, l'energia e lo sviluppo economico sostenibile (Italian National Agency for New Technologies, Energy and Sustainable Economic Development)
ENEA-INMRI	Istituto Nazionale di Metrologia delle Radiazioni Ionizzanti (National Institute of Ionizing Radiation Metrology)
EOB	End of Bombardment
FDG	Fluorodeoxyglucose
FOM	Figure of Merit
FPGA	Field Programmable Gate Array
GEANT4	GEometry ANd Tracking
G-M	Geiger Muller
GT	Gamow-Teller
HDPE	High Density Polyethylene
HPGe	High Purity Germanium
HV	High Voltage
ICRM	International Committee for Radionuclide Metrology
INFN	Istituto Nazionale di Fisica Nucleare (National for Nuclear Physics)
LET	Linear Energy Transfer
LNHB	Laboratory National Henry Becquerel
LSB	Least Significant Bit
LSC	Liquid Scintillation Counting
MAC3	Module d'acquisition de Coíncidences triples
MABs	Monoclonal Antibodies
MCA	Multichannel Analyzer
MCNP	Monte Carlo N-Particle Transport
MCS	Monte Carlo Simulations
MSB	Most Significant Bit
NaI(Tl)	Thallium-doped sodium iodide
NIM	Nuclear Instrumentation Module
NIST	National Institute of Standards and Technology
NM	Nuclear Medicine
NMIs	National Metrology Institutes
OPBG	Ospedale Pediatrico Bambino Gesù

PC	Proportional Counter
PET	Positron Emission Tomography
PMI	Primary Metrology Institutes
PMT	Photomultiplier Tube
PS	Plastic Scintillator
PSD	Pulse Shape Discrimination
PTFE	Polytetrafluoroethylene
QDC	Charge to Digital Converter
RDM	Radioactive Decay Module
RIT	Radioactive Iodine Therapy
RNT	Radionuclide Therapy
SEP	Single Electron Peak
SI	International System of Units
SIF	Italian Physical Society
SIR	International Reference System
SIRTI	International Reference System Transfer Instrument
SNR	Signal-to-Noise Ratio
SPECT	Single-Photon Emission Computerized Tomography
TAT	Targeted Alpha Therapy
TDC	Time-to-Digital Converter
TDCR	Triple-to-Double Coincidence Ratio
tSIE	transformed Spectral Index of the External Standard
TTT	Trigger Time Tag
UG	Ultima Gold
VME	Versa-Module Electronic
^{186}Re**-HEDP**	Rhenium-186-hydroxyethylidene diphosphonate

List of Tables

List of Figures

Contents

Chapter 1

Radionuclides use in Nuclear Medicine

1.1 Introduction

A branch of medicine that uses ionizing radiation to treat illness or obtain information about the functioning of a person's particular organs is called *Nuclear medicine*. In the majority of cases, physicians use this information to construct an accurate diagnosis of the patient's diseases immediately. The disorders of the human organs function such as bones, thyroid, liver, heart, and many other organs can be simply brought to light and imaged. In many situations, diseased organs or tumors can be treated by using radiation [1, 2].

Technetium-99m (^{99m}Tc) is the most common radionuclides used in diagnosis, accounting for 80% of all nuclear medicine procedures worldwide, with some 30 million procedures per year. The utilize of radiopharmaceuticals in diagnosis is growing at over 10% per year [3]. Nuclear medicine offers adequate tools for radiotherapy using pharmaceutical compounds labeled with radionuclides which emit β-, α-particles, and/or Auger electrons. They will destroy mostly targeted cancer cells in their short path lengths with limited side effects. The physical, radiobiological, and radiochemical properties of the radionuclides should be well known and studied for the ideal application for targeted radionuclide

therapy. In nuclear medicine radiopharmaceutical solution are produced with the suitable characteristics for their application. In this chapter we are going to summarize the nuclear physics of medical radionuclide production. Some radionuclides used in nuclear imaging, including PET and SPECT imaging, targeted radionuclide therapy are mentioned [4].

1.2 Diagnostic techniques in nuclear medicine

Radioactive tracers which emits γ-rays use in diagnostic techniques in nuclear medicine. Generally, these tracers are short-lived radionuclides coupled to chemical compounds which allow particular physiological processes to be scrutinized. They can be given by inhalation, injection or orally. Gamma camera detects photons emitted from the point where the radioactive tracer is positioned in the organs. This helps to view organs from many different angles. The camera accumulate an image from the points from which radiation is emitted; this image is intensified by a computer and viewed by a physician on a monitor for indications of abnormal conditions [1].

Positron Emission Tomography (PET) is a more recent developed diagnosis techniques in nuclear medicine. PET machine is more precise and sophisticated technique which use radionuclides produced in a cyclotron, especially (β^+)-emitter radionuclides. Positron Emission Tomography has most important clinical role in oncology. As radioactive tracer such as fluorine-18 (^{18}F) decays and emits a (β^+), this emitted positron directly combines with a near electron upcoming in the simultaneous emission of two detectable γ-rays in opposite directions. These two emitted gamma rays are detected by a PET camera and give very precise manifestation of their origin. Since, fluorine-18 (^{18}F) has confirmed to be the most accurate method for detecting and examining most cancers. It is also widely known in cardiac and brain imaging [5].

PET/CT is a new procedures, which combines positron emission tomography (PET) with computed X-ray tomography (CT) scans to commit co-registration of the two images (PET/CT). PET/CT is qualifying 30% better diagnosis than the traditional gamma camera alone. It is a fascinating and very powerful tool which supplies unique information on a

wide ranges of diseases and cancer. The fundamental difference between nuclear medicine imaging and other imaging techniques such as *X*-rays is the position detected of the radiation source within the body of the patients. Organ disorder or malfunction are observed when the isotope is either partially taken up in the organ (cold spot) or taken up in excess (hot spot). By generating a number of images over time, an unfamiliar pattern or rate of radionuclide movement could be an indication of the organ malfunction. Nuclear imaging method has the ability to successfully scan both bone and soft tissue, which is a major advantage over *X*-ray methods [5].

1.3 Diagnostic radiopharmaceuticals

Nuclear imaging method is non-invasive studies that measure the distribution of radioactivity from within the human body under normal and pathological conditions [1]. Gamma camera is generally used for that purpose. Currently, the common clinical nuclear imaging techniques are (excluding *X*-rays) computed tomography (CT), magnetic resonance imaging (MRI), ultrasound, planar scintigraphy, positron emission tomography (PET) and single photon emission computed tomography (SPECT), and magnetic resonance spectroscopy (MRS). By producing computer-generated transverse, sagittal, and coronal slice pictures of an organ, tomographic imaging (PET and SPECT) represents high-resolution structural and functional information. Ionizing radiations are used in planar scintigraphy, SPECT and PET, except CT. The administration of medical radionuclides is necessary in these imaging techniques. In general, short-lived radionuclides are used as the tracers used in nuclear imaging. The chemical compounds are labeled with these radionuclides and allow specific physiological processes to be examined [1].

1.4 Therapeutic radiopharmaceuticals

Ionization radiation is used to destroy cancer cell or diseased tissue in therapeutic procedures, which are either curative or palliative. Meristematic tissues such as cells in the gastrointestinal tract, blood cells in the

bone marrow, and skin cells are extremely sensitive to be damaged by irradiation. Therefore, some malignant tumors can be controlled or removed by irradiation in the region where tumor is located. In external irradiation γ-rays from ^{60}Co source, or high-energy X-rays produced by linear accelerators are used for this purpose [2].

Internal radiotherapy is performed by administering or planting a source of ionizing radiation usually β- or γ-emitter radionuclides in the target location. For example, in the treatment of head and breast cancers ^{192}Ir radionuclide is used. It is constructed in wire form and is inserted into the target location through a catheter, and the implant wires are removed after administering the right dose. In brachytherapy (short-range) method, the radiation is more localized to the target tumor, and the body expose less to radiation [2, 6]. Ionizing radiation is useful to weaken or destroy malfunctioning cells in some medical conditions. In the same manner that a radioactive element is utilized for diagnostics, the radionuclide that creates the radiation can be targeted in the relevant organ. In the vast majority of cases, β-emitter radionuclides are used to damage cancerous cell, this is called radionuclide therapy (RNT) or radiotherapy [7]. Despite the fact, radioactive materials use less in radiotherapy than diagnostic in nuclear medicine, it is nevertheless widespread, important, and growing. Lutetium-177 (^{177}Lu) and yttrium-90 (^{90}Y) are becoming the main radionuclide therapy agents. ^{177}Lu is an example of therapeutic radionuclide, it is a strong beta emitter with just enough gamma to enable imaging [8]. Ytterbium-176 (^{176}Yb) is irradiated to become ^{176}Yb and decays rapidly to ^{177}Lu [9]. ^{90}Y is used in cancer treatment, especially non-Hodgkin's lymphoma, and it is more often use in envisaged, including for arthritis treatment [10]. ^{131}I and ^{32}P are also used in radiotherapy [11]. ^{131}I is used to treat the thyroid cancers and other abnormal disorder including hyperthyroidism (overactive thyroid) [12]. ^{10}B radionuclide is a new and still experimental procedure in radiotherapy, which centralizes in the tumor [13]. In order to produce alpha particles to kill the cancer cells, the patient is irradiated with neutrons which are strongly absorbed by the boron. Actinium-225 (^{225}Ac) is readily available now for Targeted Alpha Therapy (TAT), from which the daughter Bismuth-213 (^{213}Bi) is obtained (via 3 alpha decays) to label targeting molecules [14]. Significant medical study is being conducted cross the world into the utilize

of radionuclides attached to highly specific biological chemicals namely immunoglobulin molecules (monoclonal antibodies).

1.5 Production methods for medical radionuclides

Radionuclides utilized in nuclear medicine clinics are man-made by either charged particle accelerators, nuclear reactors, or radionuclide generators. Generally, the natural radionuclides are unsuited for medical applications. Despite the fact that, the majority of natural radionuclides are long-lived or they are heavy elements that can not be used in physiological processes. Radionuclides used in nuclear medicine with essentially different properties can be produced for each production procedure, and specify their clinical applications. Currently, in nuclear medicine all radionuclides are produced artificially either in a particle accelerator by compulsory altering the nuclear structure of a stable target material or in a nuclear reactor.

There is a new production process, which is based on 14 MeV neutron beam obtained by Deuteron-Tritium (D-T) fusion reaction. Some experiments to produce with the 14 MeV neutron beam of the Frascati Neutron Generator (FNG) both ^{99}Mo [15] and ^{64}Cu [16] has been performed. Currently, 80% of the medical radioisotopes are manufactured in a nuclear reactor by neutron activation, and the remaining radionuclides are produced by particle accelerators, mostly with cyclotrons [3]. This ratio will apparently change, as cyclotrons have several advantages over a nuclear reactor: (i) the amount of radioactive waste generated by cyclotrons is not as much as in nuclear reactor and less hazardous; (ii) the manufacturing is decentralized, i.e., cyclotrons are located in hospitals, this means that the delivery of pharmaceuticals to patients are more secured and excluding the possibility of a transportation accident; (iii) the controlled chain reactions is not needed, thus there is no possibility of nuclear-power accidents or proliferation [1].

1.5.1 Reactor production

Nuclear reaction is a process of the bombardment of the nuclei of heavy target by energetic particle such as neutron, proton, alpha particle, or a heavy ion. For a long time, nuclear reactors have provided an environment that is suited for bombarding a specific target with neutrons of different energies. Neutron can interact easily with the heavy target nuclei at low energy, because neutron has zero charge, it does not has to overcome the Coulomb barrier. Indeed, neutron activation is the bombardment of a target nuclei by neutron projectiles. The low energy neutrons have more probability of taking place this reaction, because they basically spend more time around the target. On the concept of nuclear fission, medical radionuclides are produced using nuclear reactors. In nuclear fission process a heavy unstable nucleus splits into two fragments, producing 2-3 free neutrons and releasing a enormous amounts of energy. ^{235}U is a common target for neutron projectile bombardment. When the ^{235}U target nucleus bombarded by a neutron $^{236}U^*$ is formed. $^{236}U^*$ is totally unstable and initiates nuclear fission immediately and releasing more neutrons. Different fission products can produced each time with a different probability.

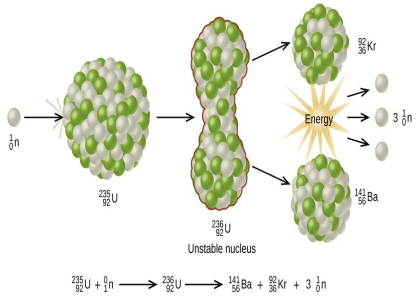

Figure 1.1: Slow neutron reacts with fissionable ^{235}U nucleus, it is absorbed and an unstable ^{236}U nucleus is formed. The ^{236}U nucleus then rapidly splits into two smaller fragments (in this case, ^{141}Ba and ^{92}Kr) along with number of neutrons (usually two or three), This results in the release of a tremendous quantity of energy.

$^{235}U + n \rightarrow^{236} U^* \rightarrow^{141} Ba +^{92} Kr + 3n$ is an example of very known nuclear reaction, where Barium and Krypton are the fragment products of the excited $^{236}U^*$ as the results of the nuclear fission, with three released neutrons as shown in Fig. 1.1 [1]

Figure 1.2 shows that the atomic mass of the fragment products are significantly different from each other, and the free neutrons that have been released might lead to further fission processes in the surrounding material and causing chain reaction. Extreme neutrons will be required for fission fragment stability, and requiring further decay through emission of β-particles. The total energy released in each fission event is about 200 MeV [1].

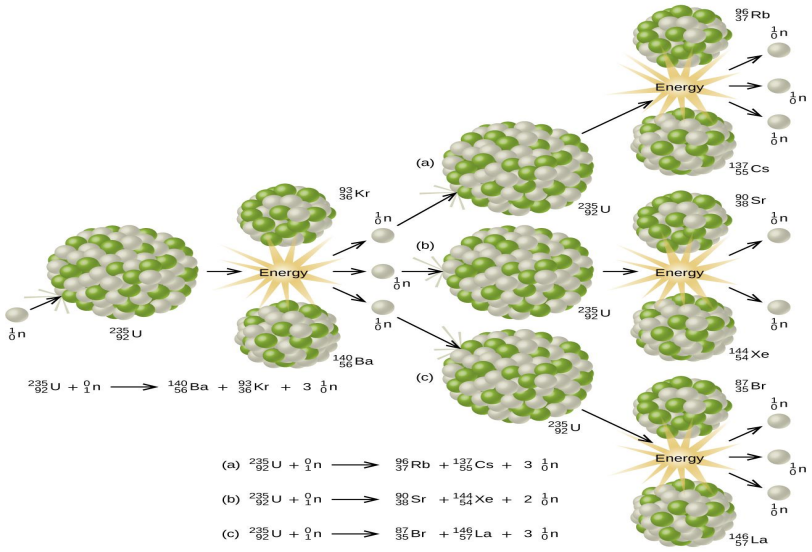

Figure 1.2: The fission process of the ^{235}U, produces 2 or 3 neutrons and two fragments products, each of free neutron is able to cause fission of another nucleus, the chain reaction is happened if this process continuous.

In certain cases, the fission fragment products themselves or a daughter product of these (after disintegration) can be a radionuclide used in medicine. Alternatively, targets of particular materials can be positioned around the reactor core to be bombarded by fission neutrons and activated by neutrons to produce a desired radioactive product. There are two types of reactions that can occur as a result of neutron activation:

1. (n, γ) reaction: A neutron is captured by a target nucleus, which is subsequently converted into an excited product nucleus. γ-ray is released as a result of de-excitation. In that case, the target and product are different isotopes of the same element. For slow (thermal) neutrons, this reaction is the most typical.

2. (p, γ) reaction: A neutron is captured by a target nucleus, which then ejects a proton. The product and target are different chemical elements.

Considering the (n, γ) reaction, it leads that a product is the same element as the target, chemical separation techniques become useless for extracting the product. Consequently, the product will not be *carrier free*, and the specific activity of the medical radionuclides is limited. As a result, many radionuclides used in nuclear medicine could be produced through neutron activation are instead obtained through nuclear fission to optimize the specific activity, e.g., ^{99}Mo (the parent of ^{99m}Tc). In some cases, the product following a (n, γ) reaction decays to a daughter product that is of medical interest, which can therefore be distinguished from the target, e.g., ^{125}Xe is produced by neutron activation of ^{124}Xe, which later decays to ^{125}I, a medically used radionuclide that can be extracted [1]. Radionuclides made through fission and neutron activation will decay and emits β-particles as they have a neutron rich nucleus, they can be used in nuclear medicine for therapeutic purposes. Daughter products dispose to decay through γ-emission, they are useful and ideal for diagnostic imaging. The table 1.1 shows several medical radionuclides produced by fission and neutron activation.

Table 1.1: Medically used radionuclides produced in nuclear reactors, either from induced fission or through neutron activation of targets, and examples of their biomedical application.

Radionuclide	**Decay Mode**	**Reaction**	**Applications**
^{99}Mo	β^-	$^{98}Mo(n,\gamma)^{99}Mo$ fission of ^{235}U	The Parent of ^{99m}Tc, ^{99}Mo is used as radionuclide generator.
^{131}I	β^-, γ	$^{130}Te(n,\gamma)^{131}Te$ β^- ^{131}I	Diagnosis and treatment of thyroid disorder, include metastasis thyroid Cancer.
^{90}Y	β^-	$^{89}Y(n,\gamma)^{90}Y$	Therapeutic radionuclide commonly used in radioembolization to treat liver canceras a label for peptide based therapies.
^{177}Lu	β^-, γ	$^{176}Lu(n,\gamma)^{177}Lu$ $^{176}Yb(n,\gamma)^{177}Yb$ $^{177}Yb \rightarrow^{177} Lu$	Targeted therapy via peptide labeling (neuroendocrine tumors and metastatic prostate cancer).
^{186}Re	β^-, EC	$^{185}Re(n,\gamma)^{186}Re$	Targeted therapy, including metastatic bone therapy.
^{32}P	β^-	$^{31}P(n,\gamma)^{32}P$	Brachytherapy label for pancreatic disease; treatment agent for some myeloproliferative disease.
^{125}I	EC, γ	$^{124}Xe(n,\gamma)^{125}Xe$ EC ^{125}I	Brachytherapy (brain tumors, prostate cancer); labeling of antibodies for nuclear medicine studies (research).
^{67}Cu	β^-	$^{67}Zn(n,p)^{67}Cu$	Labeling of peptides for treatment of NETs, meningioma (currently under trial)
^{223}Ra	α	$^{226}Ra(n,\gamma)^{227}Ra$ $\rightarrow^{227} Ac \rightarrow$ $^{227}Th \rightarrow^{223} Ra$	Target therapy for bone metastases.

1.5.2 Charged particle accelerator production

Medical radionuclides can also be formed using charged particle accelerator such as cyclotron by irradiating stable targets [17]. In such circumstances, the projectile particle usually a deuteron, proton or an alpha, is accelerated before bombarding a stable target to high energies about (10 – 100 MeV). The charged particles need to be accelerated to high energies in contrast to nuclear reactions including neutrons to overcome the Coulomb barrier of target nuclei. The radionuclides generated in cyclotrons will be neutron deficient, by comparison to those radionuclides generated in a nuclear reactor which have a neutron excess. As a result, they will decay differently, by electron capture and positron emission. Figure 1.3 describes the operation of the cyclotron [17]. Cyclotron made-up of two hollow electrodes due to their appearance called 'D's, a potential difference (AC current) applied across them. The entire configuration is established within a magnetic field. The charged particles are emitted from the ion source positioned at the center gap of the negatively charged D. Due to the magnetic field the charged particles follow a curved path. The frequency of the alternating current supply is such that the current switches at the time corresponding to the charged particle arrival at the gap between the D, subsequently accelerating it across the gap with an increasing radius of trajectory each time. The charged particle can be fired towards a target material after being fully accelerated, where it prompts nuclear reactions to generate relevant radionuclides [18].

Radionuclides produced in cyclotron have tendency to decay via β^+ emission or electron capture, these products generally have high specific activity. The chemical and physical separation process of the products are easy and successful, because there is a huge difference in atomic number of the product and target. However, due to the smaller target regions and lower beam intensity in cyclotron compare to a reactor, cyclotron produce smaller quantities of the production. This means that, radionuclides produced in cyclotron are often more expensive compare to the nuclear reactor products.

The on-site synthesis of valuable radionuclides is possible thanks to cyclotrons housed in hospital or cyclotron PET center in a special constructed concrete called bunkers [19]. This may be utilized to afford the

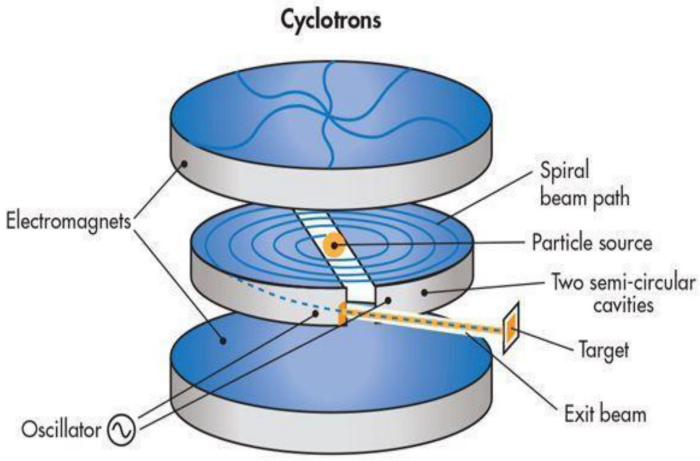

Figure 1.3: Diagram of Cyclotron, illustrating the path of a charged particle accelerated across the gap between hollow electrodes inside a magnetic field. The particle increases speed and so radius of the curved path, to produce a nuclear reaction before being triggered at a target.

hospital on-site among other PET center in surrounding areas. Additionally, it may provide short half-lived radionuclides to certain sites with some flexibility for research purposes [18]. Worldwide, there are more than 950 medical cyclotrons in operation, and that number is steadily rising [20]. The physics of nuclear reactions may be used to determine the properties of the PET radionuclides, which are created by a compact medical cyclotron. A compact medical cyclotron is designed and improved to produce PET radioisotopes [17]. The high performance, reliability, compactness, and cost-effectiveness are important keys for a compact medical cyclotron, and research is progressing and advancing in this direction. With more PET scan operations being performed, there is a continuously growing demand for more affordable compact medical cyclotrons to han-

dle the PET radioisotopes market. According to the purpose they use, cyclotrons come in a variety of sizes [18]. 70 MeV cyclotrons recently installed in some research laboratories to produce specific radioisotopes (e.g., ^{82}Sr for ^{82}Rb generators) [21]. Alpha particles or deuterons can be accelerated, and also beams of different energy range can be provided [18]. As well as, 30 MeV cyclotrons are also installed in radiopharmaceutical companies where SPECT radionuclides (especially, ^{123}I with a half-life of 13 h) are produced or in research laboratories. 15–25 MeV cyclotron are the most common medical cyclotrons and are excellent tools for ^{18}F production, which is the most requested and common radioisotope in PET applications [22]. The 18/18 MeV IBA compact medical cyclotron available at Cannizzaro Hospital is shown in Fig. 1.4 [18].

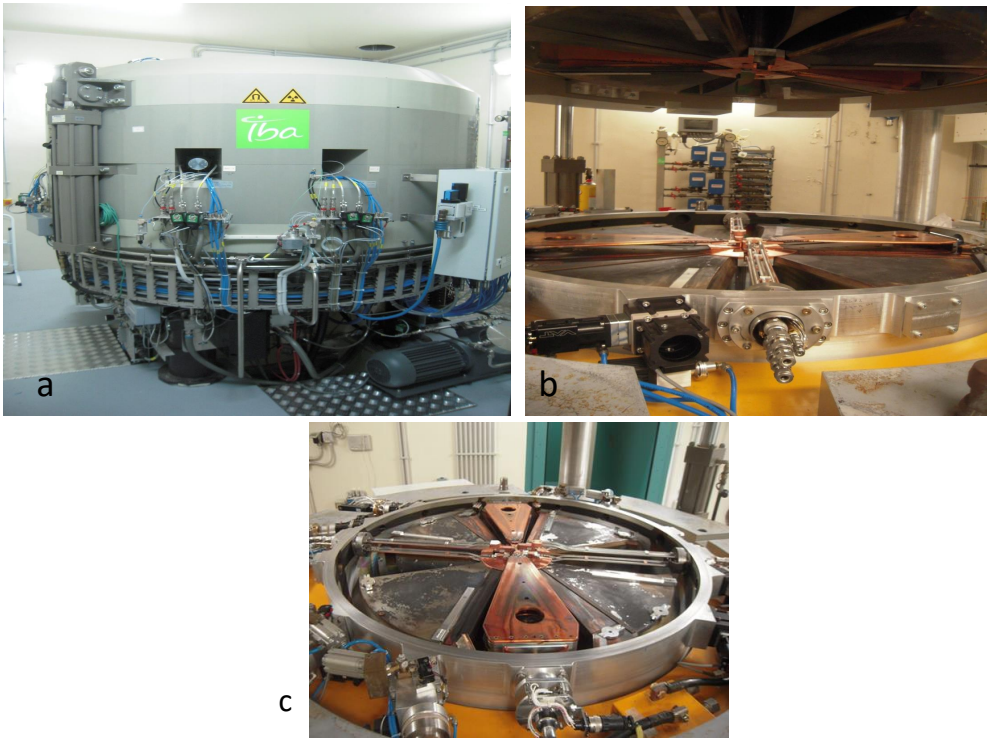

Figure 1.4: (a) The 18/18 MeV IBA compact medical cyclotron at Cannizzaro hospital, Sicily, Italy. (b) The two D parts of the 18/18 MeV IBA cyclotron. (c) Central region.

The cyclotron in the radiopharmaceutical laboratory at Cannizzaro hospital is capable of producing more than 296 GBq of ^{18}F in 2 h with a beam of 65 μA at 18 MeV. The radiopharmaceutical laboratory at the Cannizzaro hospital became today one of the state-of-the-art PET radioisotope production centers in the Sicily region in Italy, with over 5000 PET patients per year; it supplies five Sicilian centers every day with PET radiopharmaceuticals [18]. As the number of available kinds of particle accelerators with the varieties characteristics aimed at radionuclide production for nuclear medicine has also widened, the field of nuclear medicine has broadened. Table 1.2 shows some common medical radionuclides produced in cyclotron. A point of difference in the table 1.2 below is the production of ^{225}Ac, a therapeutic radionuclide produced in the cyclotron that uses alpha emissions for targeted therapy, most recently metastatic prostate cancer [1].

Table 1.2: Common medically used radionuclides produced by a cyclotron (∗production can also be achieved in high powered linear accelerator).

radionuclide	**Decay Mode**	**Reactions**
^{18}F	β^+, EC	$^{18}O(p,n)^{18}F$
^{11}C	β^+	$^{10}B(d,n)^{11}C$
^{123}I	EC	$^{121}Sb(\alpha,2n)^{123}I$
^{67}Ga	EC	$^{68}Zn(p,n)^{67}Ga$
^{111}In	EC	$^{111}Cd(p,n)^{111}In$
$^{225}Ac^*$	α	$^{226}Ra(p,2n)^{225}Ac$

1.5.3 Radionuclide generator production

Generators are a convenient procedure to produce radionuclides on-site and can be an alternative way to cyclotrons for producing short-lived radionuclides for quick and regular clinical use. In radionuclide generator a short-lived daughter radionuclide can be separated form the longer-lived parent as it decays, and can be used in clinic immediately. $^{99}Mo/^{99m}Tc$ generator is the most common generator, which is the basic for several

disciplines of nuclear medicine [3]. The generator system depends on transient equilibrium state between the parent and daughter, which basically permits the daughter to decay at the rate of the parent, and extending its lifetime. In radionuclide generator, ^{99}Mo is generated in high specific activity as a fission product in reactors. It is loaded into a column made of porous alumina resin. The parent, ammonium molybdate, is adsorbed onto the column. The ^{99m}Tc generated through decay is less tightly bound and can be eluted by a flow of saline through the column. The chloride ions exchange with the $^{99m}TcO_4^-$ (but not the MoO_4^{-2} ions) when the saline solution is passed through the column, and generating sodium pertechnetate $NaTcO_4$. Consequently, ^{99m}Tc-pertechnetate is generated in a sterile form with high specific activity and a pH suitable for radiopharmaceutical preparations see Fig. 1.5. The $^{99}Mo/^{99m}Tc$ generator can be eluted mostly twice per day for relatively a week before being replaced [3]. With this method a large quantity of ^{99m}Tc can be produced daily for clinical use without any losses due to the radionuclide transportation [1].

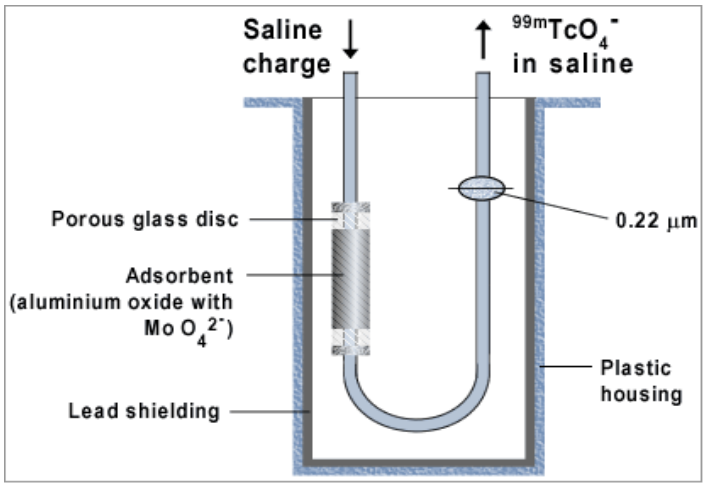

Figure 1.5: ^{99m}Tc radionuclide generator

Generally, by a continuous or discontinuous (or bolus) method one can separate a daughter radionuclide from the parent. The continuous method involves elution of the daughter radionuclide from the generator as it is formed followed by its direct use. The bolus method involves a single elimination of all the available daughter activities. This can be repeated after an appropriate intervening time during which the daughter re-grows. This method is employed when the daughter is not very short-lived, as in the case of ^{99m}Tc. The most suitable time for elution to gain maximum daughter radioactivity is at approximately four times the daughter half-life. Some examples of commonly used radionuclide generators are listed in the table 1.3 [1].

Table 1.3: Medical radionuclide generator system.

Parent(half-life)	Decay Mode	Daughter(half-life)	Decay Mode
$^{99}Mo(67\ h)$	β^-	$^{99m}Tc(6\ h)$	γ-emission
$^{68}Ge(271\ h)$	EC	$^{68}Ga(68\ mins)$	β^+, EC
$^{90}Sr(28.8\ yrs)$	β^-	$^{90}Y(2.7\ days)$	β^-
$^{82}Sr(25.5\ days)$	EC	$^{82}Rb(75\ sec)$	β^+

1.6 Radionuclides emitting beta particle in medicine

1.6.1 Fluorine-18

Fluorine-18 (^{18}F) emits positron with (97%) and electron capture with (3%) probabilities, and positron endpoint energy is 653 keV, the half-life of ^{18}F is 109.8 minutes. The current technique for ^{18}F production is the irradiating of a small volume of enriched $H_2^{18}O$ in a metal target by protons of energies from near threshold (approximately 3 MeV) up to about 20 MeV [18, 23, 24]. Due to its almost ideal chemical and nuclear characteristics, ^{18}F is the radionuclide that is most frequently used for PET routine diagnostics. The use of the $^{18}O(p,n)^{18}F$ reaction on ^{18}O-enriched water is the most effective method and delivers ^{18}F of high molar radioactivity [18]. The half-life of 109.7 min allows time-consuming multi-step radiosyntheses as well as extended PET studies of slower biochemical processes.

The most important route for obtaining ^{18}F-labeled compounds is nucleophilic substitution based on no-carrier-added ^{18}F, which is directly available from the target without any carrier addition [25]. The beam current that the water target is able to cope with is limited by vaporization/cavitation in the target water volume. The $^{18}O(p,n)^{18}F$ reaction for production of elemental fluorine offers the opportunity to produce larger quantities, at the expense, however, of being rather more complicated. There are two target materials that are used for the production of ^{18}F. The most widely used target for the production of ^{18}F fluoride is water enriched in the ^{18}O target [18]. However, more recently, a proposal to use oxygen gas in a two steps procedure has been suggested [26]. The co-production of ^{13}N via the $^{16}O(p,\alpha)^{13}N$ reaction should be taken into account when using ^{18}O of lower enrichment (< 90%). Because the atomic radius of fluorine is similar to that of hydrogen in most molecules, fluorine can be used as pseudohydrogen. Fluorine can be introduced into molecules using its electronegative and nucleophilic. The best known and widely used ^{18}F labelled radiopharmaceutical is $[^{18}F]$FDG which is a glucose analogue in which the hydroxyl group on the 2-carbon of a glucose molecule is replaced by a fluoride atom [18, 27]. Cancer diagnosis and management (diagnosis of malignancy, grading malignancy, staging disease, residual disease, detection of recurrences, measuring response to therapy, to identify the site of disease, to identify the primary tumour when secondary cancers are present) is the most important clinical application of $[^{18}F]$FDG [28]. $[^{18}F]$FDG is also used for the study of metabolism in the brain and heart and for the detection of epilepsy [27].

1.6.2 Carbon-11

Carbon-11 (^{11}C) decays 100% by positron with a maximum β^+ energy of 968 keV with half life 20.4 min. Because carbon is the building block of all organic matter, ^{11}C can be substituted into these molecules without apparent disruption of the functional nature of the molecule [29]. In the Cannizzaro hospital ^{11}C is produced by bombarding the natural nitrogen with proton via nuclear reaction ^{14}N(p, α)^{11}C. Radioactive carbon dioxide ($^{11}CO_2$) and methane ($^{11}CH_4$) will be produced from a gas target made by mixing a gas containing N_2 + 0.5–1% O_2 at a pressure of 17–19 bar, which

allows the complete absorption of the beam inside the chamber [18]. In most cases, the ^{11}C is inserted in such a way as to produce an analogue of the target molecule; thus, this new molecule must be fully characterized with respect to its functional capacity. While, there are a number of routes to produce ^{11}C. The ^{14}N(p, α)^{11}C reaction using natural nitrogen gas is the recommended mode. The production of ^{11}C from nitrogen has been studied extensively since the mid-1960s [30, 31]. The excitation function for the $^{14}N(p,\alpha)^{11}C$ reaction. The target material for producing $^{11}CO_2$ is nitrogen with a small percentage of O_2 (0.1–0.5%) [31, 32]. ^{11}C-methionine and ^{11}C -choline is used for the measurement of oxygen consumption in the heart and brain; for the detection of different types of malignancies, reflecting the amino acid utilization and prostate imaging respectively [25].

1.6.3 Gallium -67

Gallium-67 (^{67}Ga) decays to stable ^{67}Zn by electron capture. Its decay emissions include γ-rays of 93.3 keV (37.0%), 184.6 keV (20.4%) and 300.2 keV (16.6%) with half-life: 3.26 day. Gallium-67 is commonly produced by using enriched ^{68}Zn targets through the $^{68}Zn(p,2n)^{67}Ga$ nuclear reaction [5]. The target material is enriched ^{68}Zn. Gallium-67 behaves in the body in a similar way to ferric iron. It is commonly used as a trivalent citrate compound for nuclear medicine imaging, and is a valuable agent in the detection and localization of certain neoplasms and inflammatory lesions.

1.6.4 Germanium-68 /Gallium-68

Germanium-68 (^{68}Ga) is mainly used as a calibration source for PET. The decay of ^{68}Ge to ^{68}Ga gives a long lived, pure positron, source for use in PET instruments. ^{68}Ga is a positron emitter for clinical PET applications that can be produced by a $^{68}Ge/^{68}Ga$ generator without cyclotron. The $^{68}Ge/^{68}Ga$ generator is ideally suited to on-demand availability of ^{68}Ga for biomedical experiments and clinical applications.

$^{68}Ge/^{68}Ga$ generator system is developed using polysaccharide-based adsorbents and direct application of the generator eluted ^{68}Ga-citrate to PET imaging of tropical infectious diseases. Gallium-68 finds significant

applications in assessments of blood–brain barrier integrity as well as for tumor localization. It is also widely used as a source for the attenuation correction of most positron emission tomography. It is an ideal PET radiotracer, owing to its non-halogenated and non-volatile chemical properties and its 68 min half-life, which permits chemical manipulation for the production of many PET radiopharmaceuticals.

The ^{68}Ga eluent from these generators can be used for the production of various ^{68}Ga-labeled radiopharmaceuticals, such as ^{68}Ga-DOTA-TOC for detection of somatostatin receptor-expressing cancer tissues [33]. However, little progress towards using ^{68}Ga in clinical applications has been made, due to the long synthesis times required by manual production of ^{68}Ga labeled PET imaging agents.

The nuclear reactions for the production of ^{68}Ge are the alpha reaction on natural zinc and the proton reaction on either natural gallium or more often on enriched ^{69}Ga. Germanium-68 is long lived $T_{1/2} = 271$ days, and attempts to produce it on medium energy accelerators are not generally made due to the low production yields. The primary source for the parent radionuclide is from the spallation processes available at large energy accelerators, where parasitic position and operation are available [5].

1.6.5 Techentium-99m

The growth of nuclear medicine has been due mainly to the availability of ^{99m}Tc radiopharmaceuticals; this single isotope is used in over 80% of all diagnostic procedures. Each year, roughly 25 million procedures are carried out with ^{99m}Tc radiopharmaceuticals [3]. The availability of short lived ^{99m}Tc (half-life: 6 h) from the $^{99}Mo/^{99m}Tc$ generator, as the daughter product of long lived ^{99}Mo (half-life: 67 h), is a major factor behind the universal use of this radioisotope [9]. ^{99m}Tc have been used for medical imaging of tumors, cancers and other metabolism-related diseases via PET and SPECT. ^{99m}Tc radiopharmaceuticals are used in several diagnostic procedures, from the use of pertechnetate for thyroid uptake to the use of ^{99m}Tc-octreotide derivatives for imaging neuroendocrine tumours. Owing to its multiple oxidation states, ^{99m}Tc has a versatile chemistry, making it possible to produce a variety of complexes with specific desired characteristics, which is a major advantage of ^{99m}Tc for radiopharmaceu-

tical development. ^{99m}Tc is easily produced by the decay of the parent ^{99}Mo by eluting compact and transportable $^{99}Mo/^{99m}Tc$ generator systems that are almost always available in nuclear medicine departments.

1.6.6 Iodine-121

Iodine-121 (^{121}I) has a half-life of 2.12 h and decays with 94% electron capture and 6% positron emission. There is a prominent γ-ray at 212.2 keV, which can be used in gamma camera images. It decays to ^{121}Te, which has a long half-life and decays with the same 212.2 keV γ- ray [34]. The half-life of the metastable state is 69 min, and the half-life of the ground state is 4.9 h. Indium-110m is an isotope that decays by positron emission 62% of the time and by electron capture the remainder of the time. Indium-110 has some interesting production problems since it has a metastable state with a 69.1 min half-life, which decays by electron capture to the ^{110}In ground state. There is one route that does not proceed through the metastable state and this is through the ^{110}Sn parent. Thus, one way to produce pure ^{110}In is to produce pure ^{110}Sn and use it as a generator for the ^{110}In [35, 36]. The only practical method of production is from the $^{122}Te(p,2n)^{121}I$ nuclear reaction on highly enriched ^{122}Te [37].

1.6.7 Iodine-123

The most widely used cyclotron produced radiohalogen is probably ^{123}I. It has gradually replaced ^{131}I as the isotope of choice for diagnostic radiopharmaceuticals containing radioiodine. It gives a much lower radiation dose to the patient, and the γ-ray energy of 159 keV is ideally suited for use in a gamma camera. The γ-ray will penetrate tissue very effectively without an excessive radiation dose. A large number of radiopharmaceuticals have been labeled using ^{123}I, and the number is increasing. ^{123}I decays 100% by electron capture, with two main γ-rays at 0.028 and 0.160 MeV [38]. The targets used for production of ^{123}I can be grouped into three types: solid targets, liquid or molten targets, and gaseous targets. ^{123}I is commonly produced in all three types of target, depending on the energy of the cyclotron being used and on the availability of enriched ^{124}Xe as a target material [39].

1.6.8 Iodine-124

Although ^{124}I has often been considered as an impurity in preparations of ^{123}I, it does have attractive attributes for use in some PET radiopharmaceuticals [40]. The half-life of 4.2 days is long enough for localization with monoclonal antibodies, and the 23% positron decay allows imaging with PET. The use of ^{124}I is becoming more widespread. ^{124}I has potential as both a diagnostic and a therapeutic radionuclide [41]. ^{124}I has many gamma emissions and some low energy beta emissions, as well as the two high energy positron emissions. The best nuclear reaction for the production of ^{124}I is the $^{124}Te(p,n)^{124}I$ reaction on enriched. The target for production ^{124}I is limited to solid targets. The target is either elemental tellurium or tellurium oxide [42, 43]. The targets are identical to those used for the production of ^{123}I from tellurium. The target plates can be made from either platinum or tantalum. Elemental tellurium can be electrodeposited onto the target plate. Tellurium oxide is usually melted into a cavity on the target plate [44].

1.6.9 Iodine-131

^{131}I is a β-emitting radionuclide with a physical half-life of 8.1 days, a principal γ-ray of 364 keV and a principal β-particles with a maximum energy of 0.61 MeV, an average energy of 0.192 MeV, and a range in tissue of 0.8 mm. More than 50 years (in the 1930s and 1940s) have passed since Radioactive Iodine Therapy (RIT) was introduced for treating hyperthyroidism caused by Graves' disease [45]. Today, it is used in nuclear medicine both diagnostically and therapeutically. In therapy, it is used for treatment for an overactive thyroid, a condition called hyperthyroidism. RIT is also used to treat different types of thyroid cancer [11].

Therapy with ^{131}I means the oral administration of ^{131}I as sodium iodide. ^{131}I is a fission product of ^{235}U along with a lot of others. ^{131}I is produced by the irradiation of Tellurium-130 in a nuclear reactor according to the reaction: $^{130}Te(n,\gamma)^{131}Te \ \rightarrow^{131} I$. In medical applications, ^{131}I is added to NaOH solution containing 0.02 M Na_2SO_4 with pH= 9.0-12.0. Its activity concentration usually is equal or higher than 1000 mCi/ml (for high concentration) and 200-1000 mCi/ml (for low concentration) [46].

1.6.10 Nitrogen-13

Nitrogen-13 (^{13}N) decays by pure positron emission (100%) to stable ^{13}C. The end point energy of the positron is 1.19 MeV. Several compounds incorporating ^{13}N have been made, but the time of accumulation in the body is short and so the physiological processes that can be studied must be rapid [47]. ^{13}N is made by bombarding of distilled water with protons via nuclear reaction $^{16}O(p,\alpha)^{13}N$. With relatively low-energy bunch of proton in cyclotron (10 MeV) can be efficient production yield 3.7 GBq(100 mCi) achieved by irradiation for 20 minutes. Using a mixture of water and ethanol is obtained more useful chemical form ammonia ($^{13}NH_3$). Another form also used is nitrate anion ($^{13}NO_3^-$) [48].

By far the most widely used compound of ^{13}N for PET is the chemical form of ammonia. It is used as a blood flow tracer and has found utility in cardiac studies to determine areas of ischaemic or infarcted tissue. The most common reaction is the $^{16}O(p,\alpha)^{13}N$ reaction on natural water [48]. The final common reaction is the $^{12}C(d,n)^{13}N$ reaction on natural carbon, the targets for production of ^{13}N can be solids, liquids or gasses, depending on the chemical form of the nitrogen that is desired. The chemical form can also be changed by a number of other factors, such as the dose and dose rate to the target, the pH of liquid targets and the physical state. The first target for production of ^{13}N was a solid target of boron, which Joliot and Curie [49] bombarded with an alpha particle beam. Solid targets have been used extensively for production of ^{13}N, particularly in the form of either nitrogen gas or ammonia [50, 51].

1.6.11 Oxygen-15

Oxygen-15 (^{15}O) is the longest lived of the positron emitting isotopes (99.9% positron emission) of oxygen with 122 sec. The end point energy of the positron is 1.72 MeV. ^{15}O decays to stable ^{15}N and was one of the first artificial radionuclides produced with low energy deuterons on a cyclotron [52]. ^{15}O is used to label gasses, such as oxygen, carbon dioxide and carbon monoxide, for inhalation, and it is also used to label water for injection. The major purpose of these gasses and liquids is to measure blood flow, blood volume and oxygen consumption in the body. The ex-

citation functions for $^{14}N(d,n)^{15}O$ and $^{15}N(p,n)^{15}O$. Gaseous targets are, for the most part, used for these compounds. ^{15}O containing compounds can be made either directly in the target [53] or outside the target in a separate recovery module. Gas targets are usually made of nitrogen and are bombarded with either protons or deuterons, depending on which particle is available.

1.6.12 Phosphorus-32

Phosphorus-32 (^{32}P) was the first radionuclide introduced more than 50 years ago for the palliation of pain from bone metastases. From the 1940s to 1980s it was the most widely used radionuclide. ^{32}P has also been used in therapy of polycythemia vera and leukemia. ^{32}P was one of the first radioactive isotopes to be prepared in cyclotron for therapeutic research purposes. It was produced in the Berkeley cyclotron by E. Lawrence in 1936 [54]. ^{32}P was produced by irradiating red phosphorus (^{15}P) with deuteron ($^{1}H_2$) according to the reaction [55]:

$$^{15}P_{31} +^{1} H_2 \rightarrow^{15} P_{32} +^{1} H_1 \tag{1.1}$$

The cross section of the reaction is $0.18 \times 10^{-27} cm^2$. Nowadays, with the development of nuclear reactors, radiophosphorus is produced primarily from bombarding sulfur (^{16}S) with fast neutrons:

$$^{16}S_{32} + n \rightarrow^{15} P_{32} +^{1} H_1 \tag{1.2}$$

The product is practically carrier-free. ^{32}P has a physical life of 14.3 days. It emits a β-particle with a maximum energy of 1.71 MeV and an average mean energy 0.7 MeV. The mean and the maximum particle range in soft tissue are 3 and 8 mm, respectively [55].

1.6.13 Copper-64

Copper (Cu) is a transition metal with atomic number 29, known since ancient times. It is an important trace element for most organisms. In humans, copper plays a role as a cofactor for numerous enzymes, such as Cu/Zn-superoxide dismutase, cytochrome c oxidase, tyrosinase, ceruloplasmin, and other proteins, crucial for respiration, iron transport and

metabolism, cell growth, and hemostasis [56, 57]. ^{64}Cu-labeled peptides for targeted cancer therapy/imaging are one of the largest groups of copper radiopharmaceuticals currently researched. They are built of a targeting peptide such as bombesin or octreotide analogue, a linker, and a bifunctional chelator (BFC), commonly tetraazamacrocycle derivate, like tetraazamacrocyclic (TETA) or tetraxetan (DOTA). The peptide binds to a specific receptor expressed by cancer cells, while copper isotope-BFC moiety allows localization of the tumor by positron emission detection. Attractiveness of peptides for targeted radiotherapy, in comparison to monoclonal antibodies, comes from their good tissue distribution, fast clearance, low immunogenicity, and inexpensive, automated production [58]. Additionally, ^{64}Cu-labeled antibodies for PET imaging are trastuzumab (breast cancers expressing human epidermal growth factor receptor 2 or HER2), cetuximab (targeting EGFR-epidermal growth-factor receptor expressing tumors), TRC105-Fab (targeting CD105), and etaracizumab (antibody against human $\alpha_\nu\beta_3$ integrin) [58].

^{64}Cu is a highly unusual isotope because it decays by three processes, namely, positron, electron capture, and beta decays [59]. This property allows either cyclotron or reactor production, with the latter route resulting in either low specific activity (n, γ) or high specific activity (n, p) products [60]. In principle, the combination of these radioactive emissions can be exploited for carrying out both diagnosis and therapy using the same radiolabeled species, thus providing an example of clinical approaches collectively referred to as 'Theranostics' [61]. The theranostic approach is an established tool for specific molecular targeting, both for diagnostics and therapy. Radionuclides used for theranostic radiopharmaceuticals are typically produced in nuclear fission reactors or bio-medical cyclotrons. Another alternative route for producing an emerging theranostic radionuclide, is using 14 MeV fusion neutrons [16]. This can allow predictions to be made about the ^{64}Cu activity that can be produced by irradiating more material for more time, in order to deal with the requests coming from the nuclear medicine laboratories [16].

At present, the most common production method for ^{64}Cu utilizes the $^{64}Ni(p,n)^{64}Cu$ reaction [62, 63]. The target for producing ^{64}Cu is enriched ^{64}Ni (99.6%). The ^{64}Ni (typically 10–50 mg) is prepared and electroplated onto a gold disk using a procedure modified from Piel et al. [64]. The

target is bombarded on the cyclotron. Recently, Obata et al. reported the production of ^{64}Cu on a 12 MeV cyclotron, which is more representative of the modern cyclotrons currently in operation [65].

After bombardment, the ^{64}Cu is separated from the target nickel in a one-step procedure using an ion exchange column. Typically, 18.5 GBq of ^{64}Cu are produced with a 40 mg ^{64}Ni target and a bombardment time of 4 h. The specific activity of the ^{64}Cu ranges from 47.4 to 474 GBq/μmol (1280 to 12800 mCi/μmol). The typical yields for ^{64}Cu productions are 0.2 mCi/μA·h per mg ^{64}Ni. The enriched ^{64}Ni can be 85–95% recovered as previously described and reused for future bombardments, which contributes to the cost-efficiency of this method of ^{64}Cu production [66].

Another method of ^{64}Cu production is the $^{64}Zn(n,p)^{64}Cu$ reaction in a nuclear reactor [67]. Most reactor-produced radionuclides are produced using thermal neutron reactions, or (n, γ) reactions, where the thermal neutron is of relatively low energy, and the target material is of the same element as the product radionuclide.

1.6.14 Copper-67

^{67}Cu releases beta particles with mean energies and abundances of 121 keV (56%), 154 keV (23%) and 189 keV (20%) that are suitable for therapeutic purposes and photons with energies and abundances of 91 keV (7%), 93 keV (16%) and 184 keV (49%) that are suitable for imaging purposes. ^{67}Cu contains ^{64}Cu radioimpurity as a co-product. Due to its excellent physical and biochemical properties for radioimmunotherapy, Copper-67 (^{67}Cu) is being actively investigated by several groups as a radioimmunotherapeutic agent [68]. ^{67}Cu is referred as isotope of high priority and due to a 2.6 day half-life and suitable β-emission (141 keV, avg) is ideal for use with Monoclonal antibodies (MABs) and other tumor targeting compounds. ^{67}Cu has a cross section value gradually increasing, above 60 MeV-high energy reactions.

^{67}Cu is produced by the $^{68}Zn(p,2p)$ reaction, which also produces $^{64}Cu(T_{1/2} = 12.7\ h)$,$^{61}Cu(T_{1/2} = 3.4\ h)$, and other radionuclides. ^{61}Cu decays rapidly to negligible activity, but ^{67}Cu remains present in appreciable quantities for days. The ratio of ^{67}Cu to ^{64}Cu to ^{61}Cu activity is typically 1:7:10 at end of bombardment, or 1:0.5:0.0001 when received by

the customer (48- 72) h later. To produce radiopharmaceutical of adequate amount and specific activity, ^{67}Cu-2IT-BAT-Lym-l is usually prepared for clinical use within 24 h of receipt of the radionuclide [69] at which time the activity of ^{64}Cu is still significant. Because the half-life of ^{64}Cu (12.7 h) is much shorter than that of ^{67}Cu (61.9 h), the ratio of ^{64}Cu to ^{67}Cu decreases after the end of bombardment (EOB). The average amount of ^{64}Cu as a percent of total activity in the supply at the time of delivery, typically 36-48 h after EOB , is 43% (range (35-61) %). In addition to photons (1346 keV (0.5%)), ^{64}Cu emits positrons that generate annihilation photons (511 keV (36%)). These high-energy photons readily penetrate the septum of a gamma-camera collimator and can thus alter quantization of the intended ^{67}Cu radiopharmaceutical.

1.6.15 Strontium-89

Strontium-89 (^{89}Sr) is the most commonly used radionuclide in the treatment of metastatic bone cancer [70]. ^{89}Sr is a pure beta emitter. It has a physical life of 50.5 days and maximum β-particle energy of 1.46 MeV. The maximum and the average range in soft tissue are approximately 6.7 mm and 2.4 mm, respectively. At the present time, there are two major methods of ^{89}Sr production [71]. The first consists of irradiating a highly enriched target of $^{88}Sr(^{88}Sr > 99.9\%)$ with neutrons according to $^{88}Sr(n,\gamma)^{89}Sr$ reaction. This is a simple production taking place in thermal neutron reactors. The second method, based on threshold reaction with emission of charged particles according to $^{89}Y(n,p)^{89}Sr$ reaction, occurs in fast flux reactors. The small cross section of the reactions ($6 \times 10^{-27} cm^2$ and $0.3 \times 10^{-27} cm^2$ respectively) restricts the productivity of these two methods. Consequently, there is a need for a more efficient method for the production of ^{89}Sr. Recently, a new way for ^{89}Sr production with a solution in a reactor was proposed [72]. Corresponding to this way, the gaseous radionuclide ^{89}Kr decays to ^{89}Sr:

$$^{89}Se \rightarrow^{89} Br \rightarrow^{89} Kr \rightarrow^{89} Rb \rightarrow^{89} Sr \tag{1.3}$$

In this case the cross section is almost 500 times greater than in neutron capture reaction. This new technology produces almost no radioactive waste with principal advantage of high ^{89}Sr productivity [72].

1.6.16 Yttrium-90

Yttrium-90 (^{90}Y) has been used in medicine since 1960, in order to treat various kinds of benign and malignant tumors. ^{90}Y is a pure β-emitter with a physical half-life of 64.1 h (2.67 days) and it decays to stable Zirconium-90 (^{90}Zr). The β-rays emitted by its decay have an average value of 0.9367 MeV while their maximum energy reaches 2.284 MeV. Its average range in tissue is about 2.5 mm and its maximum about 11 mm while the distance within which the β-particle transfers 95% of its energy to the target tissue is about 5.94 mm. Therefore, it is more suitable for therapeutic use and it has been measured that one GBq (27 mCi) of ^{90}Y delivers a total absorbed radiation dose of 50 Gy/kg. In therapeutic use in which the isotope decays to infinity, 94% of the radiation is delivered in 11 days [73, 74]. ^{90}Y can be produced in two different ways, depending on whether the specific activity is low or high. Low specific activity ^{90}Y is produced in a nuclear reactor by neutron activation of the non-radioactive ^{89}Y, when ^{89}Y captures a neutron and becomes the radioactive β-emitter ^{90}Y. This product is of very low specific activity, due to the small neutron capture cross-section of ^{89}Y, but its radionuclide purity is generally very high. For very high specific activity ^{90}Y (that is used for target therapy), a radionuclide generator system of Strontium-90 (^{90}Sr) is used, and it is based on the fact that ^{90}Sr decays to ^{90}Y.

Four types of $^{90}Sr/^{90}Y$ generators have been developed: 1) Ion exchange-based generator 2) Single stage of Supported Liquid Membrane (SLM) based generator 3) Two stage SLM based generator and 4) Electrochemical generator. The best of these generators is the electrochemical system as it yields around 97–98% of ^{90}Y deposition. Other advantages of this generator are that it is based on equilibrium, as the parent element is very long-living ($T_{Sr_{1/2}} = 28.8$) years and it gives a short-living daughter ($T_{Y_{1/2}} = 64.1\ h$). In that way, a great quantity of pure and high specific activity ^{90}Y can be produced, with a small amount of ^{90}Sr for a great period. However, the installation of such generators in nuclear medicine departments is not easily realized because of the long-lived waste that requires careful handling and storage [75].

1.6.17 Lutetium-177

Lutetium-177 (^{177}Lu) has found a variety of applications in biomedical fields. Its main usage is in the treatment of neuroendocrine tumors but its applicability in the treatment of colon cancer, metastatic bone cancer, non-Hodgkin's lymphoma, lung, ovarian, prostate cancer, and gastroenteropancreatic tumors has also been studied.

^{177}Lu can be directly produced with a relatively high specific activity by neutron activation of ^{176}Lu. Enriched target material is required for this production route since the natural abundance of ^{176}Lu is only 2.6%. As an alternative production route, ^{177}Lu can be obtained as carrier-free from beta decay of Ytterbium-177 (^{177}Yb) produced by neutron activation of ^{176}Yb (indirect production). Again, enriched target material is required but it may be recycled since the neutron capture cross section is only 2.4 b so resulting in negligible burn-up of ^{176}Yb. The direct production route is obviously more attractive; however, most of the medical applications require ^{177}Lu of high specific activity. Such products can be prepared at many reactors only by the indirect production route. ^{177}Lu with half-life of 6.71 days turns into the stable Hafnium-177 (^{177}Hf). It emits beta radiation with a maximum energy of 498 keV and low energetic gamma rays of 208 and 113 keV with 10% and 6% abundance, respectively, which enables direct monitoring of the activity distribution in patients' body with a gamma camera and subsequent dosimetry [76].

1.6.18 Rhenium-186

The use of Rhenium-186-hydroxyethylidene diphosphonate (^{186}Re-HEDP) in bone pain palliation from multiple metastases has been proved to be highly justified and efficient. It is used for palliation because no single approach has been shown to prolong life. Advances in imaging enable us to evaluate the spatial distribution of radioactivity in tumors and normal organs over time [77]. ^{186}Re-HEDP is the most usually used as a bone-seeking radiopharmaceutical in patients with bone metastases originating from breast or prostate cancer regarding toxicity, pharmacokinetics, and bone marrow dosimetry as well as the palliating effect on bone pain [78].

^{186}Re-HEDP was first developed at the University of Cincinnati. HEDP

is strongly adsorbed on hydroxyapatite in vitro. In vivo, it is markedly concentrated on primary and metastatic bone lesions. In 1979, there was a first suggestion as a possible use of ^{186}Re in the treatment of osseous metastases [79]. However, it took until 1986 to generate therapeutically useful bone-seeking compounds, when Deutsch and Maxon were able to purify the ineffective mixture originally reported by Mathieu [80]. Bone-seeking radiopharmaceuticals have traditionally been used to image tumors in bone, but, depending on the carrier ligand and the energy of the radioactive label, these agents can also be used to treat primary or metastatic tumors in bone [81].

1.6.19 Rhenium-188

Rhenium-188 (^{188}Re) is an attractive radionuclide because of its physical properties and its production in-situ by a $^{188}W/^{188}Re$ generator. ^{188}Re obtains a variety of therapeutic applications. The most predominant application is in bone palliation while it is also used in the treatment of liver tumors and non-Hodgkin's lymphomas. Experimentally, it has been also used for endovascular brachytherapy and treatment of ovarian and breast tumors.

The production of ^{188}Re can be employed by two reactions in nuclear reactors. The first reaction is: $^{187}Re \rightarrow^{188} Re \rightarrow^{188} Os$ (stable) while the second one is: $^{186}W \rightarrow^{187} W \rightarrow^{188} W$ (69.4 days, β-emission)$\rightarrow^{188}Re$ (16.9 h, β-emission)$\rightarrow^{188}Os$ (stable). In $^{187}Re(n,\gamma)^{188}Re$ reaction, the target is metallic rhenium or oxide in natural abundance or enriched in ^{187}Re. Due to the high costs of the enriched target material this reaction has no importance for the routine production. ^{188}Re has a significant advantage as it can be obtained by a Tungsten-188/Rhenium-188 generator system. Thus, the known benefits of the generators can be used. The parent radionuclide ^{188}W, formed by the double neutron capture on ^{186}W with β-decay produces ^{188}Re which decays an energetic β-particle with a maximum energy 2.12 MeV and a gamma-photon (155 keV, 15%) [82]. Tungsten-188 is loaded on the alumina generator as tungstic acid and it is eluted with saline. $^{188}W/^{188}Re$ generator, from a chemical point of view, is almost the same as a $^{99}Mo/^{99m}Tc$ generator system, which is extensively studied. However, there is a major difference that origi-

nates from the availability of the mother radionuclides (^{99}Mo and ^{188}W) as a carrier free. The production process of ^{188}W results in a significantly carrier-added ^{188}W product (specific activity < 10 Ci/g of ^{188}W, typically 4-8 Ci/g) [83] unlike ^{99}Mo which is generally produced from the fission of ^{235}U. Hence, the adsorption column of an $^{188}W/^{188}Re$ generator is considerably larger than that of a $^{99}Mo/^{99m}Tc$ generator at the same radioactivity. As a result, a large amount of elution is required to elute ^{188}Re at a reasonable quantity. In order to solve this problem concentration methods are utilized [84].

Chapter 2

Radioactive measurement techniques

2.1 Introduction

The development and application of both nuclear power and nuclear medicine have been the major interests in nuclear science for almost half a century [85]. Associated with that are the increasing demands for standards of radioactivity in order to define its unit of measurements, i.e. Becquerel (Bq) and improved accuracy for radionuclide with a wide variety of decay schemes. For activity standards, it is not possible to have a physical representation of the Becquerel which is applicable to all radionuclides. As a consequence, a standard for any particular radionuclide will only be suitable as a measurement standard for the same radionuclide. This presents considerable difficulty for radioactivity measurements as there are hundreds of different radionuclides, all of which have their own particular decay schemes with different energies, decay rates, intensities and types. Furthermore, there is no one method or detector that can be used for the measurement of all radionuclides. Therefore, standardization of a particular radionuclide involves a particular study of its decay scheme, radiation particle interaction with matter and measurement technique [85]. The activity measurement can be classified as being either direct or indirect. Direct measurements are the measure-

ments in which the activity is determined from count rate data alone, without reference to any activity determined from previous experiments. Direct measurements are sometimes referred to as *"absolute"* measurements, and standards so produced are often designated as *"absolute"* or *"primary"* standards. The direct measurements are highly accurate and precise measurements. Indirect measurements are made by performing comparisons with the primary standards through a reference instrument such as an ionisation chamber or gamma ray spectrometer. The standards so produced are often designated as *"secondary"* standards. *"Tertiary"* standards are made traceable to secondary standards.

There are a variety of absolute methods for activity determination, as described by Allen [86] and NCRP [87]. They can be classified into the following categories. The first is defined solid-angle counting [88] and 4π-counting [89, 90, 91, 92]. In defined solid-angle measurements, a point source is placed not too close to the entrance window of a detector and the system is in a vacuum. The detection is made within a defined solid angle much less than 4π steradians ($\Omega << 4\pi$) and the effects of absorption or scattering by either the source itself or its surroundings are kept minimal and all particles incident upon the sensitive volume of the detector are recorded. Then the activity can be determined from the count rate, and the solid angle subtended at the source by the detector.

The counters are designed such that the solid angle is well-defined and directly measurable. When the solid angle increases beyond 10% of 4π steradians the defined-solid-angle method becomes unreliable, mainly because the effects of absorption and scattering are increasing and can no longer be estimated with sufficient accuracy. Defined-solid-angle counting has been used for measuring alpha particles with energies of several MeV, and photons in the energy range of 1 to 80 keV, in other words, those particles which are "lightly scattered but heavily absorbed" [87]. For β-particles, which result in much more absorption and scattering in the source itself and detector window, the method is not appropriate. If the solid angle is increased to 4π steradians and energy is above threshold, every radiation particle can be detected, and the count rate is then a direct measure of the disintegration rate. This eliminates the need for an accurate definition of the solid angle and its associated scattering problems. The angle needs no longer be considered. 4π-counting has been

used for measuring charged particle emitters where the source is made very thin, placed on a very thin source mount, and counted within a windowless detector subtending an angle of 4π steradians around the source. Forms of 4π counting, in which the detection efficiency is nearly 100 percent are: 4π gas proportional counting of a very thin source, internal gas counting of radionuclides in gaseous form, and liquid scintillation counting of energetic alpha and beta particle emitters.

These methods are relatively simple in procedure, but they involve some corrections such as self-absorption, and their accuracy are often limited. Coincidence counting is the most powerful method for the absolute measurement of radioactivity. Coincidence counting is used for the absolute radioactivity measurement of a source when each nuclear event involves two distinguishable radiations being emitted in prompt succession. Although there are some variations in the method with regards to the choice of detector type and the selection of radiations detected, the fundamental principle of the coincidence techniques is the same.

The $4\pi\beta - \gamma$ coincidence method is used for radionuclides that disintegrate by emission of α or β particle, or an X-ray (as a result of electron capture), followed by a gamma ray in prompt succession. The gamma-gamma coincidence counting is used for radionuclides that emit two gamma rays in cascade, also simultaneously for example of annihilation of β^+. The development of new standards is mostly the result of user demand. The effectiveness and accuracy of a standard relies upon the absolute standardization techniques and their subsequent development and dissemination to meet the requirements of the user communities. The development, maintenance and dissemination of the activity standard are the main task of the National Metrology Laboratory.

Following the discovery of X-rays in 1895 by Roentgen [93], H. Becquerel discovered radioactivity by accident in February 1896 [94], when using naturally fluorescent minerals to study the properties of X-rays. In Becquerel's paper, he reported that the double sulphate of uranium and potassium emitted certain rays which gave a reactive impression on a photographic plate even when exposed to no light. In other words, the emission occurred irrespective of whether or not the salt was caused by fluorescence. He realized that the emission came from uranium itself, even in the dark. Radioactivity, which was always present on the Earth,

had been discovered. Further experiments showed that uranium minerals were the only phosphorescent minerals to show this effect [95]. On 7 March 1896, H. Becquerel showed that this radiation had the important property of discharging electrified bodies [96]. Later, H. Becquerel reported that this discharge was due to the fact that the gas through which the radiation passes is made temporarily to conduct electricity [97]. This discharging power is similar to that of "Roentgen rays".

In November 1896, J. J. Thomson and E. Rutherford theorized that the rays produce positively and negatively charged carriers throughout the volume of the gas surrounding the charged body, and that the rate of production of the charge carriers is proportional to the subjected radiation [98]. In 1899, E. Rutherford published a detailed comparison of the nature of the discharge produced by “uranium radiation” with that produced by “Roentgen rays” [99]. The ability of uranium radiation to “ionize” gasses formed the basis of a method for the accurate quantitative analysis and comparison of the radiations.

In July 1898, P. and M. Curie [100] discovered polonium which was 60 times more radioactive than uranium. In the same year, M. Curie discovered radium which was 400 times more radioactive than uranium [100]. M. Curie introduced the shorthand term “radioactivite” (radioactivity) to describe the “activite radiante de l’uranium” [Becquerel, 1903]. A year earlier, in 1897, J.J. Thompson, had discovered the electron. has given a good review of the discovery of radioactivity and evolution of quantities, units and standards in radioactivity [101].

In 1899, E. Rutherford identified two types of radiation emitted by uranium minerals, namely the alpha rays, that produced the far greater part of ionization, but was completely stopped by a thin sheet of paper, and the beta rays, that produced much less ionization, but were much more penetrating.

In 1900, even more highly penetrating radiations emitted from radium, the gamma rays, were discovered by P. Villard. By successfully deflecting α-particle from radium and its decay products with both magnetic and electric fields, Rutherford showed that α-particles were positively charged. In 1909, Rutherford and Royds first proved that α particle was an ionized helium atom projected at high speed from a disintegrating atom [102].

In 1914, J. Chadwick first demonstrated that the spectrum of β-radiation was continuous [103]. The continuous spectrum was for a long time completely unexplained, until Fermi presented a successful quantitative theory of the shape of β-ray spectra and the lifetime of β-ray emitters in 1934 [104]. The theory was based on Pauli's neutrino hypothesis and was quite satisfactorily able to account for the relation between the decay rate and maximum energy of the β-particles. Furthermore, the shape of the spectrum was calculated.

The theory was soon extended to all possible types of interactions between heavy and light particles in β-decay. Progress has been more rapid since then, and by the early 1950s many of the fundamental problems concerning β-ray spectra had been solved. Since Henri Becquerel discovered the radioactivity in 1896, radionuclides have been used in a diverse range of applications within medicine, science and industry and the development of the technique of quantification of radioactive sources has never stopped.

2.2 Review of radiation detection techniques

The earliest radiation particle-detection device consisted of a thin layer of zinc sulphide (ZnS) crystal; the scintillation by α-particles striking the ZnS screen were observed. The first devices were only sensitive to the α- and β-particles. In 1908, Rutherford and Geiger used what they called an "electrical method" to detect α-particles expelled from uranium, thorium, radium, and actinium [105]. They constructed a simple gas ionization detector (see Fig. 2.1 reproduced form [105]) in order to determine by a direct method, the number of α-particles expelled from a definite quantity of radioactive matter. The detector consisted of a brass cylinder and a central insulated wire connected to an electrometer.

The outer cylinder was charged to a negative potential. The cylinder contained air or gas at a reduced pressure. This detector is considered as a primary innovation in gas counters. Rutherford and Geiger continued developing their technique and by 1912 had increased their average counting rate for α-particles from the 3 to 5 counts per minute to around 1000 counts per minute [106].

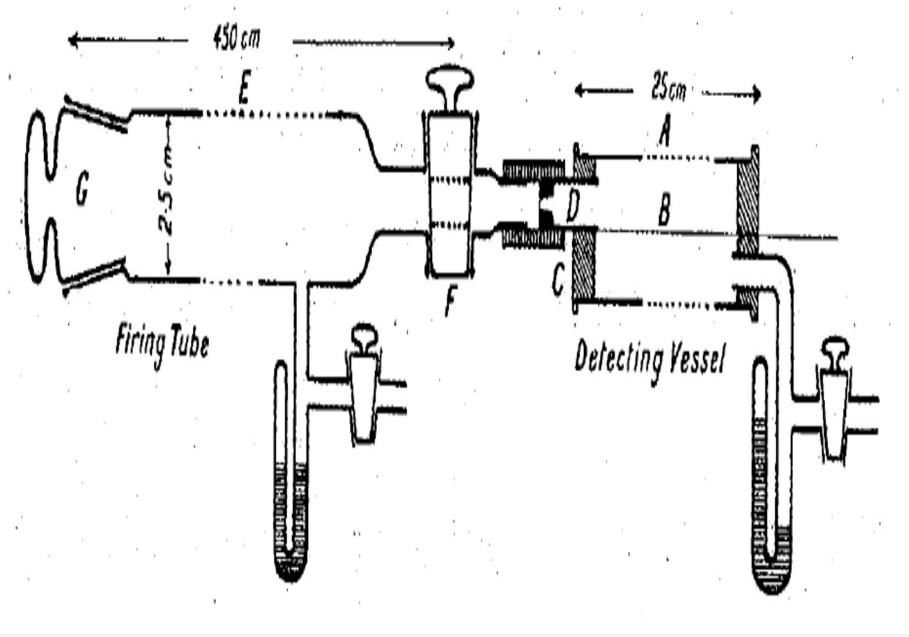

Figure 2.1: The first detecting vessel built by Rutherford and Geiger in 1908. It consists of a brass cylinder A and a central insulated wire B passing through ebonite cork C at the ends. In the ebonite cork C was fixed a short glass tube D which has a circular opening. The α-particles entered the detecting vessel through this opening. A large stop-cock F was attached to one end of the long glass tube E. The other end of the glass tube was closed by a ground stopper G.

In 1928, Geiger and Müller built a gas-filled detector based on ionisation. It was this type of detector which later became commonly known as the Geiger-Müller counter, or G-M tube. The counter employs gas multiplication to greatly increase the charge generated by the original ion pairs formed along the radiation track. It functions only as a simple counter of radiation-induced events because all pulses from a G-M tube are of the same amplitude regardless of the number of original ion pairs generated. It cannot be used as a radiation spectrometer. Due to the simplicity, low cost, and ease of use, the G-M counter is still widely used. It was in the same year that Geiger and Klemperer discovered the proportional region

of the gas ionization which laid the foundations for "proportional counting" [107]. With the proportional property, α- and β-particles could be distinguished by the difference in ionization produced.

2.2.1 4π counting of α- and β-particles

Although 4π-counting was originated in 1944 by Simpson [108] who described a counter with geometry close to 4π steradians, the first real 4π counter was reported by Haxel and Houtermans in 1948 [109]. Since then a number of 4π counting chambers of a variety of designs have appeared. In a 4π counter, the count rate equals the disintegration rate N_0 if absorption in the source or source mount can be neglected. This is still true when a nuclide emits more than two radiation particles per disintegration, provided the time interval between the two radiations is less than the resolving time of the counter and associated electronics. Thus, the system is insensitive to γ-rays and internal conversion electrons following β- or α- decay. The system is also insensitive to the scattering effect since any discharges subsequent to that corresponding to the primary event caused by repeated scattering of one particle will occur within the counter resolving time. Therefore, 4π-counting eliminates not only geometry correction, but also secondary radiation and scattering effects.

The introduction of the 4π proportional counter in late 1940s was to meet the requirements of good energy resolution, high detection efficiency, wide-range amplitude response and sufficient short resolving time. In common with the G-M tube, a 4π proportional counter is a gas-filled detector, operated in pulse mode and utilizes the phenomenon of gas multiplication to amplify the charge generated by the original ion pairs created within the gas. The difference is that for a proportional counter each original electron leads to an avalanche that is basically independent of all other avalanches formed from other electrons associated with the original ionizing event. Therefore, the collected charge is proportional to the number of original electrons, i.e. proportional to particle energies. 4π proportional counters were initially operated at atmospheric pressure. Therefore, they are also called "gas flow proportional counter". These counters are filled with methane gas which flows through the counter at atmospheric pressure. The counters have

two plateaus: at the lower voltage for α-particles and at higher voltage both for α- and β-particles. The energetic β-particles deposit only a small fraction of their energies in the counter sensitivity volume. The counters do not give any information concerning the particle energy, but only detect events induced by the particles. High pressure was used at a later time and these counters are called "pressurized proportional counter" [110, 111].

The counters are used for X-ray and Auger-electron detection in electron capture nuclide measurements. The pulse height is truly proportional to the energy deposited. These counters are operated under different pressures; they maintain a constant pressure over a long period of measurement. They have small absorption of X- or γ-rays in the walls of the counter. Although a 4π counter detects all the ionizing radiation emitted from the source, the major problem associated with 4π-counting is source self-absorption of radiation (and on a small scale the absorption of radiation by the source-mount). The precise evaluation of absorption by the source and source-mount is difficult. Therefore, one should aim to reduce the absorption to as small an amount as possible. The way of reducing source self-absorption is obviously to improve the source preparation technique. One of the methods of source preparation is to evaporate a liquid drop on the source mount. If the area of the source can be kept constant, reduction of the solid content (inactive carrier content) of the drop will reduce the source self-absorption and an extrapolation to zero source weight may be made to determine the activity for zero absorption. However, it is found that evaporation produces aggregates of crystals. Other source preparation techniques, such as using wetting agents like Ludox (colloidal silica) [112], Catanac [113] and aluminum treatment [114] have been investigated. These wetting agents act as nucleating agents in the crystallization process and produce a large number of small source crystals. The use of VYNS thin film [90] of a superficial density of $5 - 20\ \mu gm/cm^2$ reduces the absorption of radiation in the source mount to a negligible level, although, for the work of the greatest precision and particularly that with the weaker β-emitters, the absorption loss in the source mount still needs to be accurately evaluated and corrected. The use of very thin films is nevertheless still of considerable advantage, since the magnitude of the correction is reduced, and the final disinte-

gration rate value is less sensitive to the errors in the correction. Despite these improvements in the source and source-mount preparation, the absorption was still of great concern. It was desirable to develop a new direct measurement technique. The $4\pi\beta(LS) - \gamma$ coincidence counting technique was then developed to overcome this problem.

2.2.2 Gamma-ray detection

Before considering the $4\pi\beta - \gamma$ coincidence counting, let us review the detection of γ-rays. In 1948, Hofstadter [115] first reported the detection of γ-rays using a sodium iodide crystal to which a trace of thallium iodide had been added in the melt. The crystal produced an exceptionally large scintillation light output compared with the organic materials that had previously received primary attention. This discovery, more than any others, started the modern era of scintillation spectrometry of gamma radiation. This crystalline scintillator remained for almost 20 years the most important for gamma ray spectrometry. The most extraordinary property of NaI(Tl) is its excellent light yield, giving high detection efficiency for X- and γ-rays. The scintillation counter has always been at a basic disadvantage in comparison with the other methods of primary charged particles. Its resolution has kept it in the role of an energy sensitive detector rather than spectrometer. Even the gas proportional counter is capable of approximately four times better resolution than the scintillation counter (500 eV per photoelectron versus 30 eV per ion pair, where the relative resolution is proportional to $(signal)^{-1/2}$) [116]. Nowadays, scintillation detectors are not considered as high-resolution instruments, although they are still widely used for applications that need simplicity of use rather than high energy resolution. However, their high detection efficiency provides great merit for their use in coincidence measurements. We used NaI (Tl) in our coincidence counting systems in this project. In 1949, MacKay first reported the detection of α-particles in the vicinity of the depletion layer of a reverse-biased germanium point-contact diode [117]. However, it was not until 1956, when Mayer and Gossick published results of a study on germanium surface-barrier detectors of a few square millimeters that the development of broad area junction detectors began [118].

The first gold-silicon surface-barrier diode detector was described by Davis [119] in 1958. Since then, silicon has been used almost exclusively for charged particle detectors, because high resolution can be obtained at room temperature. Unfortunately, the low atomic number of silicon (Z = 14) makes such detectors unsuitable for γ-ray spectroscopy. In 1962, the advent of lithium-ion drift compensates germanium (Z = 32) technique [120] overcame this problem. In 1965, Tavendale [121] developed the large volume, high sensitivity coaxial Ge(Li) detector. The Ge(Li) detector became commercially available in the early 1960s and served as the common type of large volume germanium detector for two decades. In 1970, very high purity germanium containing $\sim 10^{10}$ electrical impurities per cm^3 was successfully grown by Hall [122]. The widespread availability of high purity germanium in the early 1980s provided an alternative to Ge(Li) and manufacturers have now discontinued production of Ge(Li) detectors in favor of the HPGe type. A major reason for this evolution is the much greater operational convenience afforded by HPGe detectors. Whereas Ge(Li) detectors must be continuously maintained at low temperature, HPGe detectors can be allowed to warm to room temperature between uses. In general, the important performance characteristics, such as detection efficiency and energy resolution, are essentially identical for Ge(Li) and HPGe detectors of the same size. Current development in γ-ray spectrometry no longer focuses on increasing the energy resolution of a system. Instead, they pursue higher throughputs of signal and higher detection efficiency. High signal throughput is achieved by the improvement of electronic equipment. Higher efficiency is achieved by growing large crystals and improving source detection configurations. While an HPGe detector has been used almost exclusively for γ-ray spectroscopy, it still suffers from limitations in the detection efficiency and the requirement of cooling for optimum resolution. A detailed review of the development of Ge detectors was given by Alexiev et al.[123].

2.2.3 The development of $4\pi\beta - \gamma$ coincidence counting

2.2.3.1 Coincidence counting

The coincidence method can be applied to events where the radioactive substance emits several coherent rays in the same disintegration process simultaneously, or in cascades. In their experiment, Geiger and Werner[124] in 1924 demonstrated that, with two observers, each using a low-power microscope to record the scintillation resulting from α-particles striking a ZnS(Ag) screen, the efficiency of each of the observers could be determined by the number of counts recorded by each observer, as well as the number of events which were coincident. This was considered as the earliest known application of coincidence counting.

In the late 1920s, electronic components for coincidence were developed [125, 126, 127]. This resulted almost immediately in the widespread use of coincidence counting in cosmic ray measurements. These measurements were chiefly concerned with the responses of separate Geiger counters to particles and were not associated with the measurement of radioactivity. For example, in Bothe and Bayer's arrangement [128], the source was placed inside the anode of a G-M counter for detecting the first particle, and this counter was surrounded by a ring of counters connected in parallel, forming the second counter of the coincidence equipment for detecting second particles. The solid angle subtended from source to counter for both rays was practically equal to 4π.

In 1940, the coincidence method was first applied to the direct measurements of radioactivity by Dunworth [129]. The possible errors due to the angular correlation of coherent rays, gamma-gamma coincidences in the beta-gamma coincidence method, scattered gamma-rays, fluctuation of the resolving time and fluctuations of the background were reviewed by Barnothy and Forro [130]. Subsequently, the $\beta - \gamma$ coincidence method, independent of detection efficiency, became a powerful technique for simple $\beta - \gamma$ emitting radionuclides provided that either the β-counter or the γ-counter was equally sensitive to all parts of the source [131]. This could be achieved by careful choice of detectors and preparation of uniform sources. Putman [131] later suggested that the uniformity of specific activity is not a necessary condition, but at least one detector should have the uniform sensitivity over the entire source. This condition

is closely approximated in practice for the γ-detector. The $\beta - \gamma$ coincidence method was particularly useful for determining the self-absorption correction in $4\pi\beta$ counting and for determining the efficiency of radiation detectors.

In principle, the coincidence method may be applied to any known decay scheme. However, the convenience and accuracy of the method decreases rapidly as the complexity of the decay scheme increases [132]. For these reasons, in the early days, the coincidence method was generally only used for measuring radionuclides that disintegrate with the emission of a single β-particle followed virtually immediately by one or more γ-rays. In practice, there are a number of corrections that need to be applied, such as those for source size, angular correlation, internal conversion, and dead-time, sensitivity of the β-detector to γ-photons, accidental coincidences and background fluctuations.

2.2.3.2 $4\pi\beta - \gamma$ coincidence counting

The $4\pi\beta - \gamma$ coincidence counting method is an improvement of the ordinary $\beta - \gamma$ coincidence method. The first and well-known paper which described the $4\pi\beta - \gamma$ coincidence counting was written by Campion [133]. Campion demonstrated that by using beta detector which has 4π geometry (high β- detection efficiency) for the coincidence method, most of these corrections are small and hence the accurate measurement of $\beta - \gamma$ emitting nuclides can be achieved. A block diagram of Campion's $4\pi\beta - \gamma$ coincidence counting system is presented in Fig. 2.2 (Reproduced from reference [133]).

The $4\pi\beta - \gamma$ coincidence counting technique can be also used for the measurements of electron capture nuclides, where the measured beta efficiency is that of the Auger electrons and X-rays associated with the electron capture process. The original $4\pi\beta - \gamma$ coincidence counting and its extended method have been used extensively for the standardization of a wide range of radionuclides [134]. The conventional $4\pi\beta - \gamma$ coincidence equation, $N_0 = \left(N_\beta \cdot N_\gamma\right) / N_c$ applies to a point source with a simple decay scheme (a single β emission followed by one or more γ-rays). N_β, N_γ, and N_c are the count rates measured by the β-detector, γ-detector, and coincidence recorder, and N_0 is the disintegration rate. The beta detector

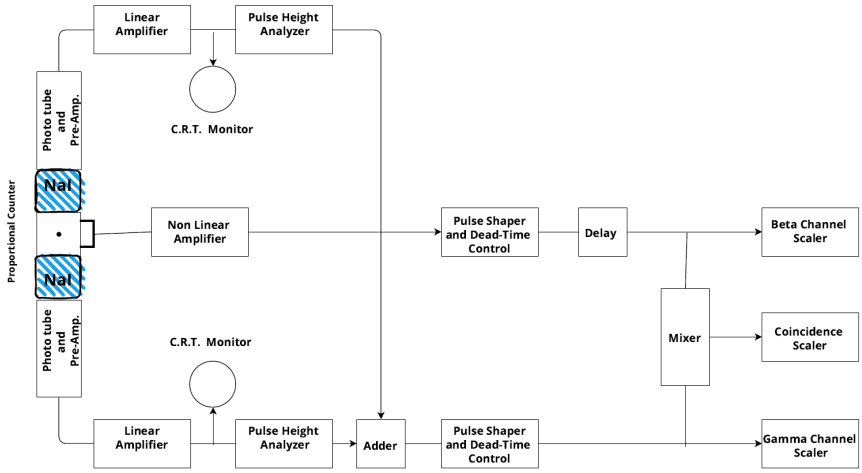

Figure 2.2: Block diagram of Campion's $4\pi\beta - \gamma$ coincidence counting system.

is assumed to respond only to β-particles, the γ-detector only to γ-rays and the coincidence recorder only to simultaneous pulses from the two detectors (true coincidences).

In any practical system, however, at least one of the detectors, usually the β-detector, is not exclusively sensitive to one type of radiation, i.e. β-particles only, but to γ-rays and conversion electrons as well. Therefore, the more general and sophisticated coincidence equation [135] has been developed and can be expressed as $\left(N_\beta \cdot N_\gamma\right) / N_c = N_0 \left[1 + K\right]$, where K is the decay-scheme-dependent correction factor, which corrects the influences of those unwanted radiations, including the γ-sensitivity of the β-detector, the detection of internal conversion electrons and different β-branches.

2.2.3.2.1 $4\pi\beta - \gamma$ coincidence extrapolation method

To eliminate these influences, the most practical technique is the $4\pi\beta - \gamma$ coincidence extrapolation method [136, 135, 137, 138]. This method requires no knowledge of the decay scheme parameters and detection efficiency, but only the observed count rate. It has proven to be the most accurate method for activity determination. However, to be able to achieve the highest accuracy with the method, the highest attainable beta detection efficiency needs to be more than 90% so that the extrapolation range can be made as short as possible. Repeating measurements under different experimental conditions is required. With the efficiency extrapolation method, a source is measured with various β-particle detection efficiencies. The apparent disintegration rate $\left(N_\beta \cdot N_\gamma\right)/N_c$ is plotted against $\left(1-\epsilon_\beta\right)/\epsilon_\beta$. Extrapolation of $\left(N_\beta \cdot N_\gamma\right)/N_c$ to $\epsilon_\beta = 1$ yields the 4π beta count rate to be $N_0 = N_\beta$ and the slope to be the correction. The relationship between the apparent disintegration rate and $\left(1-\epsilon_\beta\right)/\epsilon_\beta$ is often referred to as the efficiency function. The efficiency extrapolation method is based on the assumption that all the β-branches are subject to the same physical condition which causes the counting losses, so the inefficiencies of the various β-branches have a linear relationship. The extrapolation method eliminates the influence of conversion electrons and gamma sensitivity of the β detector. Experimentally, β-particle detection efficiencies can be varied by

1. Changing source self-absorption,

2. Adding thin absorbers, and

3. Adjust electronic discrimination levels.

Methods (2) and (3) are commonly used. Method (3) is used when the $4\pi\beta$-counter is pressurized. The three acceptable methods of efficiency variation are not theoretically equivalent [135], although experimentally the differences are insignificant [139]. The efficiency extrapolation method was first used by Steyn and Haasbroek [140] and subsequently developed by Campion et. al. [134] Taylor [141], Taylor and Merritt [142], Williams and Campion [136]. The method is now widely used for the measurements of radionuclides with complex decay schemes.

2.2.3.2.2 Theoretical correction

The decay-scheme-dependent correction K can be also derived theoretically by consideration and calculation of all elementary processes in the source, although some parameters in general have still to be determined experimentally. This method requires knowledge of decay scheme parameters and subsidiary information on some detector efficiencies. This method is based on a single measurement and has advantage of avoiding lengthy measurement procedures. When beta efficiency is low, for example, in the case of measuring a thick source, this becomes the only method to be adopted. For the correction K, γ-sensitivity and ϵ_{β_γ} of the β-detector is the most difficult parameter to determine. The original method given by Campion [133] for determining ϵ_{β_γ} was to count sources of known activity covered with absorbers, usually polyethylene, thick enough to absorb all the β-particles, and it was assumed that all the counts observed in the β-detector were due to the γ-sensitivity of the β-detector. Campion measured ^{141}Ce,^{203}Hg,^{95}Nb and ^{60}Co. ϵ_{β_γ} versus γ-ray energy was plotted. ϵ_{β_γ} was found to be in the range of approximately $0.3 - 1.1\%$ for an energy from about 200 keV to 1332 keV. However, the thickness of the absorbers required to stop all the β-particles is so large that the γ-ray interactions in the foils cannot be neglected and much higher results are obtained due to photoelectron and Compton electrons ejected into the gas from the foils. It is difficult to separate this effect from the inherent γ-ray sensitivity of the detector.

In order to overcome this problem, Williams and Campion [136] used the $4\pi\beta - \gamma$ coincidence counting efficiency extrapolation method to obtain much more accurate values of ϵ_{β_γ} as a function of γ-ray energy. With this method, ϵ_{β_γ} was obtained from the slope of the extrapolation function. A function of ϵ_{β_γ} versus γ-ray energy was plotted by measuring $^{51}Cr(E_\gamma$ = 320 keV), ^{95}Nb (765 keV), ^{54}Mn (835 keV), ^{60}Co (1332 keV) and ^{88}Y (1836 keV). ϵ_{β_γ} was found to be in the range of approximately $0.1 - 0.5\%$ for the energy about 320 keV – 1836 keV.

The accuracy of this method was later confirmed by Merrit and Taylor [143] . The method may offer much improved results compared with the original absorber method, but the use of thin absorbers to vary beta efficiency may still cause unexpected photon interactions in the absorption

foils. The range of absorber thicknesses (and hence efficiencies) that can be used is limited by the requirement that they stop a negligible number of γ-rays; otherwise the secondary electrons produced will increase the apparent ϵ_{β_γ}. The detection efficiency for conversion electrons may be reduced if considerably thick absorbers are used.

Kawada [144, 145] developed a method in which the β-efficiency was varied by changing the counter geometry from 4π to 2π, using the top- and bottom-halves of the 4π counter. The results were found to be similar to those of Williams and Campion, and Merritt and Taylor. Since this method requires no additional absorber foil and the measurements can be made without changing any physical parameter, precise results can be expected. However, this method requires modification of the instrument. There is an additional contribution to the coincidence counting rate, which arises from Compton scattering or, in more complex decay schemes, from the presence of other cascade γ-rays ($\gamma - \gamma$ coincidences). This effect can be reduced to negligible levels by appropriate energy discrimination in the γ-channel (setting a window for the γ-photopeak).

Regarding the detection efficiency of the β-counter for conversion electrons in a thin source, the efficiency for energetic conversion electrons is taken as unity in $4\pi\beta$ counter geometry [133] unless they are of extremely low energy (< 50 keV). However, for conversion electron efficiency less than unity, the event may still be recordable by detection of X-rays or Auger electrons. Perolat [146] pointed out that the accuracy of the two methods, extrapolation, and correction, are more or less equal for the simple $\beta - \gamma$ decay scheme radionuclides (e.g. ^{60}Co,^{46}Sc,^{56}Mn and ^{95}Nb). For complex decay schemes, the best accuracy are obtained by the extrapolation method (e.g.^{133}Ba,^{195}Au,$^{106}Ru - Rh$). Nevertheless, in many cases, the theoretical correction method can provide satisfactory accuracy, although it may not be as good as the extrapolation method. Some examples of using the theoretical correction method are the measurement of ^{65}Zn,^{99}Mo, and ^{59}Fe.

2.2.3.2.3 $4\pi\beta - \gamma$ coincidence efficiency-tracing technique

The $4\pi\beta - \gamma$ coincidence counting technique has been also extended to pure β-emitters by addition of suitable $\beta - \gamma$ emitters as the tracer of the

counting efficiency, the so-called efficiency-tracing technique [134, 147, 148, 149]. The method involves combining into a single counting source the pure β-emitter and an accurately known fraction of a $\beta - \gamma$ emitting "tracer". This has been achieved by (1) combining atoms of the two different nuclides into the one molecule [134], and (2) quantitatively mixing a solution of the pure β-emitter with a solution of the tracer [134]. The tracer must have a simple decay scheme which is "not-too-dissimilar" to that of the pure β-emitter. The total count rate of the mixture is found by extrapolating to 100% efficiency. The activity concentration of the nuclide being traced is obtained by subtracting the count rate due to the tracer. In fact, the tracer is used to determine the β-detection efficiency of the source. Ideally the shape and endpoint of the beta spectra of the pure β-emitter and the tracer nuclide should be the same. However, in practice this is often difficult to achieve. The effects of the shape of the beta spectra of $\beta - \gamma$ tracers and pure β-emitters are recognized, and accepted, though not without reservations [150].

The spectrum effect was investigated by Lowenthal [149]. It was found that measurements made with different $\beta - \gamma$ tracers resulted in different results on extrapolation due to the shapes of the beta spectra affecting the efficiency tracing function. If the low energy ends of the spectra are similar in shape and their end-point energies do not differ too much from each other the uncertainties are negligibly small. If the shapes of the two spectra are similar but the difference between the end-point energies is large, the uncertainties are greater. The effect could be even more serious when the shapes of low-energy sections of the spectra differ markedly. However, the study shows that there is a linear relationship of counting efficiencies among many β-emitters when homogeneously mixed. In order to avoid any differential effects due to separation of the two activities during crystallization as the source is dried, it is necessary to incorporate the two activities into the same chemical compound.^{82}Br, ^{24}Na, ^{177}Lu, ^{60}Co, and ^{134}Cs have been used as tracers [134].

2.2.3.2.4 Some additional points about $4\pi\beta - \gamma$ coincidence system

In order to maintain the linear functional relations between the inefficiency of different beta branch particles, the β-detection must be arranged

so that 1) beta efficiencies for all branches must be single-valued functions of the variable efficiency parameter N_c/N_γ , and 2) the relating functions must approach to unit detection efficiency for all branches simultaneously [135]. This requires that the β-detection geometry be 4π steradians. The source mounting arrangement, even in a 4π gas proportional counter, can reduce the effective geometry [147]. In addition, the counter should be sensitive to 25 ion pairs or less (i.e. $<$ 1 keV equivalent energy). An adequate approximate measure of the sensitivity can be obtained using a low Z electron capture source. A 4π proportional counter must be also sufficiently sensitive to high β-energies, since linear energy transfer for β-particles decreases with increasing energy up to about 1 MeV and the number of ion pairs generated in a practical counter at atmospheric pressure may not exceed 100 for energetic particles. The 4π proportional counter is usually made of aluminum, and is of the pill-box type, with a sensitive volume 3.8 - 5.9 cm in diameter and 5.1 - 7.8 cm in height. It has zero intrinsic noise, low sensitivity to γ-radiation and a recovery time of the order of 100 ns. Sodium iodide NaI(Tl) scintillation counters are currently the most satisfactory for the γ-detection, providing generally adequate energy resolution. Some laboratories have shown interest in the HPGe detector which provides much better resolution. $LaCl_3$ and $LaBr_3$ detectors have high efficiency and high resolution and could be promising alternatives for γ-detection in $4\pi\beta - \gamma$ coincidence counting.

2.2.3.3 Digital coincidence counting and other studies

The principles of the $4\pi\beta - \gamma$ coincidence counting method, as well as the nature of the corrections required, are well understood. However, valid application of these principles to actual measurements is not simple and efforts on the improvement of the accuracy of $4\pi\beta - \gamma$ coincidence counting have continued for decades. The accurate fulfillment of the linearity conditions of the gamma-ray channel was examined by Grigorescu [151] and was found to be crucial for elimination of the error from source self-absorption and the error due to absorption in source mount. Having investigated ^{59}Fe and ^{134}Cs, Miyahara and Watanabe [152] found that to obtain the highest beta efficiency, the crystallites in the $4\pi\beta$ source must be as small and uniform as possible. In the extrapolation method, a linear

function is usually used as the efficiency function, a polynomial function of second or third order is used occasionally. However, if the attainable beta efficiency is not high enough, the first-order fitting function may introduce systematic errors. This problem can be overcome by fitting a polynomial function joining both first and second order terms [153].

Other developments in the coincidence technique include replacing the 4π proportional counter with the surface barrier silicon detector for $\alpha - \gamma$ emitters [154] and using NaI crystal detectors to perform $\gamma - \gamma$ coincidence counting for a nuclide emitting two γ-rays in cascade [155, 156]. With the $\gamma - \gamma$ coincidence technique the activity is computed from the area A_1 and A_2 of the gamma photopeaks, the area A_{12} of the sum-peak, and an extrapolation of the total count-rate to zero discrimination. The coincidence equation for this technique is $N = (A_1\ A_2)\,/\,A_{12} + T$, where N is the activity of the source and T is the area under the whole spectrum. This method has been used to directly measure the activity of ^{125}I [157]. For decades, the conventional methods of data acquisition for the $4\pi\beta - \gamma$ coincidence counting technique have used dedicated analogue electronic modules such as single channel analyzers, gate and delay generators, paralysis units, time-to-amplitude converters, coincidence mixers and multichannel analyzers. The high cost of procurement and maintenance of such systems and the considerable equipment setup effort have emphasized the need for a more flexible and robust data collection process. Digital coincidence counting is a promising new approach to the absolute measurement of radioactivity. Buckman and Ius published the first paper [158, 159] introducing a digital coincidence counting system into $4\pi\beta - \gamma$ coincidence counting. The paper described a digital coincidence-counting system which comprises a customer-built data acquisition card and associated PC software. Using high-speed analogue-to-digital converters (ADCs), the pulse-trains from two radiation detectors are digitized and recorded. Processing of the pulse-trains is performed by a series of software components. The method has the advantage that once a set of pulse-trains has been recorded, it may be processed any number of times by a variety of methods. It avoids the complex and time-consuming set up procedures of a conventional analogue system. The software of the system was improved afterwards, and the system was verified with the ^{60}Co, ^{22}Na and ^{153}Sm, good results have been achieved. [160, 161].

Chapter 3

Liquid scintillation methods

3.1 Introduction

Liquid scintillation counting (LSC) techniques can be used for radionuclide activity measurement when the calculation of detection efficiency is possible or through comparison with a standard. Unlike most other radioactivity measurements, the source itself is a part of the detector and if a precise measurement is needed, standard must have a similar composition as that of the sources to measure. If a standard is not available, the detection efficiency can be calculated with special computing codes using a model of the physic-chemical and statistical processes involved in light emission, detection and counting. This model is referred to in the literature as the free parameter model, which quantifies the mean value of photoelectrons created in each photomultiplier tube after the absorption of unit energy in the scintillator. This model can be applied in two ways: by deducing the free parameter from the measurement of a tracer (CIEMAT/NIST method) [162] or by calculating this free parameter from the coincidence ratio in a specific LS counter with 3 photomultipliers tubes (TDCR method)[163].

There is a growing interest in LSC techniques in the field of radionuclide metrology, especially after the development of two quantitative LSC measurement methods: the Triple-to-Double-Coincidence Ratio (TDCR) method in 1979 [164], and the CIEMAT/NIST method [162]. These two

powerful methods based on liquid scintillation counting are generally used to measure pure beta-emitting radionuclides and have been used successfully in LS counting being established as calibration procedures for the activity measurements of a number of radionuclides [165, 166, 167]. Both methods require an accurate computation of the emission spectrum as well as the ionization quenching function to account for the non-linear energy response of the scintillation mechanism [166].

The earliest known application of coincidence counting was that, with two observers, the efficiency of each of the observers could be determined by the number of counts recorded by each one, as well as the number of events which were coincident. Later, electronic components for coincidence were developed. This resulted almost immediately in the widespread use of coincidence counting. In principle, the coincidence method may be applied to any known decay scheme [168]. Both CIEMAT/NIST and TDCR methods are counting in coincidence. In the coincidence method using liquid scintillation technique an electronic circuit receives the pulses from two or three PMTs facing the scintillator. It provides an output pulse each time the input pulses are coincident in time. Except for chance coincidences, the random noise pulses from each photomultiplier will consequently not be counted, even if they have larger amplitude than the scintillation pulses. In order to obtain a coincidence pulse, at least one photoelectron must be emitted from each photocathode [169]. It is well known that scintillation counters with two or three photomultipliers working in coincidence drastically reduce the contribution of the thermionic noise coming from the photomultipliers [170].

3.1.1 The CIEMAT/NIST method

This method, originally developed by the Centro de Investigaciones Energeticas Medioambientalesy Technologicas (CIEMAT, Spain) and the National Institute of Standards and Technology (NIST, U.S.A.) is an activity measurement method, suitable for activity determination of pure beta, beta-gamma, pure electron capture (EC) and EC-gamma decaying radionuclides using a commercial liquid scintillation analyzer [85]. The method is based on a combination of theoretical calculations related to the particular radionuclide under investigation and its emissions, as well

as theoretical calculations related to a standard tracer nuclide and its emissions together with experimental data which provides information concerning the instrument, scintillation cocktail, and radionuclide (e.g., count rate and quench indicating parameter) [162]. The main steps of the CIEMAT/NIST method are reported in Fig. 3.1 [171].

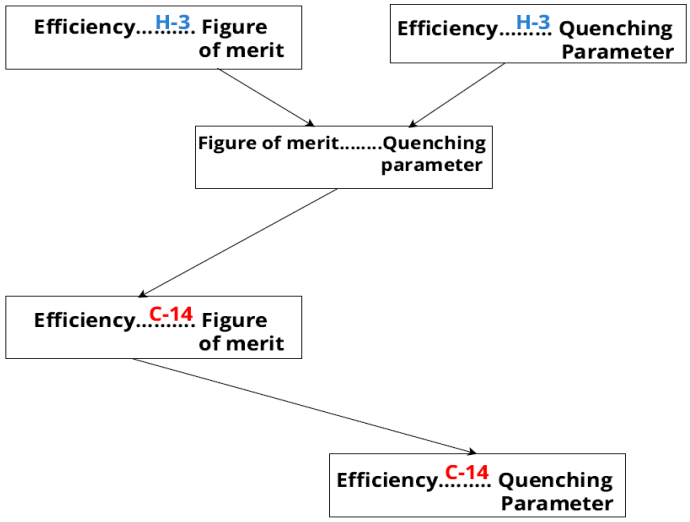

Figure 3.1: Diagram describing the application of the CIEMAT/NIST method to the standardization of ^{14}C.

The CIEMAT/NIST method originated in 1982, when Grau Malonda and García-Toraño [162] presented a method for the calculation of counting efficiency for β-ray emitting radionuclides in two- phototubes system. The authors used a set of tritium standards to obtain an experimental quenching curve, from which the β-particle counting efficiency was calculated. A quench standard curve contains a series of standards with constant absolute radioactivity and varied amounts of quench. The quench is increased from vial to vial by the addition of a quenching agent. For fundamental reasons related to the physical models used in the CIEMAT/NIST method, a low-energy tracer with a calculable spectrum is needed and up to now no alternative radionuclide with a longer half-

life is found [172]. Tritium is usually used as tracer nuclide because of its low β-particle energy ($E_{max} = 18.6$ keV), which makes the corresponding counting efficiency very sensitive to the quench parameter. Due to the very low energy, the uncertainty in tritium standard has little influence on the calculated efficiency of the more energetic β-ray emitters [173].

The method requires one to know the experimental counting efficiency of the tracer radionuclide for different degrees of chemical quench and to compute the theoretical counting efficiency at the photocathode output for different values of the free parameter M (this is defined as the amount of energy required to produce one photoelectron at the photocathode of the photomultiplier) [171]. To obtain a universal curve, which allows one to determine the counting efficiency for any radionuclide, a model for the counting efficiency as a function of the free parameter must be developed for each radionuclide. Although CIEMAT/NIST method is not a direct activity measurement method, it allows relative standard uncertainties of less than 2% to be achieved even for low energy β-emitters.

The central idea of the method consists of taking an experimental curve, counting efficiency versus quench parameter, and calculating the theoretical counting efficiency in terms of the free parameter of a given tracer radionuclide. Since both curves have in common the counting efficiency, the universal relationship between the experimental quench parameter and the theoretical free parameter can be obtained. This curve is universal in the sense that it is independent of the radionuclide but depends only on the liquid scintillation spectrometer, the vial and the liquid scintillator used. The next step is to compute the counting efficiency for the radionuclide to be standardized by applying the universal curve and taking the free parameter as a common quantity [170].

Different techniques for efficiency correction due to the quenching may be used. Among others, quench monitoring using an external standard has several advantages, being a fast and non-destructive method, allows simultaneous color measurement and works equally well for low activity samples. The external standardization correction procedure involves many methods sharing the property of using a γ-ray emitting source which may be mechanically positioned externally next to the sample counting vial. One method used to measure quench is the transformed Spectral Index of the External Standard (t-SIE). This t-SIE is cal-

culated from the Compton spectrum induced in the scintillation cocktail by an external ^{133}Ba gamma source which is positioned under the sample vial. From a mathematical transformation of this spectrum, the t-SIE value is determined, and t-SIE is a relative value, on a scale from 0 (most quenched) to 1000 (unquenched). The t-SIE parameter is independent of the sample radionuclide and of the activity in the vial and has a large dynamic range. This makes it a very reproducible means of tracking the quench of the cocktail. The t-SIE parameter is independent of the counting rate or the total accumulated counts. The t-SIE value for each sample is given directly by the liquid scintillation counter [170]. Special programs are available for the detection efficiency computation for the β-decay radionuclides. One of these is the CN2004 code with composition matched LS cocktails of a ^3H standard as the efficiency detection monitor [174].

3.1.2 The development of TDCR method

Triple-to-Double Coincidence Ratio (TDCR) method is a primary measurement method allowing the standardization of radionuclides by liquid scintillation counting when the detection efficiency is calculated from a physical and statistical model of the photon distribution emitted by the scintillating source [175, 163]. The TDCR method is widely used within the international radionuclide metrology community and was primarily developed as an absolute method for the activity measurement and standardization of beta emitting radionuclides [176].

The TDCR method does rely on decay scheme parameters to calculate the two- and three-phototube efficiencies. The advent of phototubes with high quantum efficiencies has permitted the practical application of this system. The TDCR method has become the preferred method for the absolute activity measurement of α- and β-emitters and has been extended to electron capture radionuclides and $\beta - \gamma$-emitters.

Broda from POLATOM has given an excellent review on the development of TDCR method [177]. An overview of his paper is presented as follows. The first three-phototube system Fig. 3.2a was constructed by Hoegl and Schwerdtel [178]. However, this system was used for relative measurements of pure β-emitters [179, 180]. In their experiment, the counting efficiency ϕ, was determined using a set of quenched standards.

Counting rates of the triple (N_T) and double (N_{ab}) coincidences were measured between three phototubes and a simple pair of phototubes, respectively. The experimental ratio was calculated. The function $\phi(K)$ was used to determine the activity of the measured sample.

In 1970, Kolarov et al. suggested an absolute method of determining the activity of β-emitters based on a simple detection efficiency model using two phototubes working in sum and in coincidence [181]. The major disadvantages of this method were the effect of afterpulses and thermal emission noise observed in the sum channel. The above triple coincidence LS detector and the principle of the detection efficiency model have both been the basis of the TDCR absolute method of radionuclide activity determination. The original version of the TDCR method was presented by Pochwalski and Radoszewski in 1979 [182]. In Pochwalski's system Fig. 3.2b (Reproduced from reference [177]), the outputs of three double coincidence gates (N_T) and the sum of double coincidences (N_D) (including the triple coincidences) were obtained. Note that they are different from Schwerdtel's system. The experimentally determined TDCR value, denoted by K, is given by $K = N_T/N_D$ obviously $0 \leq K \leq 1$, since the triple coincidence counting rate N_T, is always lower than the double coincidence-counting rate N_D. As the counting efficiency approaches unity, the double- and triple- coincidence counting rates will approach the disintegration rate of the source $N_T \rightarrow N_0$, $N_D \rightarrow N_0$ and the ratio K will also approach unity $K \rightarrow 1$. By extrapolating to $K \rightarrow 1$, the values of the disintegration rate, N_D can be calculated. Thus, the ratio K was found to be a very convenient experimental indicator of the counting efficiency of a given sample. In order to obtain series of pairs of count rates N_T and N_D, the efficiencies were varied by changing the optical efficiency or quenching state. Pochwalski placed a cylindrical steel wire spring around the counting vial. The number of coils appearing between the vial and photocathodes changed with the pressure applied on the spring and hence the optical efficiency of the phototubes varied.

The principle of the detection efficiency model applied to the TDCR method is based on the detection efficiency model for the two phototubes system elaborated by Kolarov et al [181]. Theoretical calculations of counting efficiency and the comparison with the experimental data for pure β-emitters for TDCR method using this model were first reported

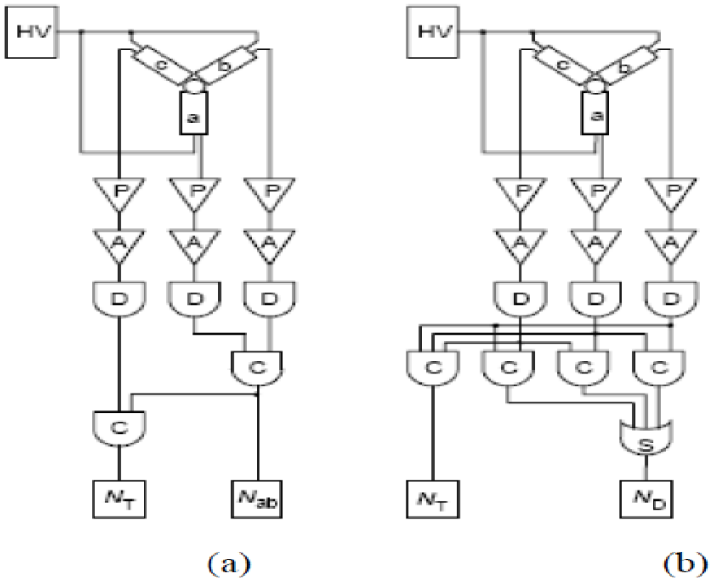

Figure 3.2: A simplified block-diagram of the three-phototube system. (a) Schwerdtel's system, (b) Pochwalski's system. HV - high voltage, P - preamplifier, A - amplifier, D - discriminator, C - coincidence gate (AND), S - summing gate (OR), N - counter.

by Broda et al [183]. This model assumed that the three phototubes had the same quantum efficiency.

In the early 1990s, the electronics of the TDCR system was modified to introduce three additional double coincidence counting outputs N_{ab}, N_{bc} and N_{ac} [184, 176, 185] in addition to the two shown in Fig. 3.2b. In this enhanced system, the electronic coincidence unit gave five outputs: three double coincidences, AB, BC and CA, one triple coincidence ABC

and a logic sum of the three double coincidences including triple coincidences, $AB + BC + CA$, as shown in Fig. 3.3 (reproduced from reference [185]). An extendable dead-time generator was incorporated in the electronic system. This type of dead-time eliminates spurious pulses caused by either phosphorescence or the residual gas in the phototube. With this system, four equations, written as below, with counting efficiencies (ϕ_{ab}, ϕ_{bc}, ϕ_{ac} *and* ϕ_T) from four coincidence channels, could be established, and the activity N_0 could be determined.

$$N_{ab} = N_0 \, \phi_{ab} \left(\varepsilon_a, \varepsilon_b \right), \tag{3.1}$$

$$N_{bc} = N_0 \, \phi_{bc} \left(\varepsilon_b, \varepsilon_c \right), \tag{3.2}$$

$$N_{ac} = N_0 \, \phi_{ac} \left(\varepsilon_a, \varepsilon_c \right), \tag{3.3}$$

$$N_T = N_0 \, \phi_T \left(\varepsilon_a, \varepsilon_b, \varepsilon_c \right), \tag{3.4}$$

In this way, the efficiencies of the individual phototubes, $\varepsilon_a, \varepsilon_b$, and ε_c, are directly determined. Thus, the assumption of symmetrical behavior of the three phototubes is no longer necessary. In fact, the real asymmetry can only be ignored for high counting efficiency. Errors introduced by the symmetry simplification increase when the efficiency decreases [186].

The TDCR parameter, being a ratio of T to D, is a convenient indicator of the quenching of the source[187]. Knowing the radionuclide energy spectrum, the model is applied to calculate the number of photons emitted by the scintillator and leading to the detection of photoelectrons in each photomultiplier. The best estimate of the source activity is the ratio of the count rate in double coincidences to the efficiency in double coincidence, which must be also equal to the ratio of the counting rate in triple coincidence to the detection efficiency in triple coincidence.

In the late 1990s, an electronic module MAC3 (module d'acquisition de coincidences triples) was developed to process the pulses delivered by the three phototubes[188]. This module replaces the complex interconnection of nine independent NIM electronic instruments. The module is illustrated in Fig. 3.4 (Reproduced from reference [177]).

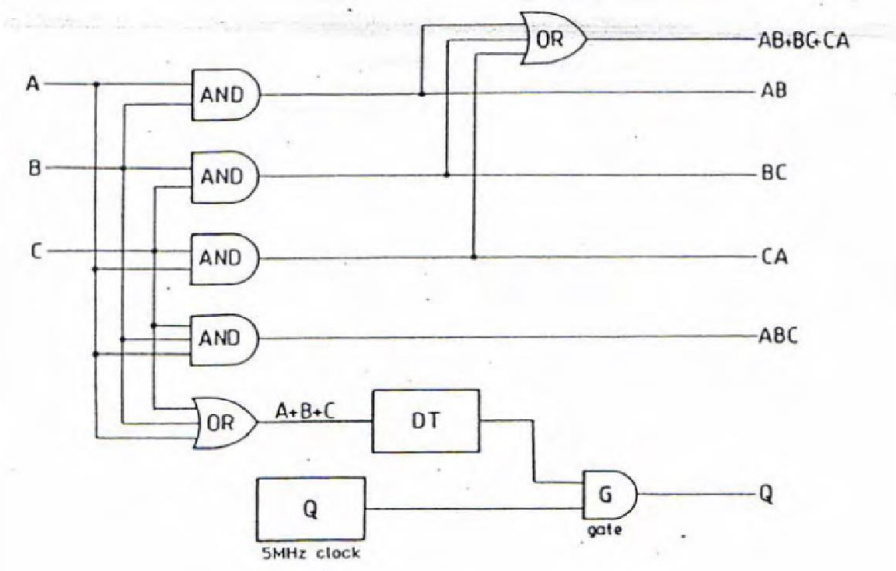

Figure 3.3: Block diagram of the TDCR coincidence unit.

In 2014, TDCR method is full digitalized at ENEA-INMRI in collaboration with CAEN. A new total digital approach was applied for processing pulses delivered by three photomultipliers in a TDCR system in which for the first time at ENEA-INMRI the CAEN digitizers belonging to the family of Desktop digitizers DT57XX were used to link directly the PMTs of home-made TDCR counters to these new front-end electronics devices. New very interesting perspectives were then opened in the TCDR acquisition and analysis by using new software codes that take into account the digitized information recorded by compact digitizer modules directly linked to the detector [189].

The TDCR device has also been applied to $4\pi\beta\,(LS) - \gamma$ coincidence counting, where the three-phototube detector is used in the beta channel and the HPGe detector in the gamma channel [190, 191]. With this ar-

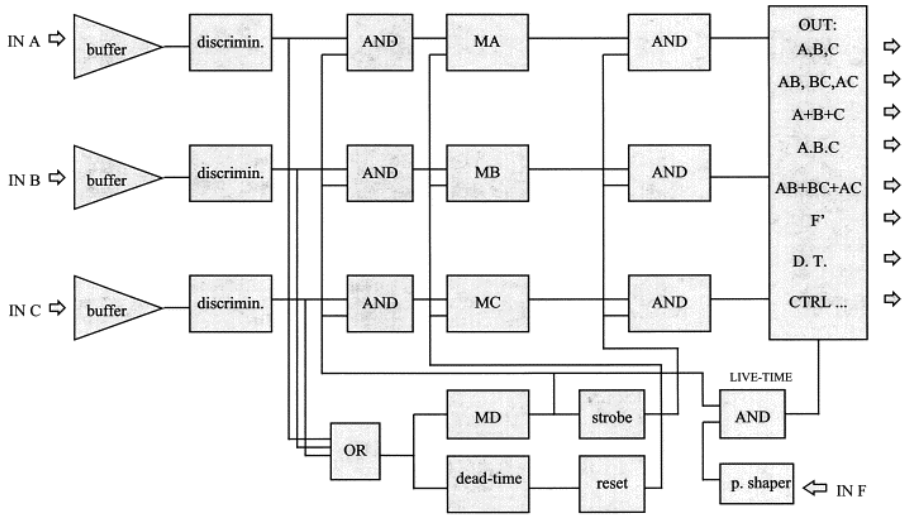

Figure 3.4: A simplified block-diagram of the MAC3 module. An incoming pulse will set memory MA, MB, and MC and, after a delay (B40 ns), will trigger the dead-time circuit. During this delay (coincidence resolving time), it is possible for additional pulses from a different channel to also be registered. After that delay, the system will not accept additional pulses until the (extendible) dead-time period has elapsed. Memories are sampled by a strobe. An arrangement of gates and buffers allows the recording of the counts in each channel.

rangement the TDCR method can be extended to a nuclide having $\beta - \gamma$ and $EC - \gamma$ decay-scheme. The system also allows a direct comparison between TDCR and the $4\pi\beta\,(LS) - \gamma$ coincidence method. Bobin and Bouchard [191] published the preliminary results of standardizing electron capture radionuclides ^{54}Mn and ^{65}Zn using the TDCR incorporated $4\pi\beta\,(LS) - \gamma$ coincidence.

A number of analysis programs have been developed and adopted for

use by several laboratories, but many laboratories have also developed their own codes in order to implement specific features or modifications of the model not found in other codes [192]. At the moment there are several TDCR analysis codes implemented especially for the case of electron capture to calculate detection efficiency and activity. Thus, the available software for TDCR counting could be, in principle, classified into pure β-emitter programs and nuclide specific programs for more complicated decay schemes [193].

A stochastic approach is investigated by implementing a comprehensive modeling of the TDCR counter based on the GEANT4 toolkit [194, 195]. This code has been selected for its capability to simulate the different processes related to the transport of charged particles and the ensuing generation of optical photons resulting from scintillation or the Cerenkov effect. One of these programs is GEANT4 code for TDCR. The program, provided [196] by LNHB - CEA, uses a Poisson statistical distribution for the number of photoelectrons generated in the cathode of PMT. The program has a small default library of input data for usual radionuclides which includes the maximum beta energy, the nature of the transition and the spectrum shape factor.

3.2 Ionization quenching

If an ionizing particle deposits energy E in a very short track length x (high dE/dx), there is a reduction in the scintillation efficiency. This loss was described by Birks [197] as "ionization quenching". Birks formulated a semi-empirical model for the rate of light output dL per unit track length dx (number of emitted photons per unit distance along the path) as following,

$$\frac{dL}{dx} = \frac{\eta_S \frac{dE}{dx}}{1 + kB\frac{dE}{dx}} \tag{3.5}$$

where, η_S is the scintillation efficiency (number of fluorescence photons emitted per unit of energy), k is the rate constant for ionization quenching, and dE/dx is the stopping power (The stopping power is defined as the average energy dissipated by the ionizing radiation per unit

path length of travel in a medium $(MeVcm^{-2}g^{-1})$ [175]). The local concentration of the core is also proportional to the ionization density, and is given by BdE/dx (the linear ionization density). The specific fluorescence in the absence of ionization quenching is:

$$\frac{dL}{dx} = \eta_S \frac{dE}{dx} \tag{3.6}$$

Therefore, $\left(1 + kB\frac{dE}{dx}\right)^{-1}$ is the reduction factor due to the ionization quench and kB is the ionization quench parameter.

The integration of equation 3.6 gives:

$$L = \eta_S \int_0^R \left(\frac{dE}{dx}\right) dx = \eta_S \int_0^E dE = \eta_S \, E \tag{3.7}$$

Therefore $\eta_S = L/E$ is the figure of merit of the scintillator when $kB(dE/dx)$ is negligible (compared with 3.5). For electrons with energy higher than 1 MeV, $dE/dx \rightarrow zero$.

When $kB(dE/dx)$ is not negligible, we have

$$L\,(E) = \eta_S \int_0^E \frac{dE}{1 + kB\frac{dE}{dx}} = \eta_S \, E \, Q\,(E) \tag{3.8}$$

where

$$Q\,(E) = \frac{1}{E} \int_0^E \frac{dE}{1 + kB\frac{dE}{dx}} \tag{3.9}$$

Thus, the figure of merit will be in this case,

$$\eta\,(E) = \frac{L\,(E)}{E} = \eta_S Q\,(E) \tag{3.10}$$

From this equation, one can see that the figure of merit is consisted of two factors: η_S, independent of the energy and $Q\,(E)$, a function of the energy but dimensionless. The energy loss in material has been calculated by many physicists, but the basic, classic derivation was due to Bloch who improved a calculation by Bethe; hence the *Bethe-Bloch* Formula [198]. The rate of energy loss is given by $(-dE/dx)$; (dE/dx) being a loss of energy, is a negative quantity. The calculation of (dE/dx) is done in such a way

as to determine the energy deposited in the medium (positive), hence the explicit negative sign for the loss of energy of the particle.

The full expression for the Bethe-Bloch formula can be written as:

$$-\left(\frac{dE}{dx}\right) = \left(\frac{e^2}{4\pi\varepsilon_0}\right)^2 \frac{4\pi N_A Z_\rho}{mc^2\beta^2 A} \left[\ln\left(\frac{mc^2\beta^2}{I}\right) - \ln\left(1-\beta^2\right) - \beta^2\right] \quad (3.11)$$

Where
c is the speed of light
mc^2 is electron rest energy (MeV)
ε_0 is vacuum permittivity
$\beta = v/c$ velocity of incident particle divided by the velocity of light
e is electron charge
Z is atomic number
I is mean excitation energy of the medium
ρ is density of the medium
A is relative atomic mass
N_A is the Avogadro number

Equation 3.8 gives the mean number of photons produced in the scintillator when an electron deposits its energy E in the liquid scintillator. It demonstrates that the dependence of the number of photons of individual scintillations upon incident electron energy E is not linear. The non-linearity increases with the mass of the particle and is a function of the LET(dE/dx) of the particle. The reason for this lack of linearity is known as ionization quenching and is related with the density of excited solvent molecules. When the concentration of these molecules is high, the interaction probability between the two excited molecules increases and the result of this interaction is that a molecule loses the excitation energy and the other one becomes super excited. A super excited molecule has a high probability to be ionized. The result is that the initial excitation energy of both the molecules is lost and a deficit of the excited energy is produced. The light output of scintillators is basically proportional to the amount of the energy deposited in the scintillator cocktail but it is known that the light output is suppressed in case of high-LET (linear energy transfer) radiation such as low-energy protons and heavy ions owing to the quenching effect.

The Birk's formula is useful for explaining the light yield of scintillators in various conditions, however Matsufuji et al. [199] pointed out that the formula cannot be applied to high LET (dE/dx) particles. This is because the Birks' formula does not consider the spatial configurations of the excited fluorescent molecules and damaged molecules explicitly, whereas the strength of energy transfer is sensitive to the distance between them.

3.3 Calculation of detection efficiency

The TDCR and CIEMAT/NIST methods are based on the free parameter model. This model assumes a statistical distribution law of the number of photons emitted by the scintillation process [163]. Both TDCR and CIEMAT/NIST methods for the calculation of the detection efficiency are based on the same statistical and physical models which occur when the ionizing particle interacts with the liquid scintillator and three assumptions are made [200]:

1. The distribution of photons emitted by a scintillator when absorbing a monoenergetic electron follows Poisson distribution;
2. The detector threshold is lower than the amplitude of the single photoelectron peak, so the detection probability of any single photon is not zero;
3. The non-linearity of the scintillation efficiency due to ionization-quenching can be described by Birks law.

It is supposed that the radioactive sample, dissolved into the liquid scintillator emits particles with energy E and each particle produces m photoelectrons at the photocathode. An assumption of the Poisson model for accounting the number of photons collected by the photocathodes of the photomultipliers is generally accepted [201]. If the emission of photoelectrons at the photocathode follows a Poisson law, the probability for obtaining exactly x photoelectrons when the expected average is m is given by the equation:

$$P(x, m) = \frac{m^x e^{-m}}{x!} \tag{3.12}$$

The photons emitted are randomly distributed within the optical chamber of the counter and can create photoelectrons in photomultiplier tubes with an overall probability of ν *(quantum efficiency)*. The resulting statistics of the number of photoelectrons, y, created is also Poisson-distributed with mean value νm.

$$P(y, \nu m) = \frac{(\nu m)^y e^{-\nu m}}{y!} \tag{3.13}$$

Experimental evidence is that the number of photons emitted is not proportional to the energy released in the LS cocktail. The detection efficiency is the detection probability, which is the complement of the non-detection probability. This second hypothesis allows one to consider that the non-detection probability is the probability to observe 0 photon, for a mean value of m. It is well known that with either the TDCR or CIEMAT/NIST method, the discrimination level has to be set just before the single photoelectron peak so that all single photoelectron pulses caused by disintegration are counted as required by the detection efficiency calculation model [202]. The distribution of photoelectrons obtained at the photocathode of a phototube is a result of three random processes: Poisson distribution for the light emission, multinomial distribution for the behavior of photons inside the optical chamber and binomial distribution for the photoelectric process at the photocathode. The counting efficiency derives directly by taking into account the formula (3.12):

$$\varepsilon = 1 - P(0) = 1 - e^{-m} \tag{3.14}$$

For a counter using three photodetectors with the same quantum efficiency ν, the detection efficiency for one PMT, 2 PMTs in coincidence, 3 PMTs in coincidence (T) and logical sum of double coincidences (D) is [203]:

Detection efficiency for 1 PMT:

$$\varepsilon_1 = 1 - e^{-\nu m/3} \tag{3.15}$$

Detection efficiency for 2 PMTs in coincidence:

$$\varepsilon_2 = \left(1 - e^{-\nu m/3}\right)^2 \tag{3.16}$$

Detection efficiency for 3 PMTs in coincidence:

$$\varepsilon_3 = \left(1 - e^{-\nu m/3}\right)^3 \tag{3.17}$$

Detection efficiency for logical sum of double coincidences:

$$\varepsilon_D = 3\left(1 - e^{-\nu m/3}\right)^2 - 2\left(1 - e^{-\nu m/3}\right)^3 \tag{3.18}$$

The above formula shows the calculated detection efficiency for the coincidence events registered in two or three phototubes for the mean number of photoelectrons produced at photocathode by monoenergetic electrons in the scintillator. A beta energy spectrum generated by a radionuclide can be described by a normalized density function $S(E)$. So, by taking into account the previous expressions, the detection efficiency of a beta particle injected in a liquid scintillator with an energy distribution $S(E)$, maximum energy E_{max} and detected by 1 PMT is thus given by:

$$\varepsilon = \int_0^{E_{max}} S(E)\left(1 - e^{-\nu m}\right) dE \tag{3.19}$$

For a system made by two photomultipliers working in coincidence and located in di-ametral position around a high reflectivity optical chamber, the detection efficiency is given by:

$$\varepsilon_2 = \int_0^{E_{max}} S(E)\left(1 - e^{-\nu m/3}\right)^2 dE \tag{3.20}$$

For a system with three-photomultiplier tube system, the detection efficiency of logical sum of double coincidence (D) is given by:

$$\varepsilon_D = \int_0^{E_{max}} S(E)\left[3\left(1 - e^{-\nu m/3}\right)^2 - 2\left(1 - e^{-\nu m/3}\right)^3\right] dE \tag{3.21}$$

and of triple coincidence (T) is given by:

$$\varepsilon_T = \int_0^{E_{max}} S(E)\left(1 - e^{-\nu m/3}\right)^3 dE \tag{3.22}$$

Taking the three previous hypothesis into account and assuming that the energy spectrum emitted by the radionuclide is described by a normalized density function $S(E)$, the ratio of the probability of the triple

coincidence divided by the probability of the double coincidence, TDCR, [204] is:

$$TDCR = \frac{\varepsilon_T}{\varepsilon_D} = \frac{\int_0^{E_{max}} S(E)\left(1-e^{-\nu m/3}\right)^3 dE}{\int_0^{E_{max}} S(E)\left[3\left(1-e^{-\nu m/3}\right)^2 - 2\left(1-e^{-\nu m/3}\right)^3\right] dE} \tag{3.23}$$

For pure beta emitters, $S(E)$ can be calculated by the Fermi function as explained in the Appendix A [205, 206, 207]. From equation 3.5 it can be seen that kB is the coefficient of the linear energy transfer (LET) dE/dx. A precise evaluation of the kB value is difficult but a best estimate can be obtained by a self-consistent calculation procedure for various values of the detection efficiency. Plotting activity values calculated from different efficiencies versus experimental TDCR, the best kB value is obtained from the one that gives constant activity value over a range of TDCR. Detection efficiency variation can be achieved using different techniques: chemical quenching, use of coaxial grey filters and defocusing of photomultiplier tubes by reducing the focusing electrode potential. The first two processes reduce the mean quantity of light emission. The last reduces the detection probability. Cassette et al. [167] indicated that the three procedures were equivalent.

3.4 The experimental setup of ENEA portable TDCR

At the Italian National Institute of Ionizing Radiation Metrology (INMRI), belonging to ENEA and located in Casaccia Research Center, the Triple-to- Double Coincidence Ratio (TDCR) method is used for absolute activity measurements and standardization of pure electron capture (EC) or pure beta emitting radionuclides [186, 183, 168]. A portable TDCR detector, made up of three photomultipliers (PMTs) working in coincidence and symmetrically arranged around a specially designed optical chamber. It allows for the measurement of radioactive material in solution of liquid scintillator, contained in a vial which is put inside the optical chamber [183, 173].

This section will describe the main components of the ENEA portable TDCR detection system (optical chamber and PMTs of the new ENEA counter, and digitizer). The ENEA portable TDCR counter was built in 2013 at ENEA-INMRI with identical performance as the TDCR counter operated for activity primary measurements in metrology [208]. This counter can be used as an on-site device for activity standardization in Primary Metrology Institutes (PMI) or it can be used in environmental applications or in nuclear medicine laboratories of the hospitals to measure the activity of a radiopharmaceutical injected into patients, such as ^{18}F or ^{11}C. ENEA portable TDCR consists of an optical chamber surrounded by the three photomultiplier tubes (PMTs) symmetrically arranged around 120^{o} the liquid scintillation vial [208]. The experimental set-up of the ENEA counter schematic diagram is shown in Fig. 3.5.

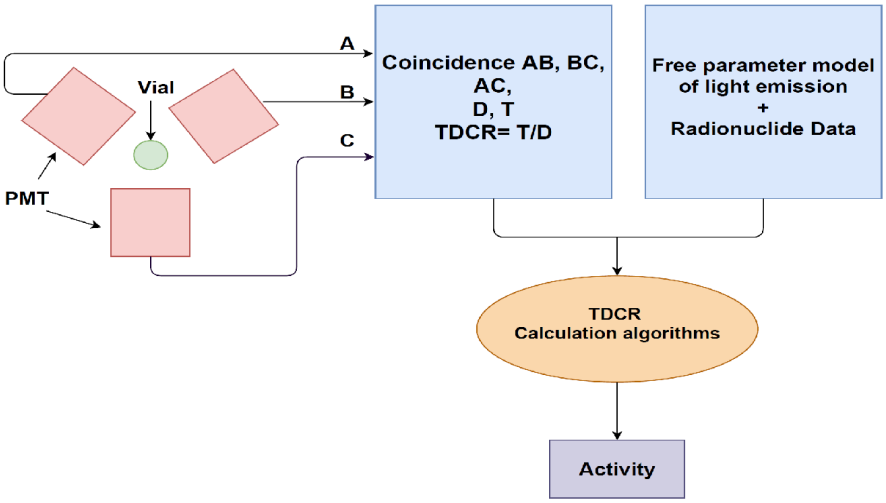

Figure 3.5: Diagram of the experimental setup of the portable TDCR at ENEA.

The portable TDCR is remarkably reducing the effort required for metrological assurance in the liquid scintillation (LS) counter; for that reason, CAEN in collaboration with ENEA-INMRI developed a front-end electronic acquisition system for the portable TDCR counter [189]. A new total digital approach was applied for processing pulses delivered by three photomultipliers in a TDCR system in which for the first time at ENEA-INMRI the CAEN products such as (CAEN DT5720 Digitizer belonging to the family of Desktop digitizers DT57XX, DPP-CI firmware, release 4.8_130.24, running on the Digitizer, and DPP-CI Control Software, release 1.3.3 running on the host station) [209] were used to link the PMTs of home-made TDCR counters to these front-end electronics devices [210]. New very interesting perspectives were then opened in the TDCR acquisition and analysis by using new software codes that take into account the digitized information recorded by compact digitizer modules directly linked to the detector [189]. The CAEN DT5720

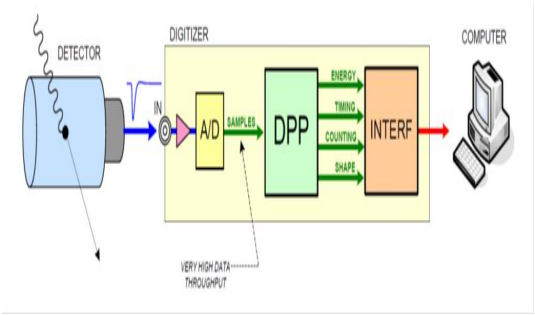

Figure 3.6: Block diagram of the digital solution.

digitizer [210, 209] is connected directly without any preamplifier to the output signals of the PMTs [208]. All the classical electronics acquisition chain based on Analog to Digital Converter (ADC), gate, traditional Linear Amplifier, and delay generator modules are completely replaced by the digitizer as shown in Fig. 3.6, and it is controlled by a computer by the CAEN (DPP-CI) Control Software [189][211].

3.4.1 The optical chamber

The ENEA portable TDCR counter optical chamber has an inner prismatic shape with equilateral base (L= 60 mm and H= 73 mm) and an outer cylindrical shape to fit precisely with this box. The optical chamber is made from white PTFE (Teflon) and it is surrounded by a black PTFE cylindrical box of (Φ= 150 mm and H= 150 mm) [208]. It is supplied with a lift and a shutter that can be used to remove or insert the vials inside the optical chamber without turning off the PMTs. Both optical shutter and lift were made of Teflon and built at ENEA- INMRI. The total weight of the portable TDCR detector is less than 6 kg. Figure 3.7 shows the new portable TDCR detector system [208] .

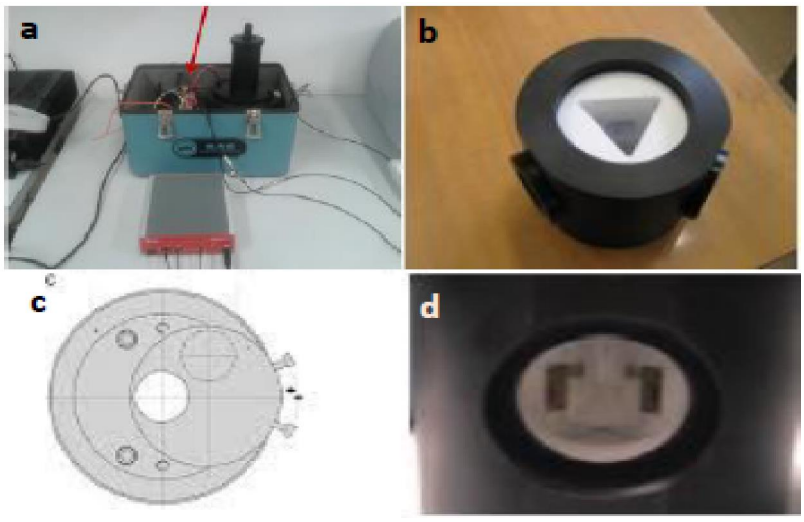

Figure 3.7: (a) The new portable TDCR system. (b) The optical chamber: external view (up), (c) The design of the optical shutter, and (d) internal view (down).

3.4.2 The photomultiplier tubes

For the new TDCR detector three Hamamatsu Photonics type R7600U-200 square package type of photomultiplier tubes (PMTs) are selected [208]. The photomultiplier tubes with small dimensions $(30\ mm \times 30\ mm)$, with 10 dynodes are used [212] as shown in Fig. 3.8. They are arranged around the optical chamber in a 120^o planar geometry around the scintillation vial (Fig. 3.6) [208]. These PMTs were selected to have a high quantum efficiency, high gain, short time of response, relatively wide range wavelength about (300 – 600 nm) [212], and relatively low supply voltage (approximately 900 V) with the cathode grounded to operate in the photon counting mode[208]. The PMTs provide good quantum efficiency with a maximum of 40% for wavelengths between 300 nm and 650 nm, which is compatible with the emission spectrum of liquid scintillators [212]. The PMTs are powered by three compacts (dimensions: $46 \times 24 \times 12\ mm^3$, weight: 31 g), on-board type HV power supply units (C4900 series, provided By Hamamatsu Photonics) [208]. The PMTs are built with the cathode at ground potential and a high positive voltage applied to the anode, which is specifically requested by ENEA-INMRI, in order to satisfy the necessary photon sensitivity for the TDCR applications and for working in photon counting mode [208]. [211].

Figure 3.8: Hamamatsu Photonics R7600U-200 square package PMT.

3.4.3 DPP- CI software

The DPP-CI Control Software is an application that manages the communication and the data acquisition from digitizers where the DPP-CI firmware is installed. The DPP-CI system allows setting the parameters for the acquisition, to configure the hardware, and to perform the data readout. It allows also to collect the histograms, and to plot and to save the list, the histogram, and the waveforms. The program can easily be interfaced to software tools for the spectroscopy analysis [211]. It is also

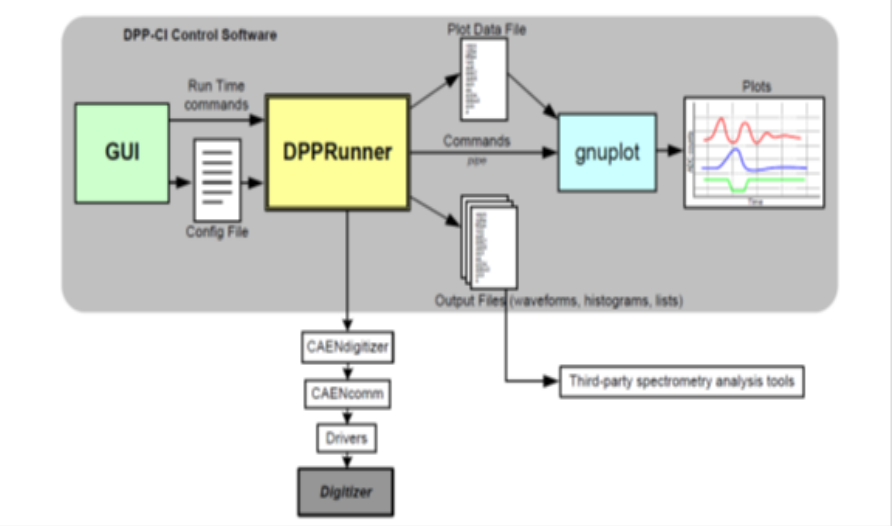

Figure 3.9: The DPP-CI Control Software block diagram.

possible to operate with multi-board systems: the front panel clock, the trigger and the general purpose LVDS I/Os connectors (VME only) make possible the synchronization of several boards. In order to manage the DPP-CI System, the host station needs either Windows or Linux operating system (OS). According to the preferred way of connection to the

digitizer, one can also take care of proper installation of USB or optical drivers in our case USB communication link with a Desktop digitizer is used. The main operations of the DPP-CI firmware are the algorithm continuously calculates the baseline of the input signal by averaging the samples belonging to a moving window of programmable size. It is possible to adjust parameters like the DC Offset, the Baseline and the Threshold in order for the Digitizer to self-trigger. One can be sure that the self-trigger option is enabled. This allows user to force the channel trigger and to visualize the signal input for the right parameter setting. When you set all the parameters correctly you can disable the SW trigger and enable the self-trigger of each channel [211]. The DC Offset is a DC value added to the input signal at the input stage of the Digitizer to fit the signal dynamic range to the ADC input dynamics. Figure 3.10 below shows the functional block diagram of the DPP-CI firmware [211]:

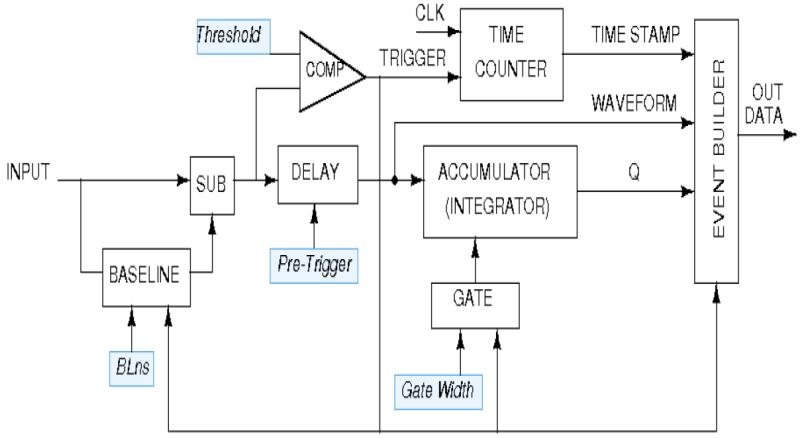

Figure 3.10: The functional block diagram of the DPP-CI firmware.

3.4.4 The digitizer

To perform the coincidence measurements with liquid scintillator counter techniques, the high-performance technology is required to process the very fast light pulses (few nanoseconds) which is emitted by a liquid scintillator when a charged particle dissipates its energy in a scintillator. For that reason, the CAEN DT5720 digitizer are used for the TDCR applications, which have high power to record very fast signals comes form the PMTs. This DT5720 digitizer device is a compact module characterized by four independent input channels, small size $(154 \times 50 \times 164\ mm^3)$, light weight (700 g) and operation capability without any crate. The board is provided with fast and precise ADCs (250 Mega Sample/s, 12 bit), analog bandwidth of 125 MHz and 2V peak-to-peak standard input dynamic range [210], making it suitable for the TDCR measurements [208]. The DT5720 version allows the setting of gate widths related in time for each triggered pulse and within a time acquisition window, as shown in Fig. 3.11.

The Gate covers in time the whole input signal pulse. In fact, the total charge Q of the signal inside the Gate window can be calculated by performing the gate integration over the input pulse. The DT5720 module elaborates and records the data and save them in a file (ASCII or Binary format) as the charge values Q and a stream of Trigger Time Tag (TTT); it means that the size of a single event is very small (typically a few bytes). The following electronic module is a waveform digitizer in which, as in a digital oscilloscope, when a trigger occurs, a certain number of samples is defined by an acquisition window and saved in a memory buffer. In order to evaluate the area of the input pulses and record timing information, the firmware performs Digital Pulse Processing (DPP) which is the main feature of the digitizer (Charge Integration, CI mode). Modern FPGA can be reprogrammed at any time by implementing DPP algorithms in it. The value of the total charge in the gated signal are recorded in an ASCII or binary file for each trigger pulse a TTT, of 4ns of resolution and, only a few bytes of information (2 bytes for charge value and 4 bytes for TTT) used per event. The digitizer provides the charge sensitivity (40 fC) and the TTT resolution and makes this device especially skilled for TDCR applications [189].

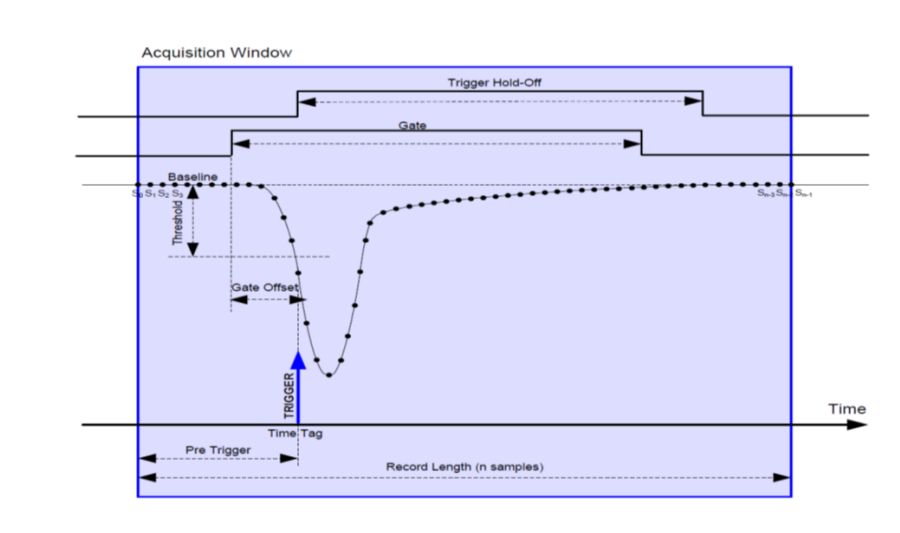

Figure 3.11: Diagram summarizing the DPP-CI parameters. The trigger fires as soon as the signal crosses the threshold value. Gate, Gate Offset, Pre-Trigger, Trigger Hold-Off, and Record Length are also shown for one acquisition window

3.4.5 Experimental measurements with portable TDCR at ENEA

The TDCR parameter can be measured by using the ENEA portable TDCR detector linked with DT5720 digitizer for low-energy pure-beta (^{3}H, ^{63}Ni and ^{14}C), for medium (^{18}F), and high-energy pure-beta (^{90}Sr and ^{90}Y) emitter radionuclides. The acquisition parameters such as: gate length, DC offset, pulse polarity, threshold level, etc., can be set, in the DPP-CI control software, independently for each channel [189]. The control software works both in histogram mode, to obtain the pulse shape spectrum as in a conventional multichannel analyzer or in oscilloscope mode in order to get the possibility to visualize the pulse shape [208].

At first, the DT5720 digitizer parameters were set with the PMTs biased around 900V and recording a typical SEP spectrum without any vial inside the optical chamber of the portable TDCR counter. For each individual channel the control software of the digitizer is used to discriminate threshold and the width of the ADC gate, in order to redact the noise and to have the whole analog pulse comes from the PMT covered completely in time by the gate pulse [208]. In order to match the PMTs for having the same gain in the three different channels, the digitizer was applied in the histogram mode or, in other words, the three Single Electron Peak (SEP) should be located at the same channel [208]. The precise adjustment of the discrimination threshold above the noise for each one of the three PMTs and under the SEP is a crucial point of the TDCR method [175]. In Fig. 3.12 a typically well separated SEP recorded by one PMT is shown.

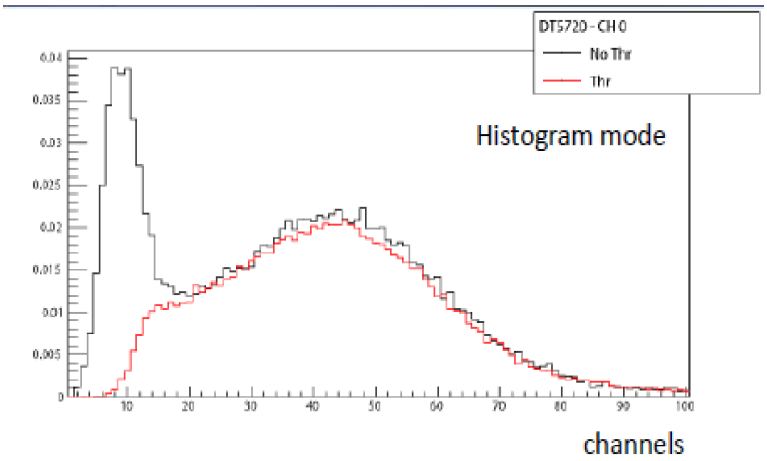

Figure 3.12: Single Electron Peak (SEP) recorded by one PMT.

The TDCR parameters for those beta emitting radionuclides measured by TDCR technique are interesting for radionuclide standardization and activity measurement in nuclear medicine applications and for other kinds of applications, such measurements on nuclear site or in the environment.

The TDCR analysis was performed by recording the Q value with an ADC gate equal to 24 ns. The sources were prepared at the radiochemistry laboratory at the ENEA-INMRI for other past experiments; the master solutions were checked by a high energy resolution HPGe detector owned by ENEA-INMRI to perform a preliminary gamma-impurity check. The sources were made, as usual, of 10 ml Ultima Gold as liquid scintillator and approximately 10 mg of radioactive solution (with different aliquots of CCl4 as a quenching agent) in 20 ml borosilicate glass vials. For background measurements one blank source was prepared containing only 10 ml of UG in the previously mentioned geometry.

3.4.6 The analysis software

The CAEN digitizers are dead-timeless acquisition devices, software is customized and written in C++ [208]. The dead-time is managed off-line by the analysis software which analyzes coincident events coming from the 3 PMTs and emulates the MAC3 logic [188].

A customized data acquisition software was implemented in order to perform a TDCR analysis on the events which are collected in a list-mode file; corresponding events from different input channels can then be compared to their TTTs when each of the acquisition channels of a digitizer are synchronized. For that reason, two data analysis software were developed, one from ENEA-INMRI and the other one from CAEN [189]. The ENEA-INMRI analysis software was implemented in the CERN ROOT frame [208]. In this part of the project ENEA- INMRI data analysis software is used for analyzing the data coming from the PMTs of the TDCR counter. This means that, when the CAEN digitizer records and organizes data in a list-mode (ASCII or Binary) file, one for each PMT, these records are read by the ENEA-INMRI data analysis software, event by event, as "leaves "of a ROOT tree file. This allows visualizing charge and timing spectra of the events recorded for each PMT of the TDCR detector. Both ENEA-INMRI and CAEN software implemented algorithms to perform the off-line TDCR analysis. In addition, to perform the off-line TDCR analysis on the same set of the events recorded by the 3 PMTs, a coincidence resolving time, $t_c\,(ns)$ window is set so allowing to compute: the single counts of each PMT (A, B, and C), the sum(S) of them, the co-

incidence counts (AB, BC, AC, D and T), the real time (t_{real}), the live time (t_{live}), and the TDCR parameter (TDCR=T/D).

After the run ends up, the data acquisition software scans the consequent event lists checking for coincidences. The recorded data stream is then analyzed by the ENEA-INMRI analysis software and values of dead time $(t_{dead} = 50\ \mu s)$ and coincidence resolving time $(t_c = 140\ ns)$ are applied. Such a dead-time length is usually long enough to eliminate the after-pulsing in liquid scintillation counting.

The ratio of $(R_T/R_{AC},\ R_T/R_{BC},\ and\ R_T/R_{AB})$ are calculated for each set of data from the net count rates of the double coincidences $R_{AC} = AC/t_{live}, R_{AB} = AB/t_{live},\ and\ R_{BC} = BC/t_{live}$ and the net count rates of the triple coincidences R_T from the three pairs of PMTs. They used to compute the efficiencies for the triple coincidences ε_T and for the logical sum of the double coincidences ε_D. TDCR value or TDCR parameter can be calculated experimentally by taking into account the ratio of the net count rate (background subtracted) of triple coincidence to the logical sum of double coincidence and it is equal to the ratio of the efficiency of triple coincidence ε_T to the efficiencies for the logical sum of the double coincidences ε_D for high statistics conditions of light emissions (i.e., for high-energy beta emitters) [177]. The TDCR parameter, obtained for different radionuclides measured using portable TDCR counter as a function of the (end-point, E_β, and mean value) energy of the beta spectrum, with the uncertainty about 1%, are shown in the table 3.1.

Table 3.1: Experimental TDCR values of different radionuclide sources

Sources	**Mean E_β(keV)**	**E_β(keV)**	**Experimental TDCR Parameter**
^{3}H	5.68	18.591	0.3106 ± 0.009
^{14}C	49.16	156.48	0.8903 ± 0.007
^{99}Tc	94.6	293.8	0.9492 ± 0.005
^{90}Sr	196.0	545.9	0.9757 ± 0.003
^{18}F	249.5	633.9	0.9917 ± 0.002
^{90}Y	926.7	2278.7	0.9910 ± 0.002

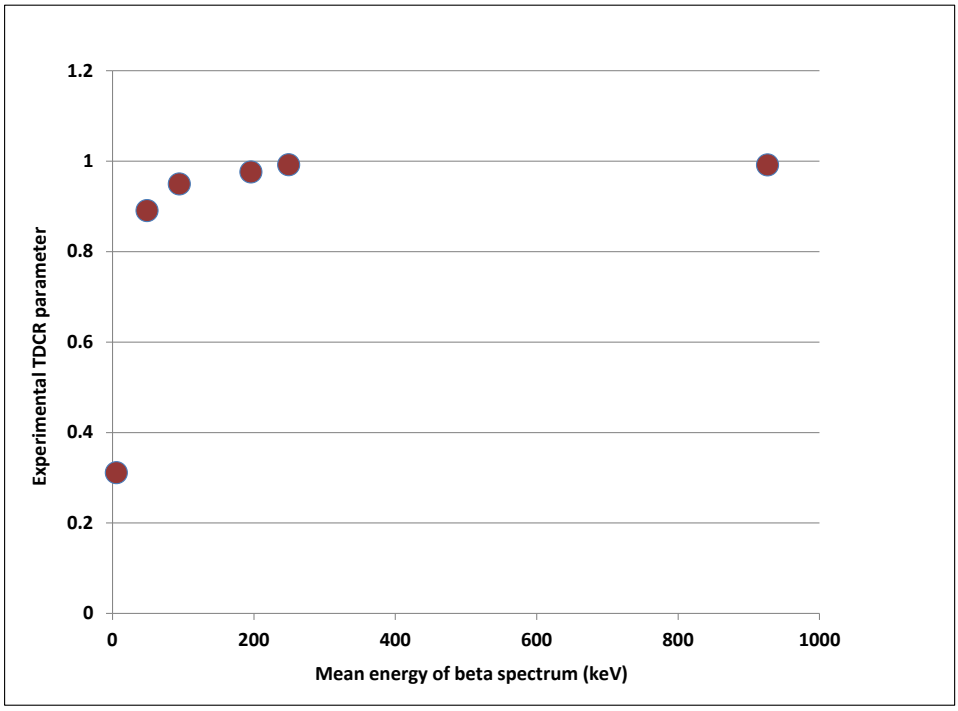

Figure 3.13: The relationship between the mean energy of beta spectrum radionuclides with experimental TDCR parameters.

Chapter 4

Monte Carlo Simulation GEANT4 Code

4.1 Introduction

The Monte Carlo method was first developed in the 1940s at the Los Alamos National Laboratory by Stanislaw Ulam [213]. It represented a key technique in determining the stopping power and energy deposited by neutrons in shielding materials. This problem could not have been solved by deterministic mathematical methods, and Stanislaw Ulam was the first one to suggest using random number distributions in modeling physical processes and extracting the desired quantities. The Monte Carlo simulation technique has overcome the shortcoming of the numerical method used for simple geometries based on the radiation transport equations [193]. Although Monte Carlo simulation has been used for a few decades in many areas of experimental physics such as nuclear and particles, it has only gained interest in radiation physics in recent decades due to the great advance of computing power. Monte Carlo simulation in radiation physics simulates the transport of electrons, positrons, photons and neutrons in materials with arbitrary compositions [214]. It simulates the physical process of energy loss along the path of radiation particles. The "history" of each primary particle and of the secondary particle resulting from interaction of the primary particle with the detector and

surrounding materials is tracked until all its initial energy is dissipated (or below the cut-off energy). A large number of histories (more than 10^6) must be tracked to obtain satisfactory statistics, as only a small percentage of events leads to absorption.

Indeed, nuclear physics experiments pose enormous challenges in the creation of complex yet robust software frameworks and applications. A particular importance is the ever-increasing demand for large scale, accurate and comprehensive simulations of the particles detectors used in these experiments. The demand is driven by the escalating size, complexity, and sensitivity of the detectors and fueled by the availability of moderate-cost, high-capacity computer systems on which larger and more complex simulations become possible. Similar considerations arise in other disciplines, such as: radiation physics, space science, nuclear medicine and, in fact, any area where particle interactions in matter play a role. A joint effort was made to build a more comprehensive package. As a result, the GEANT4 (GEometry ANd Tracking) "toolkit for the simulation of the passage of particles through matter" [194, 195] was created.

In response to this, a new object-oriented simulation toolkit, GEANT4, has been developed. The toolkit provides a diverse, wide-ranging, yet cohesive set of software components which can be employed in a variety of settings. These range from simple one-off studies of basic phenomena and geometries to full-scale detector simulations for experiments at the Large Hadron Collider and other facilities. In defining and implementing the software components, all aspects of the simulation process have been included: the geometry of the system, the materials involved, the fundamental particles of interest, the generation of primary particles of events, the tracking of particles through materials and external electromagnetic fields, the physics processes governing particle interactions, the response of sensitive detector components, the generation of event data, the storage of events and tracks, the visualisation of the detector and particle trajectories, and the capture for subsequent analysis of simulation data at different levels of detail and refinement. The widely used codes include GEANT4 developed by CERN in 1994-1998 [215], MCNP developed by the Los Alamos National Laboratory [216], PENELOPE by the University of Barcelona [217] and EGS4 by the Stanford Linear Accelerator Centre [218]. GEANT4 was completely rewritten in C++ with

a modern object-oriented design compared to its predecessor, GEANT3, dating back to 1982 and written in FORTRAN77. The main structure of the code is shown in Fig. 4.1.

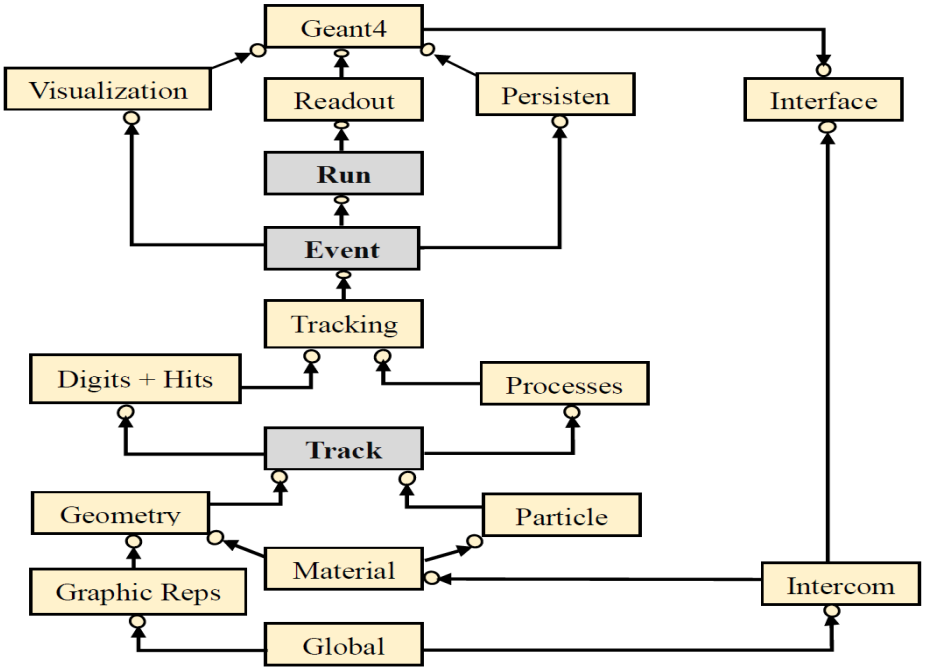

Figure 4.1: Top level category diagram of the GEANT4 package.

The lines which connect the different categories represent a dependency relationship, the circles indicating which is the category that depends on the other one, which is placed below. The most general categories are at the bottom of the chart, the higher ones depending directly or indirectly on them. The most basic category, *Global*, is concerning the system of units, constants, and random number generators. The *Intercoms* represent means to communicate between modules and between the user and GEANT4 through *Interfaces*. Going higher, there are the *Mate-*

rial, *Graphic representations*, *Geometry*, and *Particles* which are involved in defining a physical interaction and they are needed in defining a *Track* of a certain particle through matter. Each Track contains the two main parts for the passage of a particle through matter: the transport (step) and the interaction (hit). These are used by the *Processes* category which contains all different models of physical interactions and calls into action the ones that are needed in that specific interaction point. An *Event* is the sum of all the tracks produced since generating the first particle and, advancing higher in the hierarchy, the *Run* is a collection of independent events which share a common geometry and initial conditions. The categories through which the user can collect information from the simulation are *Visualization*, *Readout* and *Persistency*.

One of the many applications of GEANT4 simulations is characterizing the detection efficiency of a certain detection setup. There are many cases when standard calibration sources do not provide the desired range of energies, or they are not strong enough for testing coincidence summing effects. Another application is assisting in the design of new detectors and detection geometries in order to optimize the desired characteristics (e.g. maximizing efficiency and minimizing cost/material). The codes have been used to calculate the mean energy deposited in the gas within the active volume of the $4\pi\gamma$ counter per photon emitted from the volume source. The Monte Carlo code PENELOPE has been used to calculate ionisation chamber calibration factors (for ^{125}I, ^{109}Cd, ^{133}Ba, ^{210}Pb, ^{57}Co, ^{99m}Tc, ^{139}Ce, ^{51}Cr, ^{85}Sr, ^{95}Nb, ^{58}Co, ^{54}Mn, ^{65}Zn, ^{59}Fe, ^{56}Co, ^{60}Co, ^{22}Na, and ^{88}Y) and response function [219]. The agreement between calculated and measured factors is better than 1%. The calculation of the calibration factors of radiopharmaceuticals with short half-lives, ^{18}F, ^{99m}Tc, ^{111}In and ^{123}I, has also been performed in the same laboratory [220]. The response of $4\pi\gamma$ ionisation chamber has been simulated using MCNP code [221], GEANT4 [222] and EGS4 [223].

The Monte Carlo code GEANT4 has been used to calculate the response curve versus photon energy and calibration factors for ^{60}Co, ^{22}Na and ^{59}Fe for the ANSTO secondary standard ionisation chamber [224]. Agreement within 0.2% of the experimental values for these nuclides has been achieved, except for ^{22}Na, in which case annihilated photons need to be more carefully modelled in order to obtain higher degree of accuracy.

The Monte Carlo simulation is also used extensively to calculate the photopeak efficiency for HPGe and NaI detectors [225, 226, 227, 228, 229]. In the gamma spectrometry, the measured full energy photopeak efficiency must be corrected for cascade summing which occurs whenever two or more γ-rays from the same decay event are detected simultaneously inside the detector crystal. The cascade summing corrections have been performed using the Monte Carlo method [230]. The application of Monte Carlo simulation to the $4\pi\beta - \gamma$ coincidence counting was firstly carried out by Miyahara et al. [231]. In their work, the beta energy spectra and self-absorption of ^{134}Cs, ^{59}Fe, ^{103}Ru and ^{60}Co spherical particle sources were calculated by using the Monte Carlo method. The Monte Carlo simulation of all detection processes for ^{134}Cs in a $4\pi\beta - \gamma$ coincidence counting system was performed recently by Takeda et al. [232]. Both of the above simulations allowed the calculation of the efficiency extrapolation function.

In liquid scintillation counting, Monte Carlo is used to calculate the probability for the interaction of beta or electron capture particles, X- or γ-photons in a given scintillator and the absorbed energy distribution. The absorbed energy distribution of photons is most often calculated in discrete energy bins and the quenching function applied to each bin midpoint [193, 233]. For the modeling of the "low energy" package on the basis of Livermore data was selected for simulating photons and electrons which are created by bremsstrahlung [234]. Depending on how sophisticated the geometry description and interactions modes are, the codes might be more or less complex [235].

4.2 TDCR-GEANT4 modeling and simulation

For comprehensive modeling and simulation of the TDCR counter Monte Carlo Simulation GEANT4 code is selected. GEANT4 code has a comprehensive set of tools allows to model the TDCR counter and simulate different physical processes happening in the optical chamber. The TDCR-GEANT4 modeling and all the simulations in this project were performed with the GEANT4.9.6p01 release. Figure 4.2 represents comprehensive description of the geometry of the ENEA portable TDCR counter usnig

GEANT4 code.

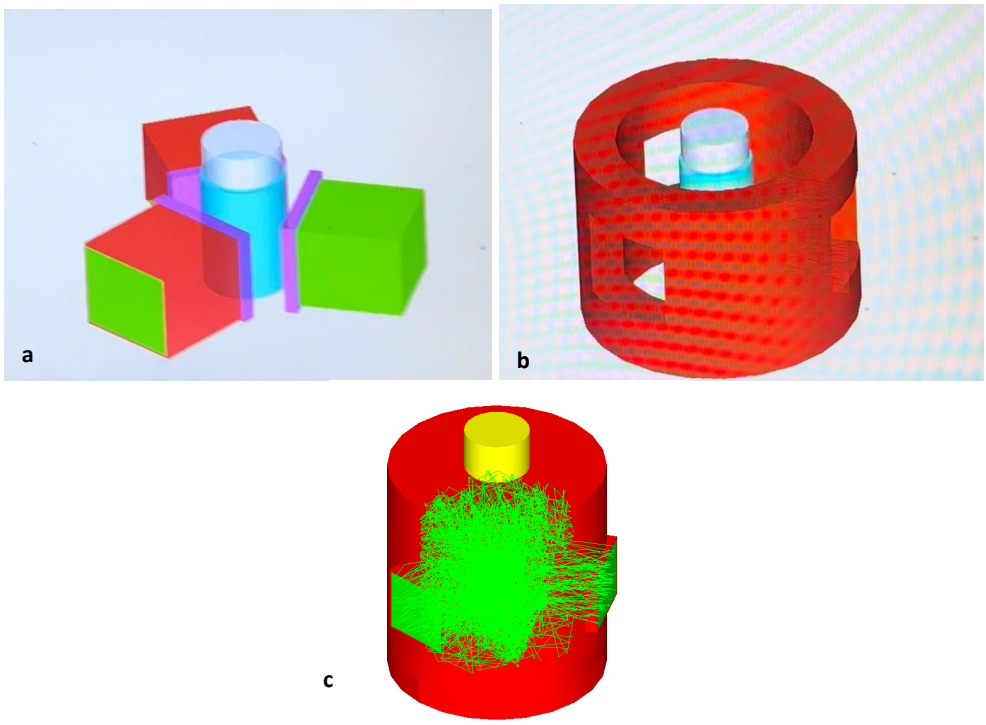

Figure 4.2: GEANT4 modeling of the TDCR counter. (a) PMTs arranged around vial inside the optical chamber. (b) Cylindrical box with three bores for PMTs. (c) Interaction of beta particle with LS solution, light is emitted in side the optical chamber.

The liquid scintillation counting must has the exact description of the liquid scintillation vial and liquid scintillator cocktail. For that reason, the atomic composition of the liquid scintillator (UG) and the dimensions of the vial are taken from the experimental set-up [196]. The standard 20 ml glass vial (borosilicate vial) is defined as a LS vial with dispersive refractive index (1.52 at 400 nm) and a polished surface. The glass vial is placed inside the optical chamber, the model of *"dielectric– dielectric"* applied for the refraction and reflection of the photon at the inner and outer scintillation vial surface [234]. The LS vial is filled with 10 ml of Ultima Gold as a liquid scintillation cocktail, it is defined as liquid water

with a dispersive refractive index (1.33 at 400 nm) and the liquid-air and liquid-vial interfaces are described as *dielectric-dielectric* boundaries. The optical chamber is made of the white Teflon. Teflon reflecting cavity is defined as *dielectric-metal* using a lambertian surface (polished surface) in order to increase the reflectivity to 95%. The center of the optical chamber is positioned 17 mm from the outer surface of the photomultiplier window, the *dielectric–metal* boundary model is used. In order to compute the photoelectrons production consistently when the photons reflect at the interface with the ultra bialkali photocathode of the PMT the model of *"dielectric-metal"* is applied. There are several optical processes happen within the fused silica window of the photomultipliers. The photocathode is simulated via its optical properties at the fused silica inner boundary, to count the number of photons refracted between both surfaces. The fused silica window is covered by the ultra bialkali photocathode and the model of *dielectric–dielectric* boundary is applied [196]. A dispersive refractive index of the fused silica material is (1.47 at 400 nm) with a polished surface. The Quantum efficiency is provided by using binomial trials for converted photons to photoelectrons in the photocathode [196]. The maximum quantum efficiency is $\sim$ 40% at 400 nm [212]. Some optical properties for the PMT model are as shown in the table 4.1 [196].

For a given application, the simulation runs according to the following steps:

1. The initial particles are randomly generated in the whole volume corresponding to the radioactive sample in the LS-vial; energy release depends on the radionuclide decay scheme.

2. optical light is produced along the track of the charged particles inside the LS-vial and also the borosilicate wall.

3. Each emitted photon is subsequently followed to account for the optical processes in the TDCR counter (refraction, reflection and absorption).

4. The photoelectrons are produced in each PMT by applying a binomial trial (using the experimental quantum efficiency) on the photons refracted at the photocathode.

Table 4.1: Some properties of the ENEA portable TDCR counter used in GEANT4 code modelling.

Detector Parameter	**Material**	**Optical Parameter**
PMT-Window	Fused Silica	**Refractive index**: 1.47 at 400 nm and 1.64 at 160 nm [236] **Surface type**: Dielectric- Dielectric
PMT-photocathode	Ultra Bialkali	**Refractive index** of Bialkali (K_2CsSb): 2.5 at 430 nm [237] **Surface type**: Dielectric-Dielectric
Optical chamber	White Teflon	**Surface type**: dielectric-Metal Lambertien-type selectivity 95%
Vial(1 **mm layer)**	Borosilicate	**Refractive index**: 1.52 at 400 nm **Surface type**: Dielectric-Dielectric
LS cocktail (10 **ml)**	Ultima Gold	**Refractive index**: 1.5 at 430 nm (correlated to the bis- MSB fluorophore)

5. The number of photoelectrons is obtained in the PMTs for each simulated event (corresponding to one disintegration).

6. The coincidences are calculated by using a second binomial trial representing the probability to reach the first dynode; at least one binomial success leads to a count in a PMT.

7. TDCR value is subsequently obtained by adjusting defocusing parameter and kB factor.

The double- and triple- coincidences are determined for each photomultiplier tube by counting the numbers of photoelectrons. The probability for photoelectrons to reach the first dynode depends on the defocusing parameter; it permits the detection efficiency variation to be simulated as experimentally found by PMTs defocusing [196].

4.3 Effect of Birks constant and defocusing darameter on TDCR value in MCS-GEANT4

In this project, we carried out two different computations to obtain the simulated TDCR parameter for ^3H, ^{14}C and ^{90}Y. We used CEA energy spectrum data for pure beta emitting radionuclides [9]. Then, we used G4RadioctiveDecay class in GEANT4 code to obtaine the energy spectrum data for pure beta emitting radionuclides above in order to compute the theoretical Monte Carlo simulated TDCR detection efficiency. The radioactive decay simulation is a standard task in Monte Carlo Simulation GEANT4 code. The simulation of the overall process uses some physical models with unknown theoretical parameters; for this reason, the Monte Carlo code is necessary to fix these parameters by comparing the simulated results against the experimental ones.

4.3.1 Measurement of Tritium

^3H emits 100% β particles with a maximum energy of 18.591 (1) keV and half-life of $T_{1/2} = 12.312(25)$ years [9]. The simulated TDCR parameter value for the ^3H radionuclide changes in the 0.2 to 0.4 range. The sets of data are corresponding to eight different kB factor values as a function of defocusing parameters used in calculation, namely (0.07, 0.08, 0.09, 0.1, 0.11, 0.12, 0.13, and 0.14) mm/MeV as shown in Fig. 4.5. From frequent processing of data for different kB, it was established that the best kB value is around kB= 0.09 mm/MeV and the defocusing parameter= 0.78. The percentage of deviation $(\Delta\%)$ of the TDCR parameter, between the experimental $TDCR_{exp}$ and the simulated one $TDCR_{sim}$, written as $\Delta\%TDCR = \left(TDCR_{sim} - TDCR_{exp}\right)/TDCR_{exp}$ at that point it is 3.06%.

In fact, this is true only for low energy beta emitter radionuclides especially for TDCR values around 0.3. The deviation of the TDCR parameter of ^3H for a different kB factor as a function of defocusing parameter is plotted in Fig. 4.3. It must be observed that the kB value has a dramatic influence on the TDCR efficiency of a ^3H source.

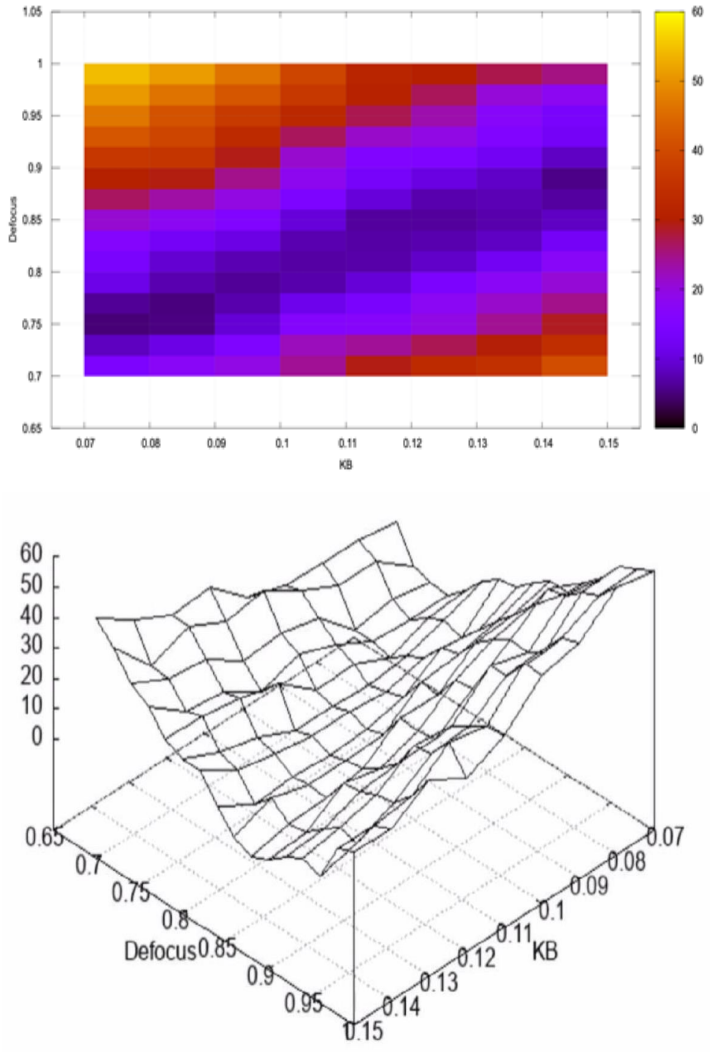

Figure 4.3: 2D and 3D relationship between the kB factor and defocusing parameter for ^3H.

4.3.2 Measurements of Carbon-14

^{14}C disintegrates 100% by β-transition with a maximum energy of 156.479 (4) keV, and half-life of $T_{1/2} = 5700(30)$ years [9]. The deviation of the TDCR parameter for the ^{14}C radionuclide for different kB factors as a function of defocusing parameter is shown in Fig. 4.5. The TDCR value is in the range of 0.80 to 0.94. The sets of data are corresponding to eight different kB factor values as a function of defocusing parameters used in calculation, namely (0.07, 0.08, 0.09, 0.1, 0.11, 0.12, 0.13, and 0.14) mm/MeV. The processing of data is repeated with different kB values. It was found that the kB value is a nearly constant for different kB factors and different defocusing parameters. The graphs showed that the deviation of the TDCR parameter for different value of kB factor as a function of defocusing parameter is very low, and it demonstrated that, in the situation of low energy radionuclides, the effect of kB on the TDCR model can be neglected when the TDCR parameter close to the 0.85.

4.3.3 Measurements of Yttrium-90

^{90}Y emits β-particles throughout a 99.983(6)% branch equivalent to the maximum energy of 2278.7 (16) keV and the half-life $T_{1/2} = 2.6684$ (13) days [9]. The TDCR detection efficiency for the pure beta emitter radionuclide ^{90}Y is roughly constant in the range 0.998 to 1.0. The sets of data are corresponding to eight different kB factor values as a function of defocusing parameters used in calculation, namely (0.07, 0.08, 0.09, 0.1, 0.11, 0.12, 0.13, and 0.14) mm/MeV. The processing of data is repeated with different kB values. It was found that the kB value is approximately constant for different kB factors and different defocusing parameters. It is clear from the graphs in Fig. 4.5, that the deviation of the TDCR parameter for different value of kB factor as a function of defocusing parameter is very low, and it is verifying that, in the case of high energy pure-beta radionuclides, the effect of kB on the TDCR model can be neglected.

On the basis of the above consideration, we looked at the deviation of the TDCR parameter for each studied radionuclide and for different kB factors and defocusing parameters. So, we were able to report in the table 4.2 the selected TDCR parameter, corresponding to the minimum

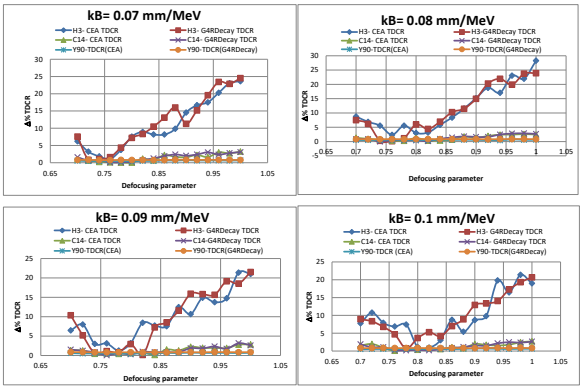

Figure 4.4: TDCR deviation for three radionuclides (^{3}H and ^{14}C as a low energy and ^{90}Y as high energy beta emitter) as a function of defocusing parameters for different kB =(0.7, 0.8, 0.9 and 0.10) mm/MeV factors

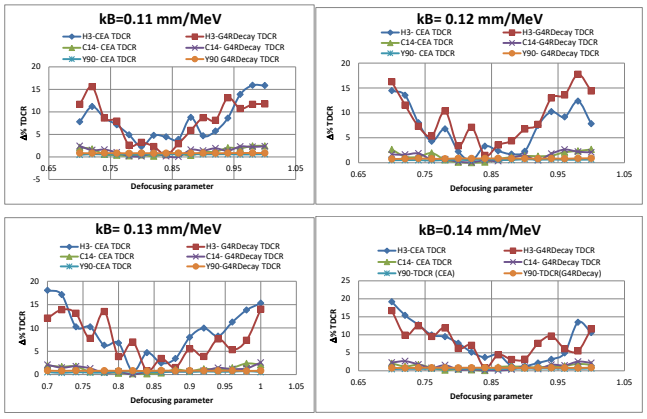

Figure 4.5: TDCR deviation for three radionuclides (^{3}H and ^{14}C as a low energy and ^{90}Y as high energy beta emitter) as a function of defocusing parameters for different kB =(0.11, 0.12, 0.13 and 0.14) mm/MeV factors

of the as a function of the mean beta energy E_β. Figure 4.6 illustrates, in particular, that the TDCR parameter depends on the energy spectrum of beta-emitting radionuclides. The relative uncertainty on a TDCR parameter increases with the decreasing of the beta energy of the radionuclides measured; in fact, for high-energy beta emitters the counting efficiency approaches unity, this means that the uncertainty is very low for these kinds of pure-beta emitters, such as (^{90}Sr and ^{90}Y).

Table 4.2: Simulated TDCR parameters for different radionuclide sources

Radionuclides	E_β**(keV)**	**Mean** E_β**(keV)**	**TDCR parameter**
^{3}H	18.6	5.68	0.3145 ± 0.05
^{63}Ni	66.98	17.434	0.7066 ± 0.1
^{14}C	157.0	49.16	0.8847 ± 0.13
^{90}Sr	546.0	196	0.9707 ± 0.01
^{18}F	634.365	249.5	0.9605 ± 0.01
^{90}Y	2278.7	926.7	0.9996 ± 0.01

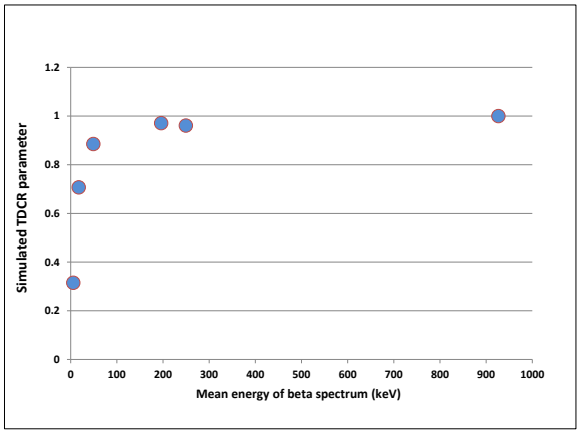

Figure 4.6: The relationship between the mean energy of beta spectrum radionuclides with simulated TDCR parameters.

By taking into account the results reported both in the table 3.1 and the table 4.2, we were able to represent in the Fig. 4.7 the experimental and simulated TDCR parameters.

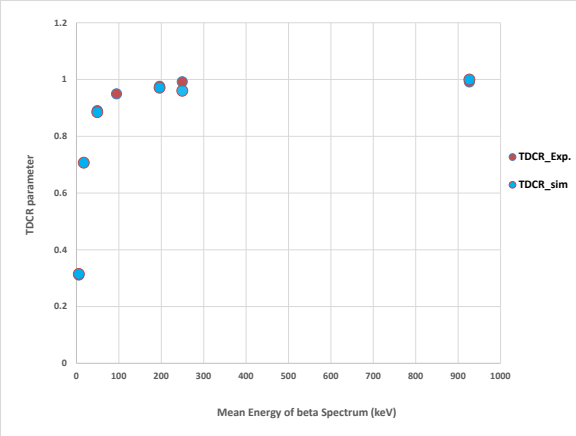

Figure 4.7: Experimental and simulated TDCR detection efficiency.

4.4 ENEA CRESCO computing facility

In this section we focused the attention on ^{18}F detection efficiency computation performed for the portable TDCR using GEANT4 as Monte Carlo simulator and the ENEA CRESCO computing facility. The use of such a heavy-duty facility was needed in order to collect in just a few months of run time a high statistics (millions of events) for radionuclides emitting secondaries at high- (order of MeV) and low- or very-low- energy, an otherwise even-larger time-consuming task. The interest for this work is also due to the fact that ^{18}F is widely used radiopharmaceuticals in nuclear medicine for Positron Emission Tomography (PET) applications and PET scanners.

Performing MCS in Liquid scintillation counter of ionizing radiations losing their energy in the scintillator is time consuming to obtain very high statistics, especially for simulations concerning very low beta emitters such as ^{3}H and ^{63}Ni. For these reasons the ENEA CRESCO computing facility was taken into account to carry out such a simulation. In particular, to test the run time necessary to perform the simulations and considering the importance of the use of the portable TDCR detector for nuclear medicine applications, the ^{18}F radionuclide was studied for all the tests performed with ENEA CRESCO. Hereafter short descriptions of

the jobs run on ENEA CRESCO.

The jobs run simulations in GEANT4 of the TDCR apparatus as described above. CRESCO system was accessed from the following front-end nodes, with username "radionuc" belonging to ENEA-INMRI:
cresco6x001.portici.enea.it
cresco6x002.portici.enea.it
Due to specific library requirements of the MonteCarlo code, it was necessary to install GEANT4 version 9.6 on

/afs/.enea.it/project/metrologia/soft/geant4_cresco6
and root 6.20.04 (thanks to one of the author i.e G.G) in
/afs/.enea.it/project/metrologia/soft/root_cresco6

The jobs, running up to about 135 hours each (depending on the number of events, and type and energy of the primary particles) are submitted to CRESCO by bsub on typically 40 cores. Their main output files, in ROOT format (of the order of tens of MB) for offline analysis, are produced on the scratch area $PFS_SCRATCH0 and then moved to the store area $PFS_POR_STORE0 using appropriate shell scripts only if successfully completed. LSF error and output files are written to AFS. In this project the TDCR parameter for radionuclide ^{18}F has endpoint energy about 634.9(5) keV [9] as shown in the table 4.3.

Table 4.3: Simulated TDCR parameters for ^{18}F radionuclide for fixed defocusing parameter= 0.95 and kB= 0.1 mm/MeV.

Radionuclides	**no.of events**	ε_T	ε_D	**TDCR ratio**
^{18}F	10000	0.9991	0.9999	0.9992

4.5 Conclusions

In this work, we performed simulations to obtain the TDCR parameter of two low-energy pure-beta (^{3}H and ^{14}C) and one high-energy pure-beta (^{90}Y) emitter. For this purpose, we carried out two different computations by using GEANT4 toolkit in which we implemented both CEA en-

ergy spectrum and G4RadioactiveDecay class for the three radionuclides above, and in order to find the theoretical TDCR efficiency.

The same code was used to study the relationship between the deviation, $\Delta\%$, of TDCR parameters (as previously defined) for ^{3}H, ^{14}C, and ^{90}Y as a function of defocusing parameters for different kB factors. This study highlights that this deviation is very strong for the very low-energy beta radionuclides such as ^{3}H. Furthermore, it can allow us to select the best kB factor for different defocusing parameters looking at the minimum of the $\Delta\%$ deviation.

The comparison between the simulated and experimental TDCR parameters for the studied radionuclides shows that, in many cases, the computed counting efficiencies fit well with the experimental ones, especially for the high-energy ^{90}Y beta emitter, measured by using the ENEA-INMRI portable TDCR detector.

Chapter 5

Radionuclides standardization at CIEMAT

5.1 Introduction

The availability of radionuclidic standards, through development and dissemination, is essential for performing accurate measurements in many application areas and disciplines involving radioactivity. These include, amongst others, the measurements needed and used for pure research on nuclear decay and reactions, for radioecological and geochemical studies, for environmental monitoring, for quality control of radiopharmaceuticals in production and administration, and for the assay of special nuclear materials in the nuclear-power and -weapons industries. These measurement standards are principally used for calibrating instruments that are used to measure radioactivity and for the monitoring of radiochemical procedures. Most standards are (or at least should be) traceably linked to national standards and to international measurement compatibilities. Primary standardization of activity is based on the detection and quantization of the emitted radiation [238]. The appropriate choices are made on the basis of the decay scheme of the considered radionuclide, showing its various transition pathways and associated probabilities [239]. The currently available decay schemes [240], with varying levels of accuracy and precision, are the result of decades of work in the field of 'Radionuclide

metrology', which comprises all aspects of radioactivity measurements, such as the determination of activity, half-life, energy levels and probabilities of decay modes. The best primary standardization methods are designed in such a way that their result is independent of the various nuclear decay data (and associated uncertainties) and their calibration based on the fundamental physical principles, not on other radioactivity measurements. The ideal method is under statistical control, i.e. all main sources of uncertainties identified and quantified, and the total uncertainty on the result preferably reduced to a minimum. Achieving a full uncertainty budget with ambitious but realistic claims on precision and accuracy constitutes one of the most challenging aspects of metrology [241]. There are some different primary standardization techniques, such as analogue coincidence counting methods, liquid scintillation counting, and gas counting.

This chapter describes the methodology applied at the Ionizing Radiation Metrology Laboratory at the Research Centre in the field of Energy, Environmental and Technology (LMRI-CIEMAT)-Madrid, Spain for the standardization of several radionuclides. This laboratory is the institute designated in Spain to provide traceability to the International System of units (SI) in the fields of Dosimetery and Activity. For this purpose, and among other functions, the LMRI participates in key international comparisons, carries out equipments calibration, and provides radionuclide standard sources. This way secondary labs/users can guarantee an adequate level of quality of their measurements. The procedure for the standardization of ^{109}Cd in the framework of an international comparison organized by BIPM is first described. Afterwards, the methodology applied to calibrate the activimeters (or dose calibrators) used by medical and pharmaceutical facilities is reported. These instruments, used to verify the activity of radiopharmaceutical after production or the dose supplied to patients, were in these case calibrated for the measurement of two common radionuclides used in diagnostic imagin, ^{68}Ga and ^{99m}Tc. The standardization of radionuclides described in this project involves several techniques in the radionuclide Metrology laboratories from CIEMAT (Spain) such as Liquid scintillation Counting using customer-built TDCR and HIDEX 300-SL methods.

5.2 The experimental setup of customer–build TDCR at CIEMAT

Liquid scintillation counting using Triple to Double coincidence ratio thecnique (TDCR) is widely used at LMRI-CIEMAT for the standardization of radionuclides. For this purpose, the laboratory has a customer-built TDCR counter, which is mainly composed of an optical chamber with three PMTs and a signal processing unit. The optical chamber was designed to optimize the light transport from the liquid scintillation sample to the photocathodes of the PMTs to improve the efficiency of the detection system as shown in Fig. 5.1a. This implies a larger optical chamber and therefore it was designed as an inner cylinder ($\Phi = 28.5\ mm$ and $H = 73\ mm$) and an outer prismatic shape ($L = 67.2\ mm$ and $H = 110\ mm$). Figure 5.1b shows this particular shape which was selected to fit the geometry of the PMTs used and to allow the vials to be placed in close proximity of the three PMTs to maximize the geometric efficiency. The optical chamber is made from white PTFE (Teflon) and it is surrounded by a duraluminum cylindrical box. There are three bores for the PMTs. They are arranged around the optical chamber in a 120^o planar geometry. The three BURLE 8850 type PMTs, a 12-stage fast-linear-focused type with bialkali photocathode and high gain at the first dynode, were selected for the TDCR detector. There is a bore from the bottom of the optical chamber to place the liquid scintillation vials. The vials can be inserted and removed via Hand-Operated Worm Gear Screw as shown in Fig. 5.1c. All the system is shielded by the cylindrical box to prevent any external light insert the optical chamber as shown in Fig. 5.1a.

The PMTs have the wavelength of maximum response (420 nm) and they have very high-quantum efficiency. The PMTs operated at 1980 V anodic voltages, which were found to be a good compromise between single electron pulse resolution and moderate dark counting rate. The PMTs are powered by HV power supply units (Mode. N1470 which is provided by CAEN). The anode of the three PMTs is connected to the MAC3 coincidence unit via fast amplifiers (NIM Model 612AM 6-channel photomultiplier amplifier) and constant fraction discriminators (NIM Model 821 Quad 100 MHz Discriminator). The outputs of the discriminators

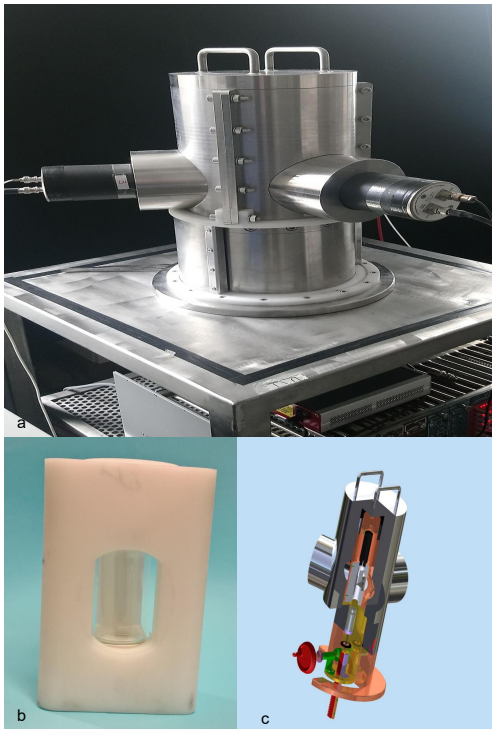

Figure 5.1: (a) The CIEMAT- TDCR system. (b) The optical chamber: external view. (c) The design of the vial lifter.

connected to the coincidence module MAC3, constructed in LNHB [188], accepts the signals from the three detection paths (A, B, C). In the present MAC3 module configuration at CIEMAT, three input channels are used for, and a forth one is used to feed in an external reference frequency of 100 kHz generated by a GPS or radio controlled receiver. If there is no reference frequency available, an internal quartz oscillator will be used as to measure the dead-time. Since the reference system is a TDCR counter connected to a MAC3 module with 40 ns implemented coincidence resolving window, all the measurements presented in this work were carried out using the same dead-time of 30 μs and a coincidence time of

40 ns. The count rates of three individual double coincidences (AB, BC, and AC), a triple coincidence (T) and a logic sum of the three double coincidences (D) are registered simultaneously by Quad scaler and preset counter timer (Mod. N1145 provided by CAEN) scalers. Counting efficiencies are calculated at LMRI-CIEMAT from theoretical models using EFFY (pure β-emitters) and NUR (electron capture, $\alpha/\beta-\gamma$ emitters) codes. These models are based on the statistical description of the physical process taking place in the counter, which comprises energy transfer from the ionizing particle, photons generation in the liquid scintillation cocktail and their conversion to electrical impulses in PMTs. Counting efficiencies depends on an intrinsic parameter of each counting configuration (combination of counter + scintillation cocktail + vial type) the so-called "free parameter", and can be calculated considering the probability to detect a specific scintillation pulse and the decay data of the radionuclide of interest as shown in Fig. 5.2. The on-line coincidence analysis is used between the different signals coming from each PMT of a TDCR system.

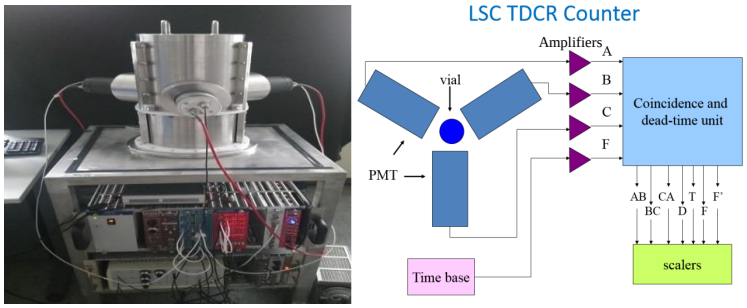

Figure 5.2: The experimental set-up and schematic diagram of the customer-Built TDCR counter at CIEMAT.

5.3 International comparison of standardization of ^{109}Cd

Cadmium-109 is widespread radionuclide used as an X-ray fluorescence source. Figure 5.3 shows the decay scheme of ^{109}Cd; it has a half-life of 461.9 days and decays by electron capture to ^{109m}Ag with the emission of a γ-ray with energy of 88.03 keV (3.79%). The de-excitation of this state is predominately through conversion electron emissions while about 3.66% undergoes gamma radiation at energy of 88.03 keV. During the EC process of ^{109}Cd or the IC process of ^{109m}Ag, electron vacancies can be created at various allowed shell states. Among all possibilities, the K-shell X-ray emission is intense and has an average rate of 1.022 per ^{109}Cd disintegration [242].

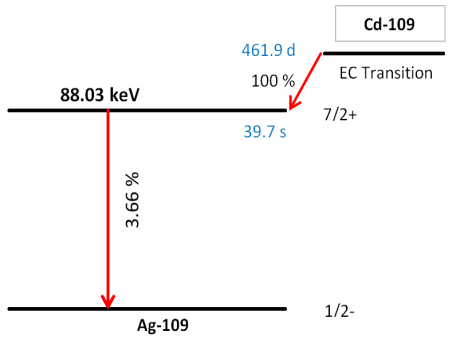

Figure 5.3: Decay scheme of ^{109}Cd

This radionuclide can be employed for calibration of detectors and as a tracer to physiological research [243, 244]. It can also be used in the energy dispersion X-ray fluorescence (EDXRF) technique [245, 246]. ^{109}Cd has been applied in physiological research on animals and plants for more than forty years which has provided useful information. This radionuclide can probably be used for inhibition of liver cancerous cells [247, 248], as well as for tissue imaging with SPECT [249]. ^{109}Cd is also used, due to its 88 keV characteristics emission, in radioprotection in solution with other gamma emitting radionuclides for calibrating by means

phantoms the internal body counters. Additionally, it can be used to investigate the ecosystem [250]. The $^{109}Cd/^{109m}Ag$ generator has been investigated for uses of venogram and angiogram. The main application of ^{109}Cd is the calibration of high-energy resolution gamma spectrometers. These spectrometers are widely used in the nuclear industry, radiation surveillance laboratories and research facilities. These spectrometers are normally calibrated using a mixed radionuclide solution that is available from National Metrology Institute; ^{109}Cd is an essential component of the mix as it provides a low-energy calibration point at 88 keV. Therefore, techniques for the accurate activity determination as well as a low uncertainty of the γ-ray emission probability are desirable.

In addition, the Measurement Method Matrix of the Consultative Committee for Ionizing Radiation, Section II (CCRI (II)) shows that measurements of ^{109}Cd may support Calibration and Measurement Capabilities of metrological institutes (CMCs) for many other radionuclides. The previous comparison of a solution of ^{109}Cd was organized by the Consultative Committee for Ionizing Radiation (CCRI) and was carried out in. Primary standardization of ^{109}Cd are challenging due to the delayed state in the daughter nuclide ^{109}Ag (half-life of about 39.7 sec). Nevertheless, the results from the comparison in 1986 showed reasonably good agreement between the participants. The results from the 1986 comparison are no longer valid to support National calibration and measurement capability (CMCs) in the General Conference on Weights and Measures CIPM MRA [251]. Consequently, the CCRI (II) decided to repeat this comparison and the Bureau International des Poids et Mesures (BIPM) volunteered to be the pilot laboratory, with the support of the Laboratoire National de Métrologie et d'Essais - Laboratoire National Henri Becquerel, France (LNE-LNHB). One method makes use of the fact that the ^{109m}Ag isomer is also part of the decay scheme of the short-lived beta emitter ^{109}Pd ($T_{1/2} = 13.7(1)h$) [242] which can be standardized by means of $4\pi\beta$ proportional counting [252] or $4\pi\beta$ liquid scintillation counting in combination with the CIEMAT/NIST method [162]. The experiments described in this project were done with several ^{109}Cd solutions. The liquid scintillation measurements were performed at CIEMAT laboratory by using customer-built system TDCR system.

5.3.1 ^{109}Cd radionuclide solution

The ^{109}Cd solution with a nominal activity concentration of 250 kBq/g on the reference date (1^{st} September 2021 12:00 UT) used in this project. It consisted of cadmium chloride in HCl of concentration 0.1 mol/L with a carrier concentration of Cd^{+} ions about 20 $\mu g/g$. An aliquot of the solution was used for the preparation of a diluted solution in order to obtain an activity concentration for ^{109}Cd. The ^{109}Cd master solution is diluted and distributed in flame sealed glass ampoules: LMRI-type ($\phi = 1.7\ cm,\ L = 8\ cm$). The mass of the solution was 2g. Homogeneity between the ampoules will be verified by ionization chamber, 4πNaI(Tl) or HPGe spectrometry measurements before dispatching to participants by the BIPM. The master solution was also measured by γ-ray spectrometry and no γ-emitting radioactive impurities were found.

5.3.2 Measurements and standardization of ^{109}Cd

The TDCR liquid scintillation samples were prepared for standardization of ^{109}Cd with two different scintillation cocktails (HiSafe 3 and Ultima Gold). Three types of 20 ml (glass with low potassium borosilicate, high density polyethylene (HDPE) and sandblasted glass) vials were used. The vials were filled with 15ml mentioned liquid scintillation cocktails and weighted portions 50-70 mg of the ^{109}Cd solution were added. A set of five ^{109}Cd liquid scintillation samples were prepared for each type of LS cocktails and for each vial. The background samples were prepared using 15ml of UG and HiSafe 3 (HS3) for each types of the vial without the radioactive source. In order to optimize the counting of double- and triple-coincidences, TDCR measurements were performed with the coincidence resolving time equal to 40 ns. Detection efficiencies of ^{109}Cd standardization by the TDCR technique were calculated using the NUR code available at LMRI-CIEMAT. NUR software (NUR means light in Arabic Language) is based on a combination of two steps as shown in Fig. 5.4: In the first one, the complete decay scheme is sampled by a Monte Carlo process, including atomic relaxation data, using the PENNUC code [253, 254], and a file is created with sets of events (independent cascades of particles and photons); in the second, the file is processed by NUR according to the par-

ticular experimental conditions of the LSC system (scintillating cocktail, vial volume, number of PMTs) to calculate the counting efficiency.

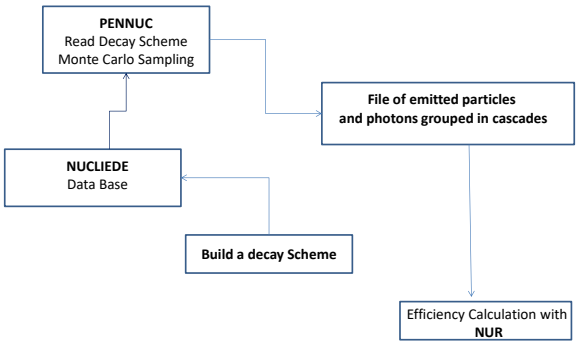

Figure 5.4: NUR Software: Creating and processing a file of events.

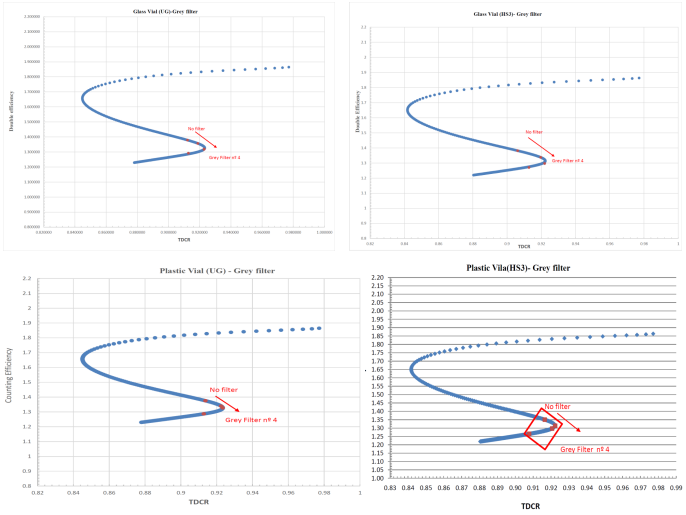

Figure 5.5: TDCR variation of ^{109}Cd as a function of double efficiency using grey filter for Ultima Gold and HS3 liquid scintillation cocktails for glass and plastic vials.

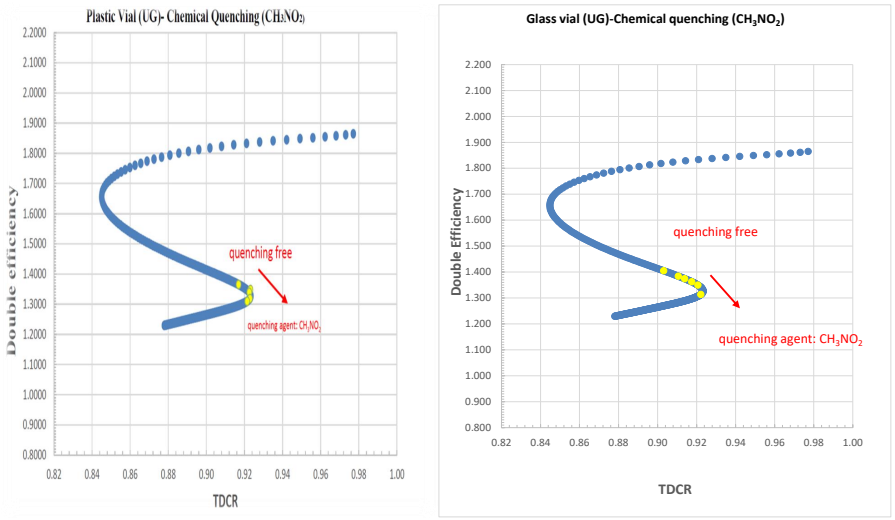

Figure 5.6: TDCR variation of ^{109}Cd as a function of double efficiency using Chemical quenching CH_3NO_2 for UG liquid scintillation cocktail for glass and plastic vials.

^{109}Cd counting efficiency (double) versus TDCR parameter is plotted in Fig. 5.5 and 5.6 for different liquid scintillation cocktails and vial types. It can be observed that the relation between the double counting efficiencies and the TDCR values are not linear. In all cases the curves show an ambiguity, this means that TDCR value for ^{109}Cd could lead to more than one value for ε_D. The TDCR curve displays the non-monotonic behavior typical of electron capture radionuclides. One could select the area of interest for the TDCR value by varying the efficiency and noting whether TDCR increases or decreases with a reduction in detection efficiency. For that reason grey filters or chemical quenching can be used to detection variation. In Fig. 5.5 grey filters with different level of grey are used, and Fig. 5.6 represents chemical quenching CH_3NO_2 which are used to vary

the detection efficiency. We were able to identify the lower part of the curve (with negative slope) as the one in which our measurements were made. When looking at the parts with high TDCR values, one can also identify a region where small changes of the TDCR parameter result in huge changes of the corresponding counting efficiency.

Figure 5.7 corresponds to the optimization of kB value. We studied the influence of varying kB on the activity concentration and efficiency values. In the four graphics, activity concentration versus efficiency for three values of kB (0.11, 0.12, and 0.13) mm/MeV are represented. The evaluation was carried out for the two scintillation cocktails and type of vials used. Optimal kB value corresponds to the line with least slope.

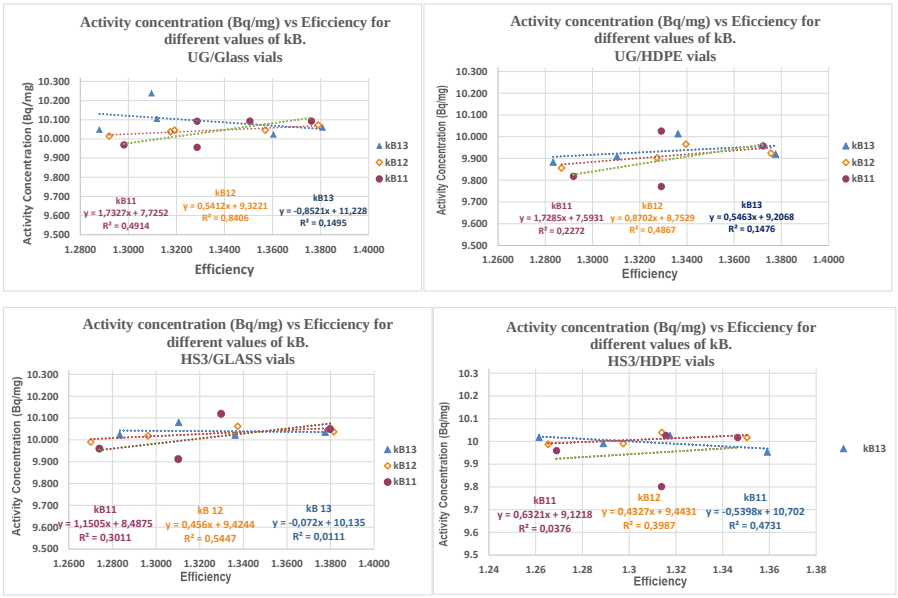

Figure 5.7: The influence of varying kB (0.11, 0.12 and 0.13) mm/MeV on the Activity concentration and efficiency values.

5.4 Activity measurement of ^{99m}Tc

CIEMAT measured and standardized ^{99m}Tc to calibrate the activity measurement form ISODER SA (Portugal). Technetium-99m is extensively used for diagnostic imaging, with more than 20 million medical scans performed annually using this radionuclide. ^{99m}Tc decays purely by isomeric transition to ^{99m}Tc, with a half-life of $T_{1/2} = 6.0067(10)$ h [240]. ^{99m}Tc is used in 80% of diagnostic nuclear medicine procedures. The majority of nuclei (99.0 (4) %) decay through the 2.1726(35) keV $\gamma_{2,0}$ transition. Internal conversion (IC) dominates the $\gamma_{2,1}$ transition (total internal conversion coefficient $\alpha_{2,1T} = 135(4) \times 10^8$ giving rise to conversion electrons with energies between E= 1.63- 2.17 keV. Internal conversion is also present in the $\gamma_{1,0}$ ($\alpha_{1,0T}$= 0.119(3)) and $\gamma_{2,0}$ ($\alpha_{2,0T}$= 40.9(8)) transitions with significantly higher conversion electron energies of E= 119.5 - 140.5 keV. In addition, X-rays in the energy ranges 2-3 keV and 18-21 keV, as well as Auger electrons in the energy ranges 1.6-2.9 keV and 14-21 keV are emitted due to electron rearrangement as shown in Fig. 5.8 [240].

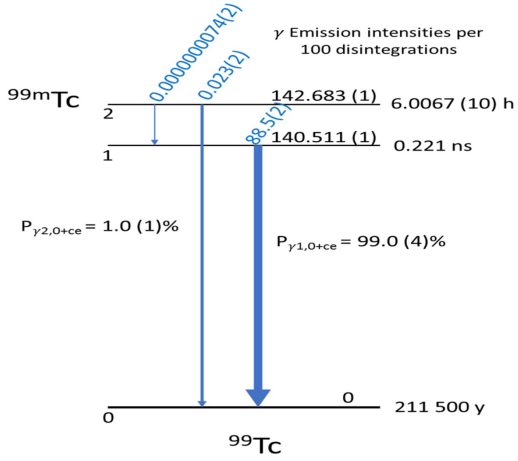

Figure 5.8: Decay scheme of ^{99m}Tc.

The solution of the ^{99m}Tc in a standard syringe volume is arrived to CIEMAT with the activity of 2 mCi. CIEMAT activimeter IG11 is used as a reference measurements to compare the measurements of the the radionuclide solution in the syringe, then compare it with the activimeter of the ISODER center. After that, a sample of 3.1745 mg of the ^{99m}Tc standard solution added to 15ml UG in 20 ml glass vial prepared for the activimeter. Then, three samples of ^{99m}Tc with masses (43.1889, 21.2786 and 23.2060) mg are prepared for the customer-built TDCR counter at CIEMAT at reference date of 1^{st} March 2022 at 14:26 UT. ^{99m}Tc solution was added to 20 ml of glass vials containing 15ml of Ultima Gold scintillation cocktail. For each vials the measurements repeated several times in order to have very accurate results on 3^{rd} March 2022 at 13:35 UT. To measure the background a blank sample is prepared with the volume described above without the radioactive solution. Sources for all standardization methods were prepared by the pycnometer technique using a Mettler-Toledo MX5 balance. The average value of the activity concentration (Ac) of ^{99m}Tc using TDCR method is 14119.00$\pm$0.53 Bq/mg at reference date. While the activity concentration 14153.41$\pm$0.48 Bq/mg using CIEMAT activimeter at the same reference date with $\Delta\%$ = 0.2.

Table 5.1: Activity measurements of ^{99m}Tc using customer-built TDCR method at CIEMAT-Madrid on 03/03/2022 at 13:35 UT.

Vial	Mass(mg)	TDCR value	Activity (Bq)	Ac. (Bq/mg)
1	43.1889	0.7181	2624.88	14186.68
2	21.2786	0.7124	1234.29	14289.64
3	23.2060	0.7126	1250.79	13880.68
Average	29.2245	0.7143	1703.32	14119.00

Table 5.2: Activity measurements of ^{99m}Tc using activimeter IG11 method at CIEMAT-Madrid on 03/03/2022 at 13:35 UT.

Mass of ^{99m}Tc (mg)	Activity (Bq)	Ac (Bq/mg)
3.1745	44.93	14153.41

5.5 Activity measurement of ^{68}Ga

Gallium-68 is one of the earliest of the positron-emitting radionuclides to have been applied to clinical medicine, dating back to the early 1960s [255]. ^{68}Ge decays by pure electron capture with the half-life of 270.95 days. The daughter nuclide ^{68}Ga disintegrates to the ground state of ^{68}Zn partially by positron emission (89.1%) with a maximum energy of 1899.1 keV, and partially by electron capture (10.9%). Most decay events lead to the emission of annihilation radiation. A simplified decay scheme is shown in Fig. 5.9. Due to its short half-life (67.83 (20)) min [9], ^{68}Ga is a useful radionuclide for PET. It provides a non-invasive method for the quantitation of blood flow and metabolism in patient studies for diagnosis and for research of disease states. ^{68}Ga also has important medical applications for neuroendocrine tumors. It is advantageous to have short-lived positron emitters to minimize the radiation exposure to the patient, and at the same time it have high enough activity to receive adequate statistical sampling in the reconstructed cross-sectional image.

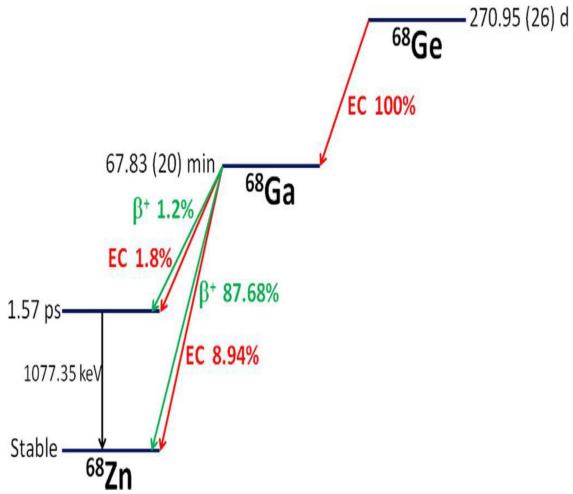

Figure 5.9: Decay scheme of ^{68}Ga.

A purified solution of ^{68}Ga was obtained by elution from a ^{68}Ge generator in HCl form at CIEMAT. Gamma spectrometry measurements were also taken to check for impurities and showed no traces of contaminants as could be expected for a solution obtained from a generator. Sources for all standardization methods were prepared by the pycnometer technique using a Mettler-Toledo MX5 balance. Three samples of ^{68}Ga from the original solution with masses between 21.06, 21.16 and 44.60) mg were added to glass vials containing 15ml of Ultima Gold scintillation cocktail prepared for the HIDEX 300-SL method. Background is measured by preparing a blank sample with the volume described above without the radioactive solution. Measurements were carried out with a HIDEX 300-LS counter, with counting times of 5 min per vial. The detection efficiency is calculated. Efficiency calculation was carried out by a Monte Carlo simulation program using data from the NUCLEIDE database [240]. Activity concentration for ^{68}Ga at the reference time was 8800.46 $\pm$0.78 Bq/mg. The specific activity for ^{68}Ga measured by activimeter (IG11) at CIEMAT. A 15 ml UG as a liquid scintillator in 20 ml borosilicate glass vial source weighing about 4.8874 mg was prepared directly from the mother solution. The specific activity for ^{68}Ga measured by the activimeter is 8708.11 $\pm$ 0.25 Bq/mg, with deviation about 1.05%.

Chapter 6

ENEA portable $4\pi\beta\,(LS) - \gamma$ coincidence detection system

6.1 Introduction

The $4\pi\beta - \gamma$ coincidence counting technique has been a powerful and widely used method for radionuclide standardization and to measure the absolute activity concentration of radionuclides [256, 133, 135]. The radionuclide activity can be measured using a direct activity measurement method, without any quenching indicating parameter and the detection efficiency without reference standard [257]. Among the currently available methods of radionuclides activity measurement, the coincidence counting technique is one of the most widely utilized in any of its variants [129, 133, 135]. This technique is formulated on the synchronized detection of two different radiations come from the same nuclear decay process. The $4\pi\beta - \gamma$ counter is used in primary metrology institutes (PMI) for primary activity measurements. The direct measurement of activity concentration can be performed for radionuclides decaying via pure β, EC, $\beta - \gamma$, $EC - \gamma$, and $X - \gamma$ without making any assumptions about the values of the detector efficiencies, branching ratios, or decay scheme parameters [258]. The principles and theory of the $4\pi\beta - \gamma$ coincidence counting method, as well as the corrections are required, and they are well understood. Nevertheless, its difficult to apply these principles to

actual measurements. Attempts to improve the accuracy and the precision of $4\pi\beta-\gamma$ coincidence counting have been ongoing for decades. Grigorescu studied the accurate fulfilment of the γ-ray channel linearity conditions [151].

Campion wrote the first and most the well-known paper that explained the $4\pi\beta-\gamma$ coincidence counting [133]. Campion showed that a $4\pi\beta-\gamma$ coincidence system principally made up of two detectors; beta and gamma detectors and an electronic unit to generate coincidence pulse by detecting synchronised gamma and beta pulses which come from the same nuclear disintegration. He demonstrated that the accurate measurement of $\beta-\gamma$ emitting radionuclides can be achieved by using the β- detector which has 4π geometry for the coincidence method, because most of the corrections are small. It is anticipated that the γ-detector responds only to γ-rays, the β-detector responds only to β-particles, and the coincidence channel records only the simultaneous pulses come from the two detectors (true coincidences) [133].

This techniques has been the focus and subjects of many papers and comprehensive reports [87, 258] since the publications of Dunworth [129] and Campion [133]. The fundamental principle of coincidence counting can be illustrated through the prototypical case of the activity measurement of a radionuclide with a simple decay-scheme consisting of an β-emission followed directly by a γ-ray from the de-excitation of the daughter radionuclide or annihilation process. The basis of the coincidence technique comes from the additional coincidence channel, which records the disintegration pulses come from both β- and γ-counters.

The activity of electron capture emitter radionuclides can be measured using $4\pi\beta-\gamma$ coincidence counting technique, where beta efficiency is measured for the Auger electrons and X-rays associated with the process of the electron capture. The standardisation of a wide range of radionuclides can be measured using the original $4\pi\beta-\gamma$ coincidence counting and its extended techniques [134]. Most laboratories have used a proportional counter in the β-channel for a long time to standardise radionuclides using the $4\pi\beta(PC)-\gamma$ coincidence method such as Laboratoire National Henri Becquerel (LNHB) and Physikalisch-Technische Bundesanstalt National metrology institute (PTB) [191, 252]. $4\pi\beta-\gamma$ coincidence system has been updated by replacing the proportional counter

with the liquid scintillation (LS) counter as a beta counter. This new coincidence counting system has been developed and improved in metrology laboratories. $4\pi\beta(LS) - \gamma$ coincidence counting system had already been implemented [259, 260, 261], but the goal was to have a complete TDCR counter as the β-channel [183, 234]. TDCR especially developed for standardization of pure β- and pure electron capture emitters, and it can be extended to simple $\beta - \gamma$ and $EC - \gamma$ emitter radionuclides.

6.2 Principles of the $4\pi\beta - \gamma$ coincidence Method

In the case of the ideal form, the $4\pi\beta - \gamma$ coincidence technique only can be applied to the standardization of radionuclides with simple decay schemes. In the simple decay scheme the β-emission is followed by coincident gamma ray, and it is supposed that gamma counters only respond to γ-ray and beta counters to β radiation. Additionally, the simultaneous pulse emission comes from both detectors only recorded by the coincidence channel [85]. The detection efficiency ε_β and ε_γ for a point source with activity n_0 is

$$n_\beta = n_0 \varepsilon_\beta \tag{6.1}$$

$$n_\gamma = n_0 \varepsilon_\gamma \tag{6.2}$$

$$n_c = n_0 \varepsilon_\beta \varepsilon_\gamma \tag{6.3}$$

where n_γ, n_β , and n_c are the counting rates of gamma, beta, and coincidence channels respectively. The total activity of the radioactivity source N_0 connected to the counting rates, N_β, N_γ, and N_c by the following expressions

$$N_\beta = N_0 \bar{\varepsilon}_\beta \tag{6.4}$$

$$N_\gamma = N_0 \bar{\varepsilon}_\gamma \tag{6.5}$$

$$N_c = N_0 \overline{\varepsilon_\beta \varepsilon}_\gamma \tag{6.6}$$

where the average values of the basic efficiencies are $\bar{\varepsilon}_\beta$ and $\bar{\varepsilon}_\gamma$. The counting efficiencies for the whole sample ε_β and ε_γ can be obtained by integrating over the surface of the sample. However, Putman [262] showed that when at least one of the detectors has the same efficiency over the whole sample, the mean value of the product $\overline{\varepsilon_\beta \varepsilon}_\gamma$ corresponds with the

product of total efficiency. The gamma detectors meet this requirement. For that reason

$$N_\beta = N_0\varepsilon_\beta \tag{6.7}$$

$$N_\gamma = N_0\varepsilon_\gamma \tag{6.8}$$

$$N_c = N_0\varepsilon_\beta\varepsilon_\gamma \tag{6.9}$$

Therefore, the activity N_0 of the radionuclides can be calculated using the following expression at zero level of approximation, it depends only on the counting rates in the beta detector N_β and gamma detector N_γ, and the coincidence counting rate detected by the both detectors N_c :

$$N_0 = \frac{N_\beta \cdot N_\gamma}{N_c} \tag{6.10}$$

The aforementioned formula illustrates how the activity of a radioactive source may be determined without knowing either the detector efficiencies ε_β and ε_γ.

Since beta detectors are often sensitive to gamma radiation, the gamma radiation detection efficiency must be included in the above expression $\varepsilon_{\beta\gamma}$. The gamma photon must not coincide with a beta particle in order to be detected as a beta count. The probability of non-detecting beta particle is $(1-\varepsilon_\beta)\times\varepsilon_{\beta\gamma}$. One can obtain the probability of counting a gamma ray in the beta detector. Then, the above equations lead to the following results

$$N_\beta = N_0\left[\varepsilon_\beta + \left(1-\varepsilon_\beta\right)\varepsilon_{\beta\gamma}\right] \tag{6.11}$$

$$N_\gamma = N_0\varepsilon_\gamma \tag{6.12}$$

$$N_c = N_0\varepsilon_\beta\varepsilon_\gamma \tag{6.13}$$

The activity of the sample can be determined by this equation

$$\frac{N_\beta N_\gamma}{N_c} = N_0\left[1+\frac{\left(1-\varepsilon_\beta\right)}{\varepsilon_\beta}\varepsilon_{\beta\gamma}\right] \tag{6.14}$$

N_0 can be obtained directly from the measured count rates N_β, N_γ, and N_c in the ideal case. The efficiencies ε_β and $\varepsilon_{\beta\gamma}$ should be known. One can solve this equation by connecting ε_β and $\varepsilon_{\beta\gamma}$ with count rates N_β, N_γ, and

N_c respectively. Typically, various values are taken for these quantities, ε_β and $\varepsilon_{\beta\gamma}$, and extrapolate to calculate activity N_0.

Additionally, there might be internal conversion (IC) in a gamma transition. The beta counter is influenced by the internal conversion of gamma transitions. This means that the internal conversion is contributed to the beta detector when the coincident β-particle is not detected with a count rate n_{ec}. Then

$$n_{ec} = N_0 \left(1 - \varepsilon_\beta\right) \varepsilon_{ce} \frac{\alpha}{1+\alpha} \tag{6.15}$$

where α is the total internal conversion coefficient and ε_{ce} is the probability of the conversion electrons detected in the beta detector. Usually, the efficiency of the converted electrons is 100%, because the energy is almost high. In the case of low energy converted electrons the detection of Auger electrons and X-rays is compensated for the converted electrons with low energy and high detection efficiencies can be obtained. In this case, $\alpha\varepsilon_{ce}$ should be replaced by

$$\sum_i \alpha_i \left[\varepsilon_i + (1 - \varepsilon_i)\varepsilon(X, A)_i\right] \tag{6.16}$$

where ε_i is the beta detector efficiency for conversion electrons of the i-shell, α_i is the internal conversion coefficient of the i-shell, and $\varepsilon(X, A)$ is the probability of at least one detected X-ray or Auger electron in the beta channel as a result of the emission of the conversion electron from the i-shell. Converted electrons can reduce the counts of γ-ray, because internal conversion electron transitions compete with emission γ-rays. Therefore, the counting rates for the γ-ray detection and the coincidence count rates are,

$$N_\gamma = N_0 \frac{\varepsilon_\gamma}{1+\alpha} \tag{6.17}$$

$$N_c = N_0 \frac{\varepsilon_\beta \varepsilon_\gamma}{1+\alpha} \tag{6.18}$$

where ε_γ is the γ-ray intrinsic efficiency. It is supposed that the emitted X-rays from internal conversion, are not detected in the gamma counter by relevant energy discrimination.

In addition, the interaction of β-particles in the gamma counter in the $4\pi\beta(LS) - \gamma$ coincidence detection system can be neglected, because the

walls of the vial in the LSC stop β-particles to reach the gamma detector. In the case of high energy beta particles, the bremsstrahlung occurs and will interact with the gamma detector. Campion studied this problem [133], he showed that errors due to this process can be neglected when the efficiency of beta detector approaches 100%. On the other hand, by adjusting the gamma detector threshold properly, this issue may be completely avoided [133].

6.3 Experimental setup of ENEA $4\pi\beta\,(LS)-\gamma$ coincidence counting system

Italian National Institute of Ionizing Radiation Metrology (INMRI) belongs to (ENEA) in collaboration with Catania University, Istituto Nazionale di Fisica Nucleare (INFN)- Catania section and Costruzioni Apparecchiature Elettroniche Nucleari (CAEN) developed a new in-situ coincidence system for activity measurement for short half-life radionuclides used in nuclear medicine which is called $4\pi\beta\,(LS)-\gamma$ coincidence counting system. The portable TDCR counter owned by ENEA-INMRI is extended at ENEA-INMRI to $4\pi\beta\,(LS)-\gamma$ coincidence system by implementing a cylindrical-type Scionix Standard 51B51/2M NaI(Tl) scintillation detector as a gamma counter. The NaI(Tl) scintillation detector consists of a scintillation material integrally coupled to a photomultiplier tube. The NaI(Tl) scintillation detector with the $(3'' \times 3'')$ crystal dimension includes a 14 pins photomultiplier with in (0.4 mm) thick aluminium housing inserted into the bottom of the TDCR counter as shown in Fig. 6.1. The new ENEA portable $4\pi\beta\,(LS)-\gamma$ coincidence system can be used in environmental applications and in nuclear medicine laboratories of the hospitals to measure the activity of a radiopharmaceutical injected into patients, such as ^{18}F,^{11}C or ^{131}I. The schematic configuration of the new ENEA portable $4\pi\beta\,(LS)-\gamma$ coincidence counting system is shown in Fig. 6.2.

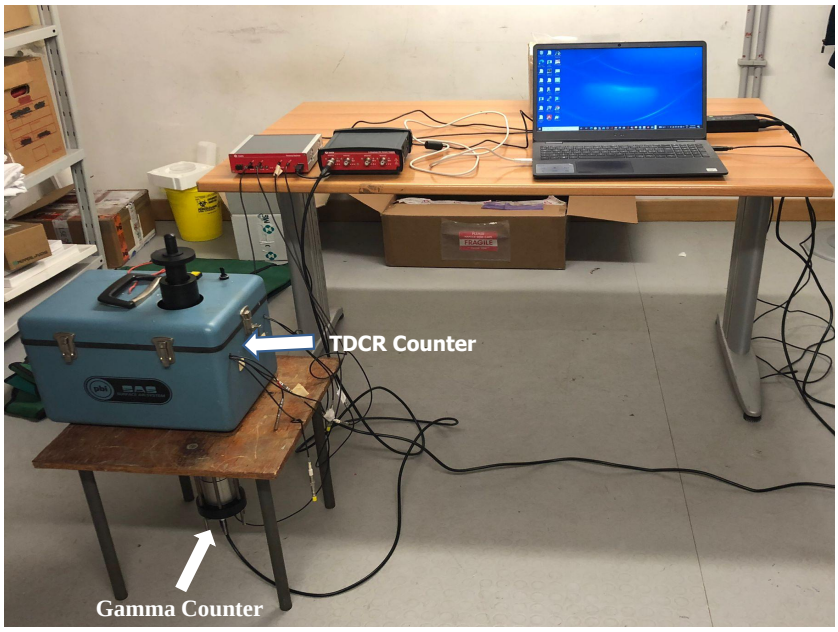

Figure 6.1: Experimental setup of ENEA portable $4\pi\beta\,(LS)-\gamma$ coincidence system.

6.4 $4\pi\beta\,(LS)-\gamma$ data analysis software

The $4\pi\beta\,(LS)-\gamma$ coincidence system is directly linked to the CAEN DT5720 digitizer. As we mentioned it in the chapter three, the CAEN DPP- CI Control Software remotely controls the digitizer. The acquisition parameters such as (gate length, DC offset, pulse polarity, threshold level, etc.) can be set independently for each channel to configure the hardware, and perform the data readout. In order to perform a $4\pi\beta\,(LS)-\gamma$ analysis on the collected event lists coming from the TDCR detector and the gamma detector, a customized TDCR DAQ software has been updated and modified. The CAEN data analysis software for $4\pi\beta\,(LS)-\gamma$ coincidence system (TDCRGamma) is customised. The software is written in C language and designed for off-line implementation of $4\pi\beta-\gamma$ coincidence counting method. Since all the acquisition channels of a digitizer are synchronized, it is possible to correlate events from different input channels comparing their TTTs.

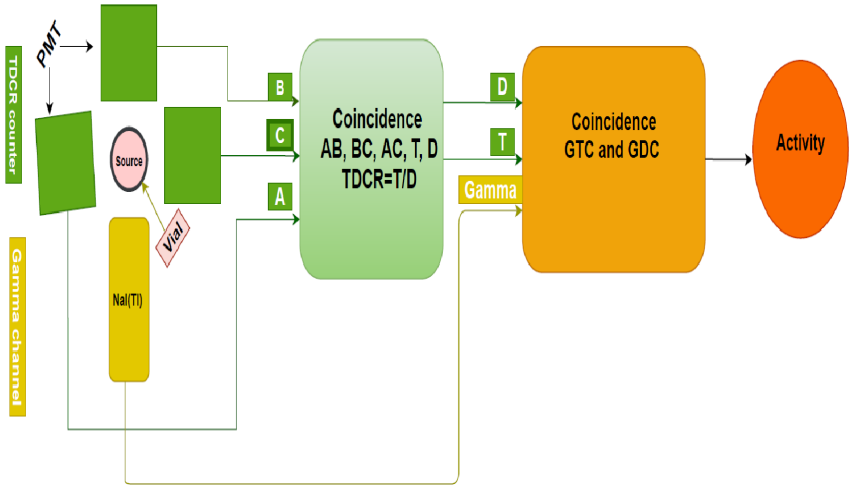

Figure 6.2: The schematic configuration of $4\pi\beta\,(LS)-\gamma$ coincidence system available at ENEA.

Once the run is over, at the first, the CAEN TDCR DAQ software scans the resulting event lists looking for coincidences between the events come from the beta channels in the TDCR counter. Afterwards, the two output files are created for both Triple N_T and Double N_D coincidences data inside the CAEN TDCR code and they are saved as a (ASCII file or binary file). These two outputs files are used as input files for the CAEN TDCRGamma code. Then, the $4\pi\beta\,(LS)-\gamma$ (CAEN TDCRGamma) DAQ software scans the resulting event lists looking for coincidences between gamma channel and beta channel (Triple and Double coincidences) output files in the TDCR counter as shown in Fig. 6.3.

This data subset from TDCR counter is used together with the set of data coming from the gamma channel. The set of events in the β-channel which are time correlated with the gamma event are taken into account. One can select the γ-energy window close to the full-energy peak of the γ-ray for the gamma channel.

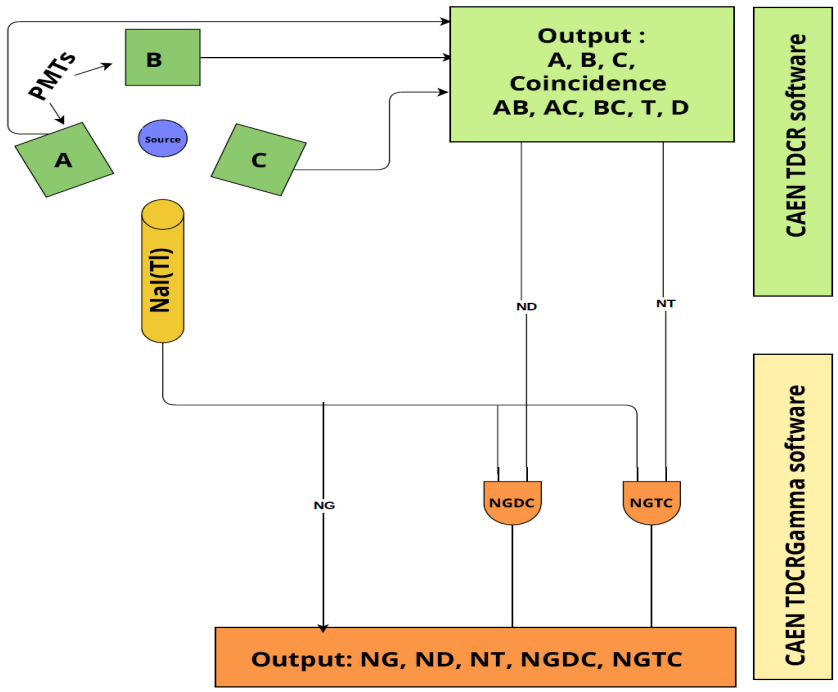

Figure 6.3: $4\pi\beta\,(LS) - \gamma$ coincidence system configuration.

Furthermore, the code will look for the event coming from the beta counter and gamma counter by looking to the minimum TTT of each events in double or triple coincidences data output files in β-counter and gamma counter to create a new coincidence window. In other word, lets assume τ_γ and τ_β are the minimum TTT of gamma and beta events respectively, and ω is the coincidence window. Moreover, if $\tau_\gamma < (\tau_\beta + \omega)$, this means that there is a coincidence between gamma channel and beta channel, otherwise there is no coincidence between the events coming from the both detectors.

Following this, the TDCRGamma software takes the minimum TTT event into account as one set of the data in the beta coincidence window

in the triple and double coincidence data files. Thus, it starts looking for coincidences with events in the gamma counter and extending the coincidence window until the event is found in the gamma channel as shown in Fig. 6.4.

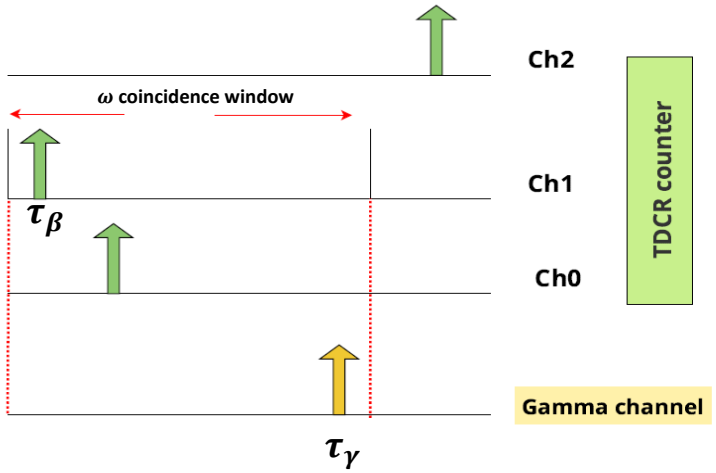

Figure 6.4: Coincidence time management for $4\pi\beta\,(LS)-\gamma$ coincidence system.

Finally, TDCRGamma software will compare the TTT for all the acquisition from the three input channels (gamma channel and the two output files from beta channel). Subsequently, the TTT for each selected event in coincidence in the TDCR counter and gamma channel will be saved. This intimates that the coincidence window for the new $4\pi\beta\,(LS)-\gamma$ coincidence system starts from the minimum time of measuring the first event in files in the beta channel until the event in the gamma channel is measured. The new time coincidence window for $4\pi\beta\,(LS)-\gamma$ coincidence system is longer than the time coincidence window of the TDCR system, because in the $4\pi\beta\,(LS)-\gamma$ coincidence system two different types of scintillator detectors are used: the organic liquid scintillation detector as a beta counter and the inorganic scintillation detector as a gamma counter.

Liquid scintillation detectors have fast light response about (3-4) ns while NaI(Tl) has slow light response more than (40- 50) ns [263]. The dead-time of the TDCR counter is longer than the selected dead-time for the gamma channel, in order to eliminate the after-pulses in the liquid scintillation counter. The recorded data stream is then analysed by the CAEN TDCRGamma analysis software. Moreover, the DAQ software implements the same algorithms of the well-known MAC3 analog module emulating its operations in terms of coincidence definition and extendable-type dead time management [188]. In particular, the CAEN TDCRGamma software ignores all those events found in the lists whose TTTs lie in a dead time window; the dead time is then extended according to the MAC3 logic [188]. As a result of this analysis, the new CAEN TDCRGamma DAQ software can provide the counting from the three channels, the single count rate, N_G, from gamma channel, the triple N_T and the logical sum of the double N_D coincidences, from beta channels, the coincidences between gamma channel with double coincidence in beta channel N_{GDC} and the coincidences between gamma channel with triple coincidence in beta channel N_{TDC} will be measured as well as real-, dead-, and live-time as shown in Fig. 6.3. The activity of the radionuclides can be measured, at the "zero order approximation", by using the conventional formula of the $4\pi\beta\,(LS) - \gamma$:

$$A = \frac{N_G \cdot N_D}{N_{GDC}} \equiv \frac{N_G \cdot N_T}{N_{GTC}} \tag{6.19}$$

Another important feature of DAQ TDCRGamma software is: the new software is able to run the $4\pi\beta\,(LS) - \gamma$ detection analysis both online or off real-time measurements and previously acquired data. This makes it possible to perform a parameter sweep analysis repeating the $4\pi\beta\,(LS) - \gamma$ detection technique on the same data set changing automatically for example the coincidence resolving time and/or dead time. It is possible, therefore, to study the behaviour of the results obtained with different parameter values applying them on the same data, without repeating the measurements several times and just by changing the parameter values in the software configuration, with no hardware operations.

Independently from CAEN, another TDCR analysis software was developed at ENEA-INMRI by implementing the MAC3 philosophy described in the CERN ROOT frame work, an object-oriented package for

physics analysis. The algorithm for the TDCR coincidence analysis was then developed by following the main idea described by Bouchard and Cassette [188] corresponding to the MAC3 "philosophy" and by taking into account the powerful CERN ROOT resources for analyzing data coming from complex detectors. Both codes can run either on Windows or Linux machine. The results obtained by the two software have been compared by measuring a standard solution of ^{18}F and ^{99}Tc with TDCR parameter by using CAEN software and ENEA software. The typical TDCR value obtained in these measurements with corresponding efficiency for logical sum of double coincidences and for triple coincidences of for both CAEN and ENEA analysis software as shown in the table 6.1. A coincidence window of $t_c = 140\ ns$ and a dead-time 50 μs were applied on the set of recorded data to perform TDCR analysis by using both software for ^{18}F. While the coincidence window of $t_c = 140\ ns$ and a dead-time 40 μs were applied on the set of recorded data to perform TDCR analysis by using both software for ^{99}Tc. The deviation in percent between the TDCR parameter $TDCR_{CAEN}$ computed by CAEN code and $TDCR_{ENEA}$ computed by ENEA code for both sources. In summary, it can be said the that both code work properly to analyse the data come from the TDCR counter. Therefore the described portable system made of digitizer, DPP and dedicated software is able to perform a complete data acquisition of the signals coming from a TDCR, providing a charge value and a trigger time tag of each pulse; the TDCR analysis can be run on the resulting data set providing also spectroscopic information of the measured sample.

Table 6.1: TDCR values for radionuclides ^{18}F and ^{99}Tc by using CAEN software and ENEA software code.

Radionuclide	**Software**	N_D	N_T	**TDCR**
^{18}F	**CAEN**	2693230	2673821	0.9928 ± 0.03
	ENEA	2693096	2673695	0.9928 ± 0.03
	$\Delta\%$	0.7126	0.005	0.00
^{99}Tc	**CAEN**	858268	812794	0.9470 ± 0.05
	ENEA	858344	812898	0.9470 ± 0.05
	$\Delta\%$	0.0088	0.012	0.00

Table 6.2: Activity measurements of radionuclides ^{18}F using TDCR and $4\pi\beta(LS)-\gamma$ methods.

radionuclide	**Method**	**Activity(Bq)**
^{18}F	TDCR	41379.69 ± 0.15
	$4\pi\beta(LS)-\gamma$	41777.06 ± 0.13
	$\Delta\%(4\pi\beta(LS)-\gamma-TDCR)$	0.09%

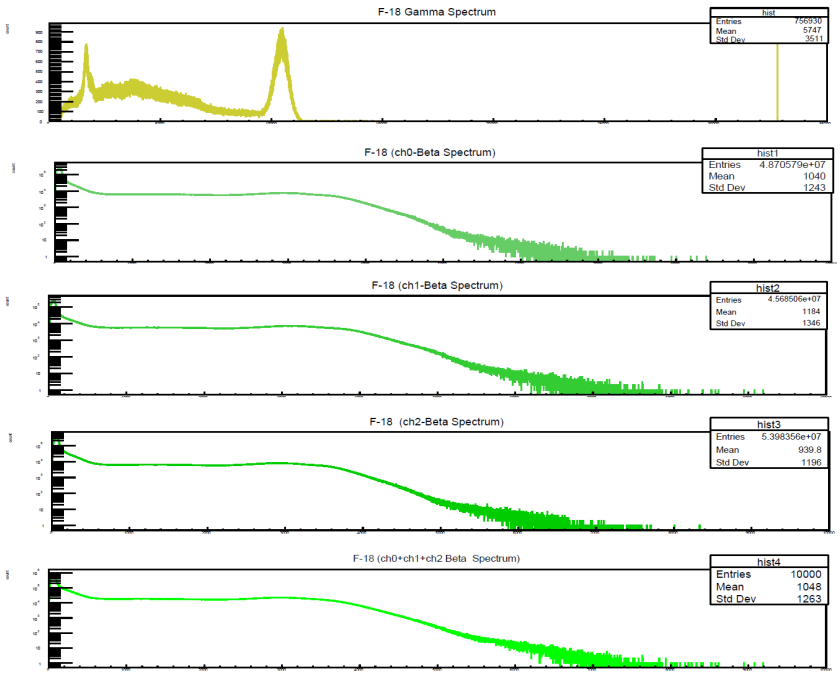

Figure 6.5: Beta and gamma Spectrum of^{18}F in $4\pi\beta(LS)-\gamma$ coincidence system.

At the same time, the activity of ^{18}F is calculated using conventional equation of $4\pi\beta(LS)-\gamma$ coincidence system Eq.6.10 without any knowl-

edge of the detection efficiency of the detectors. The γ-energy window close to the full-energy peak about 511 keV of ^{18}F for the gamma channel is selected. Table 6.2 shows that the ^{18}F activity obtained by both CAEN TDCR and $4\pi\beta(LS)-\gamma$ DQA methods is measured with a minimum deviation less than 1% between the two methods. The measurement with TDCR with uncertainty 0.5% taking into account all the aspects of the uncertainty not only the statistical uncertainty, but also the uncertainties concerning the decay model, background measurements, coincidence resolving time, dead-time, decay during measurement, decay at the reference date. The good agreements between the two methods confirms that CAEN $4\pi\beta(LS)-\gamma$ (TDCRGamma) data analysis software developed for in-situ $4\pi\beta(LS)-\gamma$ coincidence system at ENEA operates correctly.

6.5 In-situe activity measurement of ^{131}I

One of the earliest radionuclides utilised in medicine was radioactive iodine. Therefore it has been used for more than 60 years in diagnose, treat thyroid disease and thyroid cancer [264]. It is taken up and incorporated in the same way as nonradioactive iodine by the thyroid gland [264]. Iodine is necessary for the thyroid to operate normally and forms an integral part of the thyroid hormones thyroxine (T4) and triiodothyronine (T3).

Iodine is actively transferred directly into thyroid cells and organified in the colloid, supplying substrate for the production of thyroid hormone [265]. Radioiodine is administered as the iodide ion orally, it can be easily absorbed from the gastrointestinal tract and allocated in the extracellular fluid. Radioiodine is condensed in the thyroid, salivary glands, and gastric mucosa. In the normal thyroid, the trapped iodide is organified and has an effective half-life of about 7 days; in hyperthyroidism, its half-life decreases to 3–5 days. While, in thyroid cancer sometimes is lower than 3 days.

There are 53 protons and 78 neutrons in ^{131}I radionuclide. The half-life of ^{131}I is very short about eight days with beta and gamma radiation, This indicates that it takes months to decays almost in the environment [266]. When decaying, ^{131}I most frequently (89 percent of the time) with

971 keV of decay energy transforms into the stable Xenon (^{131}Xe) in two stages, gamma emits directly after beta decay as shown in the following equations [265].

$$^{131}_{53}I \rightarrow ^{131}_{54}Xe^{*} + \beta^{-} + \nu_{e}^{-} + 606\ keV \tag{6.20}$$

$$^{131}_{54}Xe^{*} \rightarrow ^{131}_{54}Xe + \gamma + 364\ keV \tag{6.21}$$

Therefore, beta particles are the main emissions of ^{131}I decay with a maximum energy of 606 keV with 89.6% abundance and 364 keV γ-rays with 81.5% abundance as illustrated in Fig. 6.6. As usual in this process, an antineutrino is also produced via beta decay, which carries off a quantity of energy of the beta decay. The colour blue in Fig. 6.6 denotes the

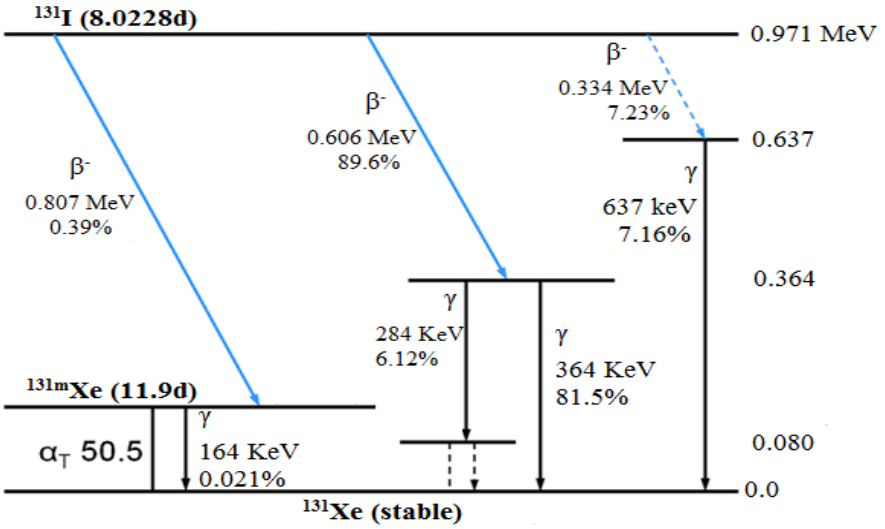

Figure 6.6: ^{131}I decay scheme

^{131}I decaying by β-emission. ^{131}I emits several β-particles with different endpoint energies. There has not been evidence of a direct transition to

the ground state of the daughter radionuclide ^{131}Xe. Transitions happen through the daughter nuclide's excited states and with a very low probability of 0.39% via the metastable ^{131m}Xe, which has a half-life of 11.9 days. The energy difference between this metastable state and the ground state is 164 keV, and the conversion of electrons is mostly emitting as a result of the disintegration of ^{131m}Xe to the ground state. Additionally, weak transitions in the ^{131}I scheme are denoted by dotted lines [265].

6.5.1 ^{131}I Sample preparation

For the measurements of ^{131}I presented in this project, the master solution of ^{131}I was provided by the nuclear medicine laboratory at the Ospedale Pediatrico Bambino Gesù (OPBG) in Rome, Italy. Then the OPBG dose calibrator was used in the Nuclear Medicine department of this Hospital for routine measurements of the ^{131}I. Two sample sources were prepared with 15 ml of Ultima Gold scintillator in 20 ml glass vials and 0.1 ml biological water to dilute the activity of the used master solution. A drop of about 0.03311 g and two drops of about 0.0665 g of the ^{131}I master solution were added to the 15 ml UG scintillation cocktail in the first and the second sample, respectively. An additional sample with 15ml of Ultima Gold scintillator without radioactive solution, was prepared for background measurements. The masses of all the samples as well as the dilution factor were determined gravimetrically using Mettler balance. The solutions were stored in the dark place for one or two hours in order to decrease the photoluminescence effect and the background noise; for that reason the solution cocktails were held in aluminium sheet.

6.5.2 Experimental measurement

The portable $4\pi\beta\,(LS)-\gamma$ coincidence system has been used directly at the Ospedale Pediatrico Bambino Gesù (OPBG) hospital in Rome, Italy to measure the activity of ^{131}I.

$4\pi\beta\,(LS)-\gamma$ coincidence system is directly linked to the CAEN DT5720 digitizer without using any preamplifier. Firstly, the correct working parameters for the new ENEA $4\pi\beta\,(LS)-\gamma$ coincidence system were set. In this case, the SEP is recorded without any vial inside the optical chamber

in order to equalise the response of each single PMT of the TDCR counter. The DT5720 digitizer was equipped with the PMTs biased around 900 V for the TDCR counter and 800 V for gamma channel. For each individual channel, the control software of the digitizer is used to discriminate the threshold and the width (typically 24 ns) of the ADC gate, in order to minimise the noise and to have the whole analog pulse coming from the PMT covered completely in time by the gate pulse [208]. In order to match the PMTs in TDCR counter for having the same gain in the three different channels, the digitizer was applied in the histogram mode or, in other words, the three SEPs should be located at the same channel in TDCR counter [189].

The NaI(Tl) detector is calibrated at ENEA-INMRI before being used for radiation detection to convert channel scale to energy scale. The shape, energy, and efficiency calibration of the NaI(Tl) detector was a method used occasionally to establish the connection between the energy of the radiation, the channel number, and the detector efficiency. Table 6.3 illustrates the typical energy and shape calibration of the amplitudes from standard (^{60}Co,^{241}Am,^{56}Mn,^{166}Ho,^{177}Lu, and ^{137}Cs) radioactive point-like sources which are used for calibration. Radioactive point-like source was positioned close to the detector. Figure 6.7 indicates the calibration curve for NaI(Tl) used in the ENEA portable $4\pi(LS)-\gamma$ detection system.

Table 6.3: Gamma photopeaks and channels number for different radionuclide used for gamma detector calibration.

Radionuclide	**Channel**	**E(keV)**
^{137}Cs	12352.9	611
^{241}Am	1149.43	59.5
^{56}Mn	15324.7	846.8
^{166}Ho	1619.72	75.95
^{177}Lu	2323.94	113.84
	4084.51	208.56
^{60}Co	22225	1184.5
	25284	1349.07

The following first-degree polynomial equation shows the relation between the energy and the channel number X

$$E = a + b \cdot X \tag{6.22}$$

where X is the spectral channel number of the center of the peak correlated to the energy E, E is the γ-ray energy photopeak in keV and , while the parameters a= -11.174 and b = 0.0538 are constants, which are calculated by the energy calibration process. By taking into account the value of a and b, one can calculate the calibrated gamma photopeakes(E_{cal}) for ^{131}I as shown in the second column of the table 6.4 and compared with ^{131}I gamma photopeaks provided at LNHB [9](E_{LNHB}) with minimum deviation $\Delta\% = \frac{(E_{cal}-E_{LNHB})}{E_{cal}} \times 100\%$.

Table 6.4: Gamma photopeaks of ^{131}I calculated using calibration curve.

Radionuclide	**Channel**	E_{cal}**(keV)**	E_{LNHB}**(keV)**	$\Delta\%$
^{131}I	1698.37	80.1763	80.185	-0.01
	5492.49	284.2999	284.305	-0.002
	6982.93	364.4857	364.489	-0.0009
	12048.08	636.9907	636.989	0.0002

To perform TDCR analysis both software ENEA and CAEN TDCR analysis software were used as mentioned in previous section. In the both software a coincidence window of t_c= 140 ns and a dead-time 50 μs were applied on the sets of recorded data in TDCR counter. Then, the β counting rate either is defined as the counting rate for the logical sum of double coincidence N_D or as the counting rate for the triple coincidence N_T. The TDCR parameter was 0.9729 using CAEN data analysis software. The TDCR value for both CAEN and ENEA analysis software were measured with $\Delta\%$ = 0.16%. The deviation in percent between the TDCR parameters which are computed by CAEN and ENEA codes for both sources as shown in the table 6.5.

The activity of ^{131}I is determined separately by using TDCR and $4\pi\beta\,(LS)-\gamma$ methods. In the TDCR method one can determine the activity of any

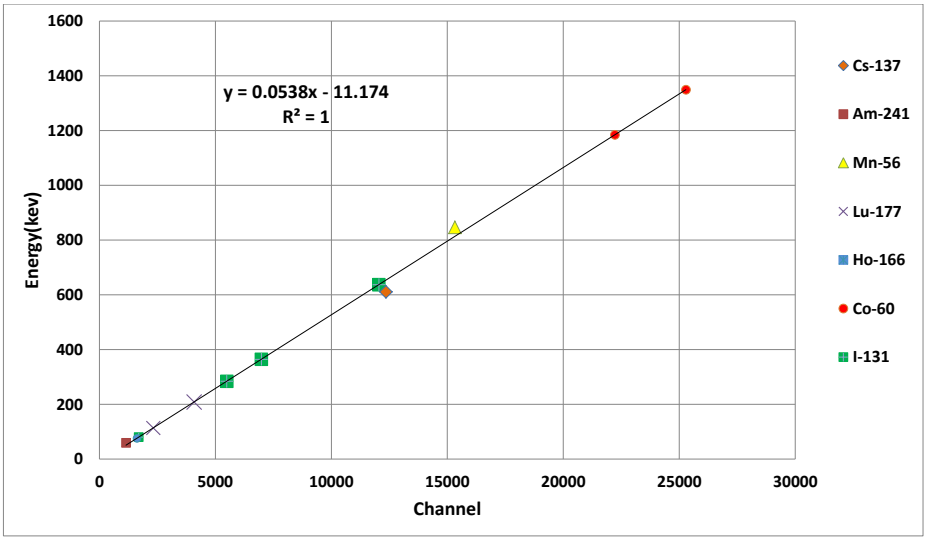

Figure 6.7: The calibration energy curves (measured) using standard point sources (^{60}Co,^{241} Am ^{56}Mn,^{166} Ho,^{177} Lu and ^{137}Cs) with NaI(Tl) detector used as a gamma counter in $4\pi\beta(LS)-\gamma$ coincidence detection system at ENEA.

radioactive source by using the following equation

$$A = \frac{R_c D}{\varepsilon_D} \equiv \frac{R_c T}{\varepsilon_T} \tag{6.23}$$

Where R_cD and R_cT are logical sum of double and triple corrected count rates for ^{131}I respectively. Corrected count rate can be calculated to correct the decay during the measurements by multiply the net count rate of logical sum of double count R_nD and triple count R_nT by correct Factor for R_cD. Another important parameters are the logical sum of double efficiency ε_D and triple efficiency ε_T which can be computed theoretically by using Monte Carlo Simulation GEANT4 code [196]. The activity of

Table 6.5: TDCR values for radionuclides ^{131}I by using CAEN and ENEA TDCR software codes.

Software	N_D **Count rate**	N_T **Count rate**	**TDCR Value**
CAEN	3808983	3699554	0.9729 ± 0.003
ENEA	3809482	3700073	0.9713 ± 0.004
$\Delta\%$	-0.013	-0.014	0.16

^{131}I is 13595 Bq and 13439 Bq with uncertainty less than 1%. The minimum deviation -0.82% and 0.34% using both CAEN TDCR and ENEA TDCR code compare to the nominal activity of ^{131}I measured at OPBG's ionization chamber at the reference date respectively.

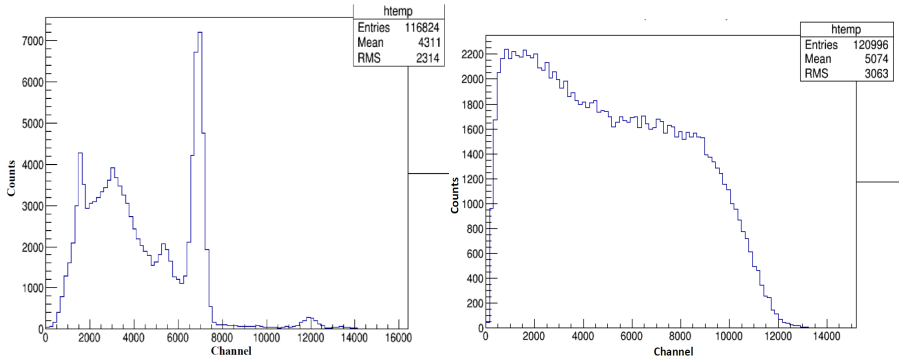

Figure 6.8: Gamma (left) and beta (right) spectrum of ^{131}I.

6.6 Extrapolation curves in the $4\pi\beta(LS)-\gamma$ techniques

The efficiency-extrapolation technique [138] is an important technique associated to the $4\pi\beta-\gamma$ coincidence detection method [133] in radionuclide metrology. Basically, the efficiency-extrapolation technique can be used to correct the counting in the β-channel associated to γ-transition events (γ-ray and X-ray, conversion and Auger electrons). The efficiency-extrapolation technique also is used to prevent systematic biases on activity calculation when the detection efficiency in the β-counter given by $\varepsilon_\beta = N_c/N_\gamma$ does not define the true value. The efficiency-extrapolation technique is completed by detection-efficiency variation in the beta counter. Generally, for each measurement, the determined activities are fitted with a straight-line equation using as a variable an expression depending on N_c/N_γ such as $(1-N_c/N_\gamma)/(N_c/N_\gamma)$. The accurate activity can be calculated by taking the y-intercept corresponding to $N_c/N_\gamma = 1$. Depending on the standardisation radionuclide and the coincidence detection technique being employed [267].

To perform the $4\pi\beta\,(LS)-\gamma$ coincidence system analysis the TTT and charge Q value were recorded with a Gate= 24 ns. The coincidence window of $t_c = 2$ μs and a dead time 10 μs were applied on the set of recorded data comes from the $4\pi\beta\,(LS)-\gamma$ detector system.

In practice, the extrapolation technique is carried out at ENEA by detection efficiency variation in the β-channel (TDCR). In this work ENEA $4\pi\beta\,(LS)-\gamma$ analysis software is used. For that reason, the count rates of the β events for different energy thresholds of beta spectrum N_β, are measured for detection efficiency variation. The γ count rates were measured using γ-window centred on the photopeak of ^{131}I gamma spectrum about 364 keV energy peak, this means that channels form 6000 to 8000 corresponding to the photopeaks 364.49 keV is selected as a gamma window for the photopeak of ^{131}I as shown in Fig. 6.8.

Then, the software records the coincidence events N_c between the selected beta spectrum and the gamma photopeak. The calculated activities are generally fitted with a straight-line equation depending on ε_β such as $\left(1-\varepsilon_\beta\right)/\varepsilon_\beta$. The true activity is determined by taking the y-intercept cor-

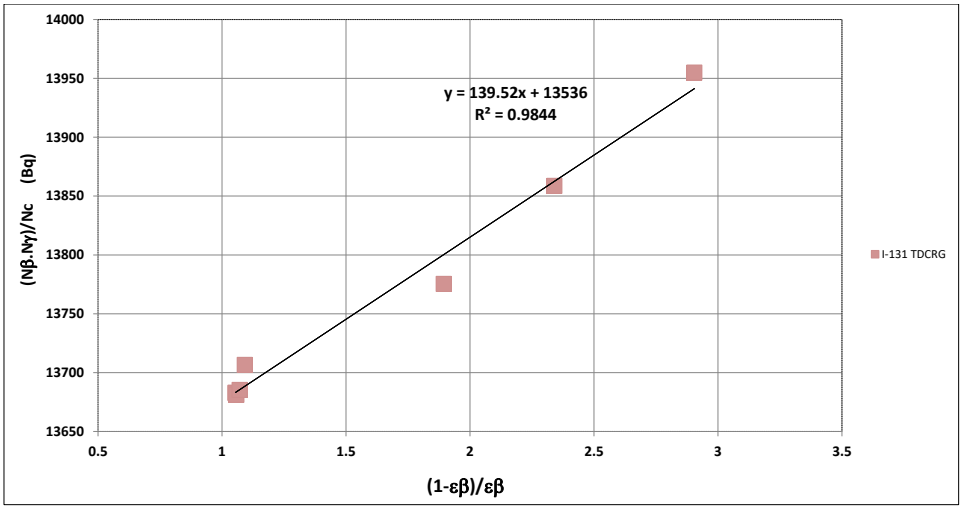

Figure 6.9: The plots of $(N_\beta \cdot N_\gamma / N_c)$ versus $(1-\varepsilon_\beta)/\varepsilon_\beta$ for efficiency variation by changing the threshold of beta spectrum for gamma window 364 keV using ENEA TDCRG software.

responding to $\varepsilon_\beta = 1$ as shown in Fig. 6.9 The activity measured of ^{131}I is 13544 Bq by using the ENEA DQA software for $4\pi\beta\,(LS)-\gamma$ method with the minimum deviation about -0.38% compare to the nominal activity of ^{131}I measured by OPBG ionization chamber. The relative standard uncertainty associated with the activity concentration determined from the sources was estimated at 0.2 %. We describe uncertainties due to measurement variability, extrapolation functions, dead-time and resolving-time effects, gravimetric links, and nuclear and atomic data. Most importantly, a thorough understanding of the measurement system and its response to the decay under study can be used to derive a robust estimate of the measurement uncertainty. The main components that contribute to the uncertainty budget are related to the efficiency extrapolation, statistics

and weighing. The result for using CAEN DAQ code for $4\pi\beta\,(LS) - \gamma$ coincidence still in progress, the analysis needs more deepen study, because it is clear that we used the first order extrapolation method. We are still checking CAEN DQA software for $4\pi\beta\,(LS) - \gamma$. The good agreement between the two methods using ENEA code confirms that the extrapolation method is work correctly.

Conclusions

For the first time portable $4\pi\beta\,(LS)-\gamma$ coincidence system has been used directly as in-situ detection system in hospital to measure the activity of short half-lived radionuclides used in nuclear medicine such as ^{131}I. The $4\pi\beta-\gamma$ coincidence counting technique is the most powerful technique for the absolute activity measurements of $\beta-\gamma$ or EC-γ emitting nuclides.

In this thesis we discussed about the development of a new portable $4\pi\beta\,(LS)-\gamma$ coincidence system for in-situ activity measurement of short-lived radionuclides used in Nuclear Medicine. The mechanical hardware for the gamma channel of the new in-situ $4\pi\beta(LS)-\gamma$ coincidence detection system which is developed at ENEA in collaboration with Catania University and INFN-Catania section, for activity measurement of short half-lived radionuclides. While, the data analysis software of the ENEA portable $4\pi\beta(LS)-\gamma$ coincidence detection system is updated and modified in CAEN, Italy. The activity of ^{131}I is determined using two different methods, such as TDCR and $4\pi\beta\,(LS)-\gamma$ coincidence methods with extrapolation technique, at the same reference date. Short half-lived radionuclides need to be standardized in-situ, because it is difficult to send the radioactive source to nuclear metrology institute. For instance, it is laborious to standarize the ^{11}C source transferring the radioactive source solution from Cannizzaro hospital in catania to ENEA-INMRI in Rome. For that reason it is important to have a portable instrument to standardize short half-live radionuclide inside radiopharmaceuticals centers. Two methods TDCR and $4\pi\beta\,(LS)-\gamma$ were used for the alternative and in-

dependent measurement of activity of ^{131}I. Independently from CAEN TDCR software, ENEA-INMRI developed new data analysis software to calculate the TDCR parameter by implementing the MAC3 philosophy described in the CERN ROOT framework, an object-oriented package for physics analysis. Then, the TDCR parameters are measured for standard solutions ^{131}I by using CAEN and ENEA software. Both codes are compatible and work properly. Another important point is that the activity measurement of the radionuclides is independent on the detection efficiency for either detectors using the $4\pi\beta\,(LS)-\gamma$ method. On the other hand, in TDCR method the detection efficiency has a crucial role in the activity measurement of the radionuclides. For that reason, one can compute the detection efficiency of the detectors by using the Monte Carlo Simulation; in this project GEANT4 Code is used.

The early years of $4\pi\beta-\gamma$ method were filled with the development of efficiency-variation methods, analogue electronics, and the theory that underlies efficiency extrapolations for various types of decay. Since then, it has become clear that appropriate uncertainty assessments require thorough understanding the experimental system and its response to the decay pathways of the radionuclide under study, as well as careful tests of the data for systematic effects or unexpected variance. Current advances are in utilizing knowledge of the measurement system make wise experimental designs, which can lead to a deeper understanding of the measurement process and its resulting uncertainties. Uncertainty components represented in this work come from $4\pi\beta(LS)-\gamma$ coincidence measurement of the massic activity of a solution of ^{131}I. Uncertainty due to background subtraction, beyond that encompassed in 'measurement variability' is 0.05%, uncertainty due to the determination of dilution factor and source masses, beyond that encompassed in 'measurement variability' is 0.05%, and standard deviation of the distribution of four different extrapolation functions is 0.31%. In most cases, the extrapolation comprises the largest component of uncertainty. Yet estimation of this component can rely on the experimenter's judgment as much as on any formula. In practice, this judgment can be based on the standard deviation of the intercept parameter using an assumed functional form of the fit. This judgment can be further informed by systematic tests of the sensitivity of the extrapolation intercept the choice of γ-ray windows,

functional form of the extrapolation and domain of the fit.

The $4\pi\beta-\gamma$ coincidence method and its variants are robust, widely applicable, primary standard methods in radioactivity metrology. Furthermore, with the $4\pi\beta(LS)-\gamma$ coincidence detection system it is possible to standardize directly on site the short-lived pure β, α, electron capture, or $\beta-\gamma$, and $EC-\gamma$ radionuclides used in Nuclear Medicine and then calibrated the devices used in the Nuclear Medicine Departments, such as activimeters, PET, SPECT, Gamma camera, etc, without moving the radioactive sources between the Hospitals and the Metrology Institutes. All the calibration, from the standard to the end-users instruments, can be performed thanks to the new technique directly on site. The ENEA portable $4\pi\beta(LS)-\gamma$ coincidence counting can be consider as an important primary standardization technique for short half-life radionuclides used in nuclear medicine in all other regions in Italy or in other countries.

Bibliography

[1] G. B. Saha, *Fundamentals of Nuclear Pharmacy* (Springer, New York, 2010).

[2] (WNA) World Nuclear Association, Radioisotopes in Medicine,Accessed on 22.05.2022 **URL https://world-nuclear.org**, .

[3] IAEA, *Technetium-99m radiopharmaceuticals : manufacture of kits* (International Atomic Energy agency, Vienna, 2008), No. 466.

[4] OECD-NEA, The Supply of Medical Radioisotopes: An Economic Diagnosis and Possible Solutions **Accessed on 22.05.2022**, (URL https://www.oecd-nea.org).

[5] IAEA *INTERNATIONAL ATOMIC ENERGY AGENCY, Charged Particle Cross-section Database for Medical Radioisotope Production: Diagnostic Radioisotopes and Monitor Reactions.*, IAEA-TECDOC-1211, IAEA, Vienna (2001).

[6] B. McCormick, MF. Wesson, L. Cox, MP. Osborne, JA. Petrek, and DW. Kinne, Int J Radiat Oncol Biol Phys. **15(3)**, 745 (1988).

[7] A. Dash, FF. Knapp, and MR. Pillai, Curr Radiopharm. **6(3)**, 152 (2013).

[8] A. Dash, MR. Pillai, and FF Jr. Knapp, Nucl Med Mol Imaging. **49(2)**, 85 (2015).

[9] Laboratoire National Henri Becquerel (LNHB), LNHB **Accessed on 21.04.2022**, (URL https://www.lnhb.fr/nuclear-data/nuclear-data-table/).

[10] GA. Wiseman and TE. Witzig, Cancer Biother Radiopharm. **20(2)**, 185 (2005).

[11] AM. Safa, OP. Schumacher, and Rodriguez-Antunez A., N Engl J **292**, 167 (1975).

[12] A. Wyszomirska, Nucl Med Rev Cent East Eur. **15(2)**, 120 (2012).

[13] D. Malouff Timothy, S. Seneviratne Danushka, K. Ebner Daniel, C. Stross William, R. Waddle Mark, M. Trifiletti Daniel, and Krishnan Sunil, Frontiers in Oncology **11**, (2021).

[14] L. Li, J. Rousseau, MG. Jaraquemada-Peláez, X. Wang, A. Robertson, V. Radchenko, P. Schaffer, KS. Lin, F. Bénard, and C. Orvig, Bioconjug Chem. **32(7)**, 1348 (2021).

[15] M. Capogni, A. Pietropaolo, L. Quintieri, M. Angelone, A. Boschi, M. Capone, N. Cherubini, P. De Felice, A. Dodaro, A. Duatti, A. Fazio, S. Loreti, P. Martini, G. Pagano, M. Pasquali, M. Pillon, L. Uccelli, and A. Pizzuto, Molecules **23**, 1872 (2018).

[16] M. Capogni, M. Capone, A. Colangeli, G. Dellepiane, A. Fazio, M. Frisoni, M. Pillon, and A. Pietropaolo, EPL **137**, 64001 (2022).

[17] IAEA, *Cyclotron Produced Radionuclides: Principles and Practice* (IAEA Tech. Rep. Ser, Vienna, 2009), No. 465.

[18] F. Abubaker, F. Scopelliti, M.A. Pometti, and et al., Radiochemistry **63**, 77–86 (2021).

[19] P. Schmor, Rev. Accelerator Sci. Technol **4**, 103 (2011).

[20] A. W. Chao and W. Chou, Rev. Accelerator Sci. Technol. **10**, 105 (2019).

[21] T. J. Ruth, Rev. Accelerator Sci. Technol **2**, 17 (2009).

[22] L. Safavi-Tehrani, G. E. Miller, and M. Nilsson, J. Radioanal. Nucl. Chem. **303**, 1099 (2015).

[23] M. R. Kilbourn, J. T. Hood, and M. J. Welch, Int. J. Appl. Radiat. Isot. **35**, 599–602 (1984).

[24] T. J. Tewson, M. S. Berridge, L. Bolomey, and K. L. Gould, Nucl. Med. Biol. **15**, 499–504 (1988).

[25] P. H. Elsinga, Methods **27**, 208 (2002).

[26] T. J. Ruth and A. P. Wolf, Radiochim. Acta **26**, 21–24 (1979).

[27] S. Yu, Biomed Imaging Interv J **2(4)**, 1 (2006).

[28] N. M. Maisey, in *Positron Emission Tomography in Clinical Medicine*, edited by D. L. Bailey, D. W. Townsend, P. E. Valk, and M.N. Maisey (Springer-Verlag, London, UK., 2004).

[29] R. A. Ferrieri and A. P. Wolf, Radiochim. Acta **34**, 69–83 (1983).

[30] H. J. Ache and A. P. Wolf, J. Phys. Chem. **72**, 1988–1993 (1968).

[31] D. R. Christman, R. D. Finn, K. I. Karlstrom, and A. P. Wolf, Int. J. Appl. Radiat. Isot. **26**, 435–442 (1975).

[32] T. Vandewalle and C. Vandecasteele, Int. J. Appl. Radiat. Isot. **34**, 1459–1464 (1983).

[33] S. R. Banerjee and M. G. Pomper, Appl. Radiat. Isot **76**, 213. (2013).

[34] Venkat R. Narra, Roger W. Howell, Raw S. Harapanhalli, Kandula S. R. Sastry, and Dandamudi V. Rao, The Journal of Nuclear Medicine **33**, (1992).

[35] H. Undqvist, and Einarsson L. Scott-Robson, S., and P. Malmborg, Appl. Radiat. Isot **42**, 447–450 (1991).

[36] F. Szelecsènyi, Z. Kovàcs, F. Tàrkànyi, and G.Y. Tòth, paper presented at 8th Int. Symp. on Radiopharmaceutical Chemistry, Princeton, NJ, 1990 (J. Labelled Compd. Radiopharm **30**, 98–99 (1991).

[37] F. D. S. Butement and S. M. Qaim, J. Inorg. Nucl. Chem. **27**, 907–917 (1965).

[38] K. Kondo, R. M. Lambrecht, and A. P. Wolf, Int. J. Appl. Radiat. Isot. **28**, 395–401 (1977).

[39] M. Uillaume, R. M. Lambrecht, and A. P. Wolf, Int. J. Appl. Radiat. Isot. **26**, 703–707 (1975).

[40] P. E. Frey and et al., J. Clin. Endocrinol. Metab **63**, 918–927 (1986).

[41] R. Weinreich and et al., J. Labelled Compd. Radiopharm **40**, 346–347 (1997).

[42] N. R. Stevenson and et al., Targetry and Target Chemistry (Proc. 6th Workshop Vancouver, 1995) TRIUMF, Vancouver 82–83 (1995).

[43] S. M. Qaim, Nucl. Instrum. Methods Phys. Res. A **282**, 289–295 (1989).

[44] Y. Sheh and et al., Radiochim. Acta **88**, 169–173 (2000).

[45] EM. Chapman, JAMA **250**, 2042 (1983).

[46] Nordion, Iodine-131 (n, gamma) Radiochemical Sodium Iodide Solution **Accessed on 22.05.2022**, (URL https://www.nordion.com).

[47] M. G. Straatmann and M. J. Welch, Radiat. Res. **56**, 48–56 (1973).

[48] R. S. Tilbury and J. R. DahlL, Radiat. Res. **79**, 22–33 (1979).

[49] F. Joliot and I. Curie, Nature **133**, 201–202 (1934).

[50] R. E. Shefer, B. J. Hughey, R. E. Klinkowstein, M. J. Welch, and C. S. Dence, Nucl. Med. Biol. **21**, 977–986 (1994).

[51] W. Vaalburg and et al., J. Labelled Compd. Radiopharm. **18**, 303–308 (1981).

[52] M. S. Livingston and E. McMillan, Phys. Rev. **46**, 439–440 (1934).

[53] H. Vera-Ruiz and A. P. Wolf, Radiochim. Acta **24**, 65–67 (1977).

[54] EO. Lawrence and D. Cooksey, Phys Rev **50**, 1131–40 (1936).

[55] AJ. Tofe, MD. Francis, CL. Slough, AK. Merritt, and WJ. Harvey, J Nucl Med **17(suppl)**, 548P (1976).

[56] S. Puig and D. J. Tiele, Current Opinion in Chemical Biology **6**, 171–180 (2002).

[57] I. Bertini, G. Cavallaro, and K. S. McGreevy, Coordination Chemistry Reviews **254**, 506–524 (2010).

[58] P. Szymański, T. Frączek, M. Markowicz, and et al., Biometals **25**, 1089–1112 (2012).

[59] I.A.E.A. Radioisotopes, *radiopharmaceuticals. Cyclotron produced radionuclides: Emerging positron emitters for medical applications:* ^{64}Cu *and* ^{124}I (IAEA Tech. Rep. Ser, Vienna, 2016), No. Reports No. 1.

[60] H.A. Williams, S. Robinson, P. Julyan, and et al., Eur J Nucl Med Mol Imaging **32**, 1473–1480 (2005).

[61] Sonke Svenson, Molecular Pharmaceutics **10 (3)**, 848 (2013).

[62] D. W. McCarthy, R. E. Shefer, R. E. Klinkowstein, and et al., Nuclear Medicine and Biology **24**, 35–43 (1997).

[63] C. Alliot, N. Michel, A. C. Bonraisin, and et al., Radiochimica Acta **99**, 627–630 (2011).

[64] H. Piel, S. M. Qaim, and G. Stocklin, Radiochimica Acta **57**, 1–5 (1992).

[65] A. Obata, S. Kasamatsu, D. W. McCarthy, and et al., Nuclear Medicine and Biology **30**, 535–539 (2003).

[66] T. J. Wadas, E. H. Wong, G. R. Weisman, and C. J. Anderson, Current Pharmaceutical Design **13**, 3–16 (2007).

[67] K. V. Vimalnath, A. Rajeswari, V. Chirayil, and et al., Journal of Radioanalytical and Nuclear Chemistry **290**, 221–225 (2011).

[68] GL. DeNardo, SI. DeNardo, CF. Meares, and et al., Antibody Immun Radiopharm **4**, 777 (l991).

[69] DW. Palmer and SA. Rao, J Nucl Med **26**, 936 (l991).

[70] C. Pecher, Univ Calif Publ Pharmacology **2**, 1117 (1942).

[71] S. Abalin, Y. Vereschagin, G. Grigoriev, and et al., United States Patient US 6.456.680 (2002).

[72] D. Chuvilin, V. Khvostionov, D. Markovskij, and et al., Appl Rad Isot **65**, 1087 (2007).

[73] R. Murthy, R. Nunez, J. Szklaruk, and et al., Radiographics **25**, S41–S55 (2005).

[74] G. Paganelli, S. Zoboli, M. Cremonesi, and et al., Eur J Nucl Med **28**, 426–34 (2001).

[75] R. Chakravarty, U. Pandey, RB. Manolkar, and et al., Nucl Med Biol **35**, 245 (2008).

[76] Z. Dvorakova, R. Henkelmann, X. Lin, and et al., App Radiat Isot **66**, 147 (2008).

[77] M. Lyra, GS. Limouris, AP. Frantzis, and et al., Eur J Nucl Med **26(553)**, 1191 (1999).

[78] De Klerk, JM. Zonnenberg, BA. Blijham, and et al., Anticancer Res **17(3B)**, 1773 (1997).

[79] L. Mathieu, P. Chevalier, G. Galy, and M. Berger, Int J Appl Radiat Isot **30**, 725 (1979).

[80] E. Deutsch, K. Libson, JL. Vanderheyden, AR. Ketring, and HR. Maxon, Int J Rad Appl Instrum B **13**, 465 (1986).

[81] VJ. Lewington, Eur J Nucl Med **20**, 66 (1993).

[82] J. Vucina and D. Lukic', Phys Chem and Tech **2**, 235 (2002).

[83] FF. Knapp, AP. Callahan, AL. Beets, and et al, Appl Radiat Isot **45**, 1123 (1994).

[84] JS. Lee, J. Lee, U. Park, and et al., Appl Radiat Isot **67**, 1162 (2009).

[85] M. F. L'Annunziata, *Handbook of Radioactivity Analysis*, 2 ed. (Academic Press, New York, 2003).

[86] R. A. Allen, in *Alpha-, Beta- and Gamma-Ray Spectroscopy*, edited by K. Siegbahn (North-Holland, Amsterdam, 1965), Vol. 1.

[87] R. Resnick, D. Halliday, and K. S. Krane, *A handbook of radioactivity measurements procedures (National Council on Radiation Protection and Measurements* (PUBLISHER, Washington, 1985), No. 58.

[88] W. Bambynek, *Precise solid angle counting, Symp. Standardization of Radionuclides* (International Atomic Energy Agency, IAEA, Vienna, 1967), p. 373.

[89] H. H. Seliger and A. Schwebel, Nucleonics **12**, 54 (1954).

[90] B. D. Pate and L. Yaffe, Can. J. Chem. **33**, 15 (1955a).

[91] B.D. Pate and L. Yaffe, Can. J. Chem. **33**, 610 (1955b).

[92] B. D. Pate and L. Yaffe, Can. J. Chem. **34**, 265 (1956).

[93] W. K. Roentgen, *Source Book in Physics* (Sitzber. Wurzberger Phys.-Med. Ges., December, 1895. Condensed English translations are given by Magie, W. F. McGraw-Hill Book Company, Inc., New York, 1895).

[94] H. Becquerel, C.R. Acad. Sci. **122**, 420 (1896a).

[95] H. Becquerel, C.R. Acad. Sci. **122**, 501 (1896b).

[96] H. Becquerel, Recherches sur une propriete nouvelle de la matiere, Paris, typographie de Firmin-Didot et Cie. .

[97] H. Becquerel, C.R. Acad. Sci. **122**, 855 (1896c).

[98] J. J. Thomson and E. Rutherford, Phil. Mag. **42**, 392 (1896).

[99] E. Rutherford, Phil. Mag. **47**, 109 (1899).

[100] P. Curie and M. Curie, C.R. Acad. Sci. **127**, 175 (1898).

[101] A. Allisy, Metrologia **31**, 467 (1994/1995).

[102] E. Rutherford and Royds, Phil. Mag. **17**, 281 (1909).

[103] J. Chadwick, Verhandl. deut. Physik. Ges. **16**, 383 (1914).

[104] E. Fermi, Z. Physik **88**, 161 (1934).

[105] E. Rutherford and H. Geiger, Proc. R. Soc. **81**, 141 (1908).

[106] H. Geiger and E. Rutherford, Philosophical Magazine and Journal of Science **24:142**, 618 (1912).

[107] H. Geiger and Klemperer, O.Z., Phys. **49**, 753 (1928).

[108] J. A. Simpson, Jr. Rev. Sci. Instr. **15**, 119 (1944).

[109] O. Haxel and F.G. Houtermans, Z. Physik **124**, 705 (1948).

[110] A. P. Baerg, Nucl. Instr. Meth. **112**, 143 (1973a).

[111] D. J. N. Bekuzarov, Nucl. Instr. Meth. **112**, 201 (1973).

[112] J. S. Merritt, J. G. V. Taylor, and P. J. Campion, Canad. J. Chem. **37**, 1109 (1959).

[113] H. A. Wyllie, Canad. J. Chem. ANSTO/M118 (1989).

[114] M. Yoshida, H. Miyahara, and T. Watanabe, Int. J. Appl. Radiat. Isotopes **28**, 633 (1977).

[115] R. Hofstadter, Phys. Rev. **74**, 100 (1948).

[116] K. Siegbahn, *Alpha-, beta- and gamma-ray spectroscopy* (North-Holland., Amsterdam, 1965), Vol. 1, p. 247.

[117] K. G. MacKay, Phys. Rev. A **76**, 1537 (1949).

[118] J. W. Mayer and B. Gossick, Rev. Sci. Intr **27**, 407 (1956).

[119] W. D. Davis, J. App. Phys. **29**, 231 (1958).

[120] D. V. Freck and J. Wakefield, J. App. Phys. **193**, 669 (1962).

[121] A. J. Tavendale, IEEE Trans. Nucl. Sci **NS-12**, 255 (1965).

[122] R. N. Hall, R. D. Baertsch, T. J. Soltys, and L. J. Petrucco, USAEC Contract No. AT (30-1) 3870 (1970).

[123] D. Alexiev, M. I. Reinhard, L. Mo, A. R. Rosenfeld, and M. L. Smith, J. App. Phys. **25**, 7 (2002).

[124] H. Geiger and A. Werner, Z. Phys. **21**, 187 (1924).

[125] W. Bothe and H. Kolhorster, Zeits. f. Phys. **56**, 571 (1929).

[126] B. H. Rossi, Zeits. f. Phys. **68**, 64 (1931).

[127] M. A. Tuve, Phys. Rev. **35**, 651 (1930).

[128] W. Bothe and V. Baeyer, Zeits. f. Phys. **95**, 417 (1935).

[129] J. V. Dunworth, Rev. Sci. Instr. **11**, 167 (1940).

[130] W. Bothe and V. Baeyer, The Review of Scientific Instruments **22**, 415– (1951).

[131] J. L. Putman, U.K. Atomic Energy Research Establ. (A.E.R.E.), Report I/M 26 (1957).

[132] A. H. Snell, *Nuclear Instruments and their uses* (Wiley, New York, 1962), Vol. 1, p. 323.

[133] P. J. Campion, Int J. Appl. Radiat. Isotopes **4**, 232 (1959).

[134] P. J. Campion, J. G. V. Taylor, and J. S. Merritt, Int. J. Appl. Radiat. Isot. **8**, 8 (1960).

[135] A. P. Baerg, Metrologia **2**, 23 (1966).

[136] A. Williams and P. J. Campion, Int. J. Appl. Ra-diat. Isot. **14**, 533 (1963).

[137] H. Houtermans and M. Miguel, Int. J. Appl. Radiat. Isot **13**, 137 (1962).

[138] A. P. Baerg, Nucl. Instr. Meth. Phy. Res.A **112**, 143 (1973).

[139] A.P. Baerg, Bowes G. C., and R. J. Adams, IAEA Symp. Standardisation of radionuclides, SM-79/12 (IAEA. Vienna) (1967).

[140] J. Steyn and F. J. Haasbroek, Proceedings of the second international conference on the peaceful uses of atomic energy, Geneva, A/Conf.15.United Nations, N. Y. 1104 (1958).

[141] J. G. V. Taylor, Can. J. Phys. **40**, 383 (1962).

[142] J. G. V. Taylor and J. S. Merritt, Bull. Am. Phys. Soc. Ser. II **7**, 352 (1962).

[143] J. S. Merritt and J. G. V. Taylor, Response of 4π proportional counter to γ-rays, in Standardization of radionuclides (IAEA, Vienna, SM-79/66) 147 (1966).

[144] Y. Kawada, T. Michikawa, and Yamashita M., Nucl. Instrum. Meth. **61**, 117 (1968).

[145] Y. Kawada, Intern. J. Appl. Rad. Isot **20**, 413 (1969).

[146] J. P. Perolat, Nucl. Instr. Meth **112**, 179 (1973).

[147] A.P. Baerg, S. Meghir, and G. C. Bowes, Int. J. Appl. Rad. Isotopes **15**, 279 (1964).

[148] A. P. Baerg, Nucl. Instr. and Meth **112**, 137 (1973).

[149] G. C. Lowenthal, Nucl. Instr. Meth. **112**, 165 (1973).

[150] J. Bryant, D. G. Jones, and McNair, Proc. IAEA Symp., STI/PUB/139, SM-79/28,(IAEA, Vienna, 1967) **7**, 47 (1967).

[151] L. Grigorescu, Int. J. Appl. Radiat. Isot **34:8**, p1151 (1982).

[152] H. Miyahara and T. Watanabe, Int. J. Appl. Radiat. Isot. **35**, 345 (1984).

[153] H. Miyahara, T. Momose, and T. Watanabe, Appl. Radiat. Isot. **37**, 1 (1986).

[154] M. F. Koskinas and M. Dias, Nucl. Instrum. Meth. in Phys. Res. A **280**, 327 (1989).

[155] G. A. Brinkman, A. H. W. Aten, JR. Veenboer, and J. TH., Int. J. Appl. Isot. **14**, 153 (1963a).

[156] G. A. Brinkman, A. H. W. Aten, JR Veenboer, and J. TH., Int. J. Appl. Isot. **14**, 433 (1963b).

[157] B. R. S. Simpson and B. R. Meyer, international comparison. 668, Sept., NAC category: ST ISBN 0-7988-4675-5. (1989).

[158] S. M. Buckman, PhD thesis, Macquarie University .

[159] S. M. Buckman and D. Ius, Nucl. Instr. Meth. Phys. Res. A **369**, 368 (1996).

[160] S. M. Buckman, J. D. Keightley, D. Smith, and M. J. Woods, Appl. Radiat. Isot. **49**, 1135 (1998).

[161] K. S. A. Butcher, G. C. Watt, D. Alexiev, H. van der Gaast, J. Davies, L. Mo, H. A. Wyllie, J. D. Keightley, D. Smith, and M. J. Woods, Nucl. Instr. Meth. Phy. Res. A **450**, 30 (2000).

[162] A. Grau Malonda and E. Garcia-Torano, Int. J. Appl. Radiat. Isot. **33**, 249 (1982).

[163] C. Ivan, P. Cassette, and M. Sahagia, Applied Radiation and Isotopes **66**, 1006 (2008).

[164] C. Bobin, C. Thiam, J. Bouchard, and F. Jaubert, Applied Radiation and Isotopes **68**, (2010).

[165] A. T. Sanz and K. Kossert, Nuclear Instruments and Methods in Physics Research A **648**, 124 (2011).

[166] K. Kossert, O. J. Nahle, and A. Grau Carles, Applied Radiation and Isotopes **69**, 1246 (2011a).

[167] P. Cassette, G. H. Ahn, T. Alzitzoglou, I. Aubineau-Laniece, F. Bochud, E. Garcia Torano, A. Grau Carles, A. Grau Malonda, K. Kossert, K. B. Lee, J. P. Laedermann, B. R. S. Simpson, W. M. van Wyngaardt, and B. E. Zimmerman, Applied Radiation and Isotopes **64**, 1471–1480 (2006).

[168] L. Mo, H.Y Wu, and C. Baldock, IEEE Transactions on Nuclear Science **54**, (2007).

[169] E. Schram and R. Lombaert, *Organic scintillation detectors: counting of low-energy beta emitters* (Elsevier Publishing Co., Amsterdam, 1963).

[170] A. Grau Malonda, in *Free parameter models in liquid scintillation counting*, edited by K. Siegbahn (Coleccio´n Documentos CIEMAT. CIEMAT, Madrid, 1999).

[171] E. Gunther, Applied Radiation and Isotopes **56**, 357–360 (2002).

[172] P. Cassette and P. Do, Applied Radiation and Isotopes **66**, 1026 (2008).

[173] L. Mo, M.J. Qin, and M. Hurry, ANSTO technical report, ANSTO/S/TN/2007-2 (2007).

[174] R. Fitzgerald, R. Colle, L. Laureano-Perez, L. Pibida, Nour S. Hammond, M. M., and B. E. Zimmerman, Applied Radiation and Isotopes **68**, 1303 (2010).

[175] R. Broda, P. Cassette, and K. Kossert, Metrologia **44**, S36 (2007).

[176] P. Cassette and R. Vatin, Nucl. Instrum. Methods A **312**, 95–99 (1992).

[177] R. Broda, Appl. Radiat. Isot. **58**, 585 (2003).

[178] A. Hoegl and E. Schwerdtel, Appl. Radiat. Isot. **52**, 643 (1963).

[179] E. Schwerdtel, Kerntechnik **8**, 517–520 (1966a).

[180] E. Schwerdtel, Atomkernenergie **11**, 324–325 (1966b).

[181] V. Kolarov, Y. Le Gallic, and R. Vatin, Int. J. Appl. Radiat. Isot. **21**, 443–452 (1970).

[182] K. Pochwalski and T. Radoszewski, IBJ Report, INR 1848/OPiDI/E/A (1979).

[183] K. Pochwalski, R. Broda, and T. Radoszewski, Appl. Radiat. Isot. **39**, 165–172 (1988).

[184] R. Vatin, *Mesure absolue de l'activite des radionucleides emetteurs beta purs par scintillateur liquide a l'aide d'un detecteur a 3 photomultiplicateurs. In: Magana, J.F. (Ed.), Mesure de l'activite des radionucleides emetteurs beta purs* (Bulletin BNM, Paris, 1991), No. 85 BNM, p. 13–21.

[185] R. Broda and K. Pochwalski, Nucl. Instrum. Methods, A **312**, 85–89 (1992).

[186] A. Grau Malonda and B.M. Coursey, Appl. Radiat. Isot. **39**, 1191 (1988).

[187] A. C. Razdolescu, R. Broda, P. Cassette, B. Simpson, and F. V. Wyngaardt, Applied Radiation and Isotopes **64**, 1510 (2006).

[188] J. Bouchard and P. Cassette, Applied Radiation and Isotopes **52**, 669 (2000).

[189] Giuliano Mini, Francesco Pepe, Carlo Tintori, and Marco Capogni, Applied Radiation and Isotopes **87**, 166–170 (2014).

[190] P. Cassette, J. Bouchard, and B. Chauvenet, Nucl. Instrum. Methods **A339**, 339–342 (1994).

[191] Ch. Bobin and J. Bouchard, Appl. Radiat. Isot. **64**, 124 (2006).

[192] B. E. Zimmerman, T. Altzitzoglou, D. Rodrigues, R. Broda, P. Cassette, L. Mo, G. Ratel, B. Simpson, W. Van Wyngaardt, and C. Watjen, Applied Radiation and Isotopes **68**, 1477–1481 (2010).

[193] D. Rodrigues, P. Arenillas, M. E. Capoulat, and C. Balpardo, Applied Radiation and Isotopes **66**, 1049 (2008).

[194] S. Agostinelli, J. Allison, and et al., NIMA **506**, 250 – 303 (2003).

[195] J. Allison and et al., IEEE Transactions on Nuclear Science **53**, 270–278 (2006).

[196] C. Thiam, C. Bobin, B. Chauvenet, and J. Bouchard, Applied Radiation and Isotopes **70**, 2195 (2012).

[197] J. B. Birks, in *The theory and practice of scintillation counting*, edited by C. G. Bell (Pergamon Press, Oxford, 1958), p. 185.

[198] M. O. El-Ghossain, International Journal of Physics **5**, 92 (2017).

[199] Naruhiro Matsufuji, Tatsuaki Kanai, Hideaki Komami, and Toshiyuki Kohno, Nuclear Instruments and Methods in Physics Research Section A: Accelerators, Spectrometers, Detectors and Associated Equipment **437**, 346 (1999).

[200] P. Cassette, in *Evaluation of the influence of wall effects on the liquid scintillation counting detection efficiency for the standardization of high-energy beta and alpha radionuclides", LSC 2001- Advances in Liquid Scintillation Spectrometry*, edited by Franz Schonhofer Edited by Siegurd Mobius, John Noakes (Department of Geosciences, The University of Arizona, Tucson, Arizona 85712 USA, 2001), pp. 45–55.

[201] R. Broda, Applied Radiation and Isotopes **66**, 1062 (2008).

[202] L. Mo, P. Cassette, and C. Baldock, Nuclear Instruments and Methods in Physics Research A **558**, 490 (2006).

[203] Nähle O. and Kossert K., *Comparison of the TDCR method and the CIEMAT/NIST method for the activity determination of beta emitting nuclides" LSC- Advances in Liquid Scintillation Spectrometry* (PUBLISHER, Paris, 2010).

[204] M. J. Qin, L. Mo, D. Alexiev, and P. Cassette, Applied Radiation and Isotopes **66**, 1033 (2008).

[205] R. D. Evans, *The Atomic Nucleus* (McGraw-Hill Book Company, New York, 1955).

[206] C. S. Wu and S. A. Moszkowski, *Beta decay* (John Wiley Sons, New York-LondonSydney, 1966).

[207] H. Behrens and L. Szybisz, Physics data, ZAED 69 (1976).

[208] M. Capogni and P. DeFelice, Applied Radiation and Isotopes **93**, 45 (2014).

[209] CAEN DT5720 digitizer, CAEN **Accessed on 21.04.2022**, (URL https://www.caen.it/products/dt5720/.).

[210] CAEN digitizer whitepaper, CAEN **Accessed on 21.04.2022**, (URL https://www.caen.it/caen-digitizer-whitepaper/.).

[211] User Manual UM2089: Digital Pulse Processing (DPP-CI), CAEN **Accessed on 21.04.2022**, (URL https://www.npl.washington.edu /TRIMS/sites/sand.npl.washington.edu.TRIMS/files/manuals-documentation/CAEN-DPCI_UserManual_rev1.pdf.).

[212] Photomultiplier Tubes R7600U Series Hamamatsu, Hamamatsu photonics **Accessed on 03.02.2022**, (URL https://www.hamamatsu.com/eu/en/product/ type/R7600U-20/index.html.).

[213] H. L. Anderson, Applied Radiation and Isotopes **14**, 96–108 (1986).

[214] S. Guatelli, D. Cutajar, B. Oborn, and A. B. Rosenfeld, *Introduction to the geant4 simulation toolkit 2011* (institutional repository for the University of Wollongong, Sydney, 2011).

[215] S. Giani and et al., CERN/LHCC 98 (1998).

[216] J. F. Briesmeister, Los Alamos National Laboratory LA-12625-M (Los Alamos, NM) (1993).

[217] F. Salvat, J.M. Fernandez-Varea, E. Acosta, and J. Sempau, Workshop proceedings, OECD/NEA 5-7 November 2001, Issy-les-Moulineaux, France, NEA/NSC/DOC (2001).

[218] W.R Nelson, H. Hirayama, and D.W.O Rogers, Stanford Linear Accelerator Centre, Stanford, California (1985).

[219] A. De Vismes and M.N. Amiot, Appl. Radiat. Isot. **59**, 267 – 272 (2003).

[220] M. N. Amiot, Appl. Radiat. Isot. **60**, 529 (2004).

[221] A. A. Khalid, Med. Phys. **29**, 12 (2002).

[222] J. J. Gostely and J. P. Leadermann, Appl. Radiat. Isot. **52(3)**, 447 (2000).

[223] H. Suzuki, K. Sibaike, H. Hashimoto, Y. Kawada, and Y. Hino, Appl. Radiat. Isot. **49 (9-11)**, 1245 (1998).

[224] M. D. S Seneviratne, Master thesis, The University of Sydney (2005).

[225] P. N. Johnston and P. A. Burns, Nucl. Instr. Meth. in Phys. Res **353**, 101 (1994).

[226] J. C. Hardy, V. E. Iacob, M. Sanchez-Vega, R. T. Effinger, P. Lipnik, V. E. Mayes, D. K. Willis, and R. G. Helmer, Appl. Radiat. Isot. **56**, 65 (2002).

[227] R. G. Helmer, J. C. Hardy, V. E. Iacob, M. Sanchez-Vega, R. G. Neilson, and J. Nelson, Nucl. Instr. Meth. in Phys. Res. **511**, 360 (2003).

[228] C. M. Salgado, C. C. Conti, and P. H. B. Becker, Appl. Radiat. Isot. **64**, 700 (2006).

[229] R. Vlastou, I. Th. Ntziou, M. Kokkoris, C. T. Papadopoulos, and C. Tsabaris, Appl. Radiat. Isot. **64**, 116 (2006).

[230] M. S. Dias, M. N Takeda, and M. F. Koskinas, Appl. Radiat. Isot. **56**, 105 (2002).

[231] H. Miyahara, M. Mizuno, and T. Watanabe, Nucl. Instrum. Meth. in Phys. Res. **228**, 397 (1985).

[232] M. N. Takeda, M. da Silva Dias, and M. Fallone koskinas, IEEE Transactions on Nuclear Science **52**, 2951 (2005).

[233] B. E. Zimmerman, Appl. Radiat. Isot. **64**, 1492 (2006).

[234] J. Bouchard and P. Cassette, Nucl. Instrum. Meth **A 505**, 72–75 (2003).

[235] Jennifer, M. Olfert, Xiongxin Dai, and P. Sheila Kramer-Tremblay, J Radioanal Nucl Chem **300**, 263–267 (2014).

[236] A. Levin and C. Moisan, In: Proceedings of the 1996 IEEE Nuclear Science Symposium **2**, 702–706 (1996).

[237] S. W. Harmer, R. Downey, Y. Wang, and P. D. Townsend, Nucl. Instrum. Methods A **564**, 439–450 (2006).

[238] T. J. Quinn, Metrologia **34**, 61–5 (1997).

[239] K. Debertin, Appl. Radiat. Isot. **47**, 423–31 (1996).

[240] Bè M-M and et al, Table of Radionuclides (vol 1—A = 1 to 150; vol 2—A = 151 to 242) and 2006 (vol 3—A = 3 to 244) Monographie BIPM-5 .

[241] S. Pomme, Appl. Radiat. Isot. **64**, 1158–62 (2006).

[242] E. Browne and RB. Firestone, in *Table of Radioactive Isotopes*, edited by V. S. Shirley (John Wiley and Sons, New York, 1996).

[243] S. Yoshida and T. Ohsugi, Nuclear Instruments and Methods in Physics research A **541**, 412 (2005).

[244] KP. Grawé and A. Oskarsson, Nuclear Instruments and Methods in Physics research A **73**, 519 (2000).

[245] D. Gupta, JM. Chatterjee, R. Ghosh, AK. Mitra, S. Roy, and M. Sarkar, Applied Radiation and Isotopes **65**, 512 (2007).

[246] J. Roboco, ML. Carvalho, AF. Marques, FR. Frreira, and DR. Chettle, Talanta **70**, 957 (2006).

[247] A. Fritioff and M. Greger, Chemosphere **67**, 365 (2007).

[248] P. Moffatt, M. Marion, and F. Denizeau, Cell Biology and Toxicology **8**, 277 (1992).

[249] R. Accorsi, AS. Curion, PR. Frallicciardi, C. Lanza, A. Lauria, G. Mettivier, MC. Montesi, and P. Russo, Nuclear Instruments and Methods in Physics research A **571**, 415 (2007).

[250] S. Liu and WX. Wang, Marine Biology **140**, 595 (2002).

[251] BIPM Bureau International des Poids et Mesures, General Conference on Weights and Measures **22nd Meeting**, (2003).

[252] E. Sch ̈ofeld, H. Janssen, R. Klein, JC. Hardy, V. Iacob, M. Sanchezvega, HC. Griffin, and Ludington MA., Appl. Radiat. Isot. **56**, 215 (2002).

[253] E. García-Toraño, V. Peyres, and F. Salvat, Computer Physics Communications **245**, 106849 (2006).

[254] E. García-Toraño, V. Peyres, M.-M. Be, C. Dulieu, M.-C. Lepy, and F. Salvat, Nuclear Instruments and Methods in Physics Research Section B: Beam Interactions with Materials and Atoms **396**, 43 – 49 (2017).

[255] H. O. Anger and A. Gottschalk, J. Nucl. Med.: Off. Publ. Soc. Nucl. Med. **4**, 326–330 (1963).

[256] J. V. Dunworth, Rev. Sci. Instr. **11**, 167 (1940).

[257] C. Bobin, J. Bouchard, S. Pierre, and et al., Appl. Radiat. Isot. **70**, 2012 (2012).

[258] Particle Counting in Radioactivity Measurements: International Commission on Radiation Units and Measurements (ICRU), ISBN 0-913394-51-3 **Report 52**, (1994).

[259] B. R. S. Simpson and B. R. Meyer, Nucl. Instr. and Meth. A **14**, 339 (1994).

[260] P. Cassette, M. M. Be, F. Jaubert, and M. C. Lepy, Appl Radiat. Isot. **60**, 439 (2004).

[261] A. Chylinski and T. Radoszewski, Nucl. Instrum. Meth. A **369**, 336 (1996).

[262] J. L. Putman, Br. J. Radiol **23**, 46e63 (1950).

[263] Roger Rusack, CERN,Accessed on 24.03.2021 **URL https://indico.cern.ch/.../Lecture3-Scintillators-Light-Detection.pptx.pdf**, (2021).

[264] F. Peter Sharp, G. Howard Gemmell, and D. Alison Murray, *Practical nuclear medicine*, 3rd ed. (Spring, New York, USA, 2005).

[265] Wal'a Al-jubeh, Ansam Shaheen, and Othman Zalloum, Radioiodine I-131 for Diagnosing and Treatment of Thyroid Diseases.Conference paper (2012).

[266] Richard J. Robbins and Martin J. Schlumberger, J Nucl Med **46**, 28S (2005).

[267] A. Williams, F. H. Hughes, and P. J. Campion, Metrologia **4**, 178 (1968).

[268] D. Smith, in *In applications of liquid-scintillation counting in radionuclide metrology*, edited by W. B. Mann and J. G. V. Taylor (BIPM, Monographie 3, Amsterdam, 1980).

[269] K. F. Flynn, L. E. Glendenin, and V. Prodi, New York: Academic (1982).

[270] D. G. Jones and A. McNair, Nat Bur. Stand. Spec. Publ **331**, 37 (1970).

[271] H. Houtermans, Nucl. Instrum. Methods **112**, 121 (1973).

[272] A. Grau Malonda, Int. J. Appl. Radiat. Isot. **33**, 371 (1982).

[273] B. M. Coursey, J. A. B. Gibson, Heitzman M. W., and J. C. Leak, Int. J. Appl. Radiat. Isot **35**, 1103 (1984).

[274] B. M. Coursey, W. B. Mann, A. Grau Malonda, E. Garcia-Torano, J. M. Los Arcos, J. A. B. Gibson, and B. Reher, Appl. Radiat. Isot. **37**, 403 (1986).

[275] N. Tsoulfanidis, *Measurement and Detection of Radiation* (Hemisphere Publishing corporation, Washington, 1983).

[276] E. H. Borai, Y. F. Lasheen, A. F. Seliman, and M. M. Abo-Aly, World Journal of Chemistry 2 **1**, 1 (2007).

[277] J. B. Birks, *Scintillation counters*, 3 ed. (Pergamon Press, University of California, 1960), Vol. 2.

[278] X. Hou, NKS-B Workshop on Radioanalytical Chemistry, November 16-20 **52**, 643 (2009).

[279] L. Y. Johansson, PhD thesis (2008).

Appendix A

Theory of Beta Decay

A.1 Introduction

We have seen that many thousands of nuclei can be produced and studied in the laboratory. However, only less than 300 of these nuclei are stable, the rest are radioactive. The vast majority of unstable nuclei lie in regions in which α decay is not important, and the nuclei undergo one or another form of beta decay in order to become more stable. In a certain sense, the stable nuclei have a balance between the numbers of neutrons and protons. Nuclei are said to be unstable with respect to β decay when these numbers are "out of balance." In a very qualitative way β decay "converts" a neutron into a proton (or vice versa) inside a nucleus, which becomes more stable while maintaining a constant mass number. Beta decay is named for the second most ionizing rays that were found to emanate from uranium samples. β-particles are either electrons or positrons that are emitted through a certain class of nuclear decay associated with the weak interaction. The naturally occurring beta rays were identified as fast moving (negative) electrons relatively easily, but it took many years to obtain a full understanding of the emission process. The difficulty lies in the fact that two particles are "created" during the decay as compared to the "disruption" of a heavy nucleus in alpha decay. In contrast to alpha decay, angular momentum plays a crucial role in understanding the process. Let us consider the simplest form of β decay to illustrate

the difficulties. The proton and the neutron are the two possible isobars for $A = 1$. We know that the neutron has a larger mass than the proton and is thus unstable with respect to the combination of a proton and an electron. Associated with the electron is a conserved quantity, expressed as the quantum number known as the lepton number. The lepton number of the negatron is by convention $+1$. The lepton number of the positron, also the antiparticle of the negatron, is -1. A free neutron will undergo β decay with a half-life of approximately 10 minutes. We might expect to write the decay equation as:

$$ {}^{1}_{0}n \rightarrow {}^{1}_{1}p + {}^{-1}_{0}e + Q \tag{A.1} $$

However, all three particles in this equation are fermions with intrinsic spins $S = 1/2\hbar$. Therefore; we cannot balance the angular momentum in the reaction as written. The spins of the proton S_p and the electron S_e can be coupled to 0 or $1\hbar$ and can also have relative angular momenta with any integral value from the emission process. This simple spin algebra will never yield the half-integral value on the left-hand side of the equation. Another fermion must be present among the products of the transformation.

Another feature of β-decay that was puzzling at first but really pointed to the incompleteness of the previous equation is that the β-rays have a continuous energy distribution. That is, electrons are emitted from a source with a distribution of energies that extends from a maximum at the Q value down to zero. Recall that if there are only two products from a reaction then they will precisely share the decay energy according to conservation of momentum. Quite dramatic pictures of the tracks of charged particles from beta decay show events in which the particles move in one direction in clear violation of conservation of linear momentum. The way out of this mounting paradox with violations of very strongly held conservation laws is to introduce another conservation law and recognize that another unseen particle must be produced and emitted. The conservation law is conservation of the number of "particles" in a reaction and the unseen particle is a form of neutrino.

A.2 Neutrino Hypothesis

Enrico Fermi in 1934 on his voyage to the new world formulated the theory of beta decay; he suggested that a third particle was needed to balance the emission of the electron in β decay. However, the existing conservation laws also had to be satisfied so there were a number of constraints on the properties of this new particle. Focusing on the decay of a neutron as a specific example, the reaction is already balanced with respect to electric charge, so any additional particle must be neutral. The electrons were observed with energies up to the maximum allowed by the decay Q value so the mass of the particle must be smaller than the instrumental uncertainties. The third constraint on the neutrino from the decay is that it must be an "antiparticle" in order to cancel or compensate for the creation of the electron, a "particle." The fourth constraint is that the neutrino must have half-integral spin and be a fermion in order to couple the total final angular momentum to the initial spin of $1/2\hbar$. Combining all these constraints we can now rewrite the previous equation properly as:

$$ {}^{1}_{0}n \rightarrow {}^{1}_{1}p + {}^{-1}_{0}e + {}^{0}_{0}\vec{\nu}_e + Q \tag{A.2} $$

The spins of the final products can be combined in two ways and still couple to the initial spin of the neutron. Focusing on the spins of the created particles, they can vector couple to $S_\beta = 1$ in a parallel alignment or to $S_\beta = 0$ in an anti-parallel alignment. Both can combine with $S = 1/2$ of the neutron for a resultant vector of $1/2$. The two possible relative alignments of the "created" spins are labeled as Fermi (F)$(S_\beta = 0)$ and Gamow-Teller (GT) $(S_\beta = 1)$ decay modes after the people that initially described the mode. Both modes are very often possible, and a source will produce a mixture of relative spins. In some cases, particularly the decay of even β even nuclei with N=Z (the so-called mirror nuclei), the neutrons and protons are in the same orbitals so that $0+$ to $0+$ decay can only take place by a Fermi transition. In heavy nuclei with protons and neutrons in very different orbitals (shells) the GT mode dominates. In complex nuclei, the rate of decay will depend on the overlap of the wave functions of the ground state of the parent and the state of the daughter. The final state in the daughter depends on the decay mode. Notice that in the example of neutron decay, the difference between the

two modes is solely the orientation of the spin of the bare proton relative to the spins of the other products. The decay constant can be calculated if these wave functions are known. Alternatively, the observed rate gives some indication of the quantum mechanical overlap of the initial and final state wave functions. The general form of β (decay of a heavy parent nucleus, ${}^{A}Z$), can be written as:

$$ {}^{A}Z_n \rightarrow {}^{A}\ (Z+1)^{+}_{N-1} + e^{-} + \bar{\nu}_e + Q_{\beta^-} \tag{A.3} $$

where we have written out the charges on the products explicitly. Notice that the electron can be combined with the positive ion to create a neutral atom (with the release of very small binding energy). This allows us to use the masses of the neutral atoms to calculate the Q value, again assuming that the mass of the anti-neutrino is very small. Thus,

$$ Q_{\beta^-} = M[{}^{A}Z] - M[{}^{A}(Z+1)] \tag{A.4} $$

Up to this point we have concentrated on the decay process in which a neutron converted into a proton. There are a large number of unstable nuclei that have more protons in the nucleus than the stable isobar and so will decay by converting a proton into a neutron. We can write an equation for β decay that is exactly analogous to the previous equation.

$$ {}^{A}Z_n \rightarrow {}^{A}\ (Z-1)^{+}_{N+1} + e^{+} + \nu_e + Q^{+}_{\beta} \tag{A.5} $$

where we have replaced both the electron and the electron anti-neutrino with their respective antiparticles, the positron, and the electron neutrino. Note in this case, in contrast to β-decay, the charge on the daughter ion is negative. This means that there is an extra electron present in the reaction compared to that with a neutral daughter atom. Thus, the Q value must reflect this difference:

$$ Q^{+}_{\beta} = M[{}^{A}Z] - M[{}^{A}(Z-1)] + 2m_e c^2 \tag{A.6} $$

where m_e is the electron mass. Recall that particles and antiparticles have identical masses. This equation shows that spontaneous β^+ decay requires that the mass difference between the parent and daughter atoms be greater than $2m_e c^2 = 1.022$ MeV. Nature takes this to be an undue

restriction and has found an alternative process for the conversion of a proton into a neutron (in an atomic nucleus). The process is the capture of an orbital electron by a proton in the nucleus. This process, called electron capture (EC), is particularly important for heavy nuclei. The reaction is written as:

$$ {}^{A}Z_n \rightarrow {}^{A}\,(Z-1)^{+}_{N+1} + \nu_e + Q_{EC} \tag{A.7} $$

where all the electrons are implicitly understood to be present on the atom. This process also has the property that the final state has only two products so conservation of momentum will cause the neutrino to be emitted with precise energies depending on the binding energy of the captured electron and the final state of the daughter nucleus. Indicating β^- decay of neutron rich nuclei, β^+ decay of proton rich nuclei and electron capture decay of proton rich nuclei. Neglecting the electron binding energies in computing the decay energetic, we have

$$ Q^{-}_{\beta} = (M_P - M_D)c^2 \tag{A.8} $$

$$ Q^{+}_{\beta} = (M_P - M_D)c^2 + 2m_e c^2 \tag{A.9} $$

$$ Q_{EC} = (M_P - M_D)c^2 \tag{A.10} $$

where M_P and M_D are the atomic mass of the parent and daughter radionuclides involved and M_e is the electron mass. Typical values of $Q^{-}_{\beta} \sim 0.5 - 2$ MeV, $Q^{+}_{\beta} \sim 2 - 4$ MeV, and $Q_{EC} \sim 0.2 - 2 - 4$ MeV. As a final point in the introduction, it is interesting to note that the analogous process of positron capture by neutron excessive nuclei should be possible in principle. However, such captures are hindered by two important facts: first, the number of positrons available for capture is vanishingly small in nature, and second, both the nucleus and the positron are positively charged and will repel one another. Compare this to the situation for electron capture in which the nucleus is surrounded by (negative) electrons that are attracted to the nucleus, of course, and the most probable position to find any s-electrons is at the nucleus ($r = 0$).

A.3 Fermi theory of beta decay

The week interaction can be written in term of the particle field wave function

$$V_{int} = g\ \psi_e^*\ \psi_\nu \tag{A.11}$$

Where g is the coupling constant that determines how strong the interaction is. Then the matrix element $V_{if} = \langle \psi_i \rangle$ can be written as

$$V_{if} = \int g\ \psi_f^* \cdot [\psi_e^* \cdot \psi_\nu^*] \cdot \psi_i\ dr \tag{A.12}$$

To first approximation the electron and neutrino wave functions can be written as plane waves as

$$\psi_e\,(r) = Ae^{i\vec{k}_e \cdot \vec{r}} = \frac{1}{\sqrt{V}} \quad e^{i\vec{k}_e \cdot \vec{r}} \tag{A.13}$$

$$\psi_\nu\,(r) = Be^{i\vec{k}_\nu \cdot \vec{r}} = \frac{1}{\sqrt{V}} \quad e^{i\vec{k}_\nu \cdot \vec{r}} \tag{A.14}$$

Where we have applied a normalization condition to determine the constants A and B. We can expand the exponential for $r \sim 0$ (the nuclear volume) as

$$e^{i\vec{k}\cdot\vec{r}} = 1 + i\vec{k} \cdot \vec{r} + \frac{\left(i\vec{k} \cdot \vec{r}\right)^2}{2!} + \frac{\left(i\vec{k} \cdot \vec{r}\right)^3}{3!} + ... \cong 1 \tag{A.15}$$

Then the wave function of electron and neutrino can be written as

$$\psi_e\,(r \sim 0) = \frac{1}{\sqrt{V}} \tag{A.16}$$

$$\psi_\nu\,(r \sim 0) = \frac{1}{\sqrt{V}} \tag{A.17}$$

Thus

$$V_{if} = g\frac{1}{V}\int \psi_f^*\,(r) \cdot \psi_i\,(r)\,dr \tag{A.18}$$

One can write the matrix element as

$$V_{if} = g\frac{1}{V}M_{if} \tag{A.19}$$

Where M_{if} is a very complicated function of nuclear spin and angular momentum states. In addition, we can use it in the Fermi Golden rule; it does not depend on the lepton's energies

$$\mid M_{if} \mid^2 \rightarrow \mid M_{if} \mid^2 F\left(Z_0, Q_\beta\right) \tag{A.20}$$

Where the Fermi function $F\left(Z_0, Q_\beta\right)$ counts for the Coulomb interaction between nucleus and the electrons. The probability of emitting an electron with a momentum p_e between p_e and d_{p_e} becomes

$$\lambda\left(p_e\right) d_{p_e} = \frac{1}{2\pi^3 \hbar^7 c^3} g^2 \left(Q - T_e\right)^2 p_e^2 \, d_{p_e} \tag{A.21}$$

Where $\mid M_{if} \mid^2$ is a nuclear matrix element representing the overlap between the initial and final nuclear states. This matrix element must be evaluated with the detailed nuclear wave functions, for example, those available from the shell model. Collecting all constants for a given decay, the probability of decay as a function of the electron momentum is:

$$\lambda\left(p_e\right) d_{p_e} = (constants) \left(Q - T_e\right)^2 p_e^2 \, d_{p_e} \tag{A.22}$$

This form (even though it is mixed with a momentum part and an energy part for the electron) clearly goes to zero at $p_e = 0$ and at $T_e = Q$ and has a maximum in between. The shape of this function is shown in Fig. A.1 .

This function is often called the statistical or phase space factor for the decay. We should be sure to note that we have made a big approximation in ignoring the charge on the emitted electron. Positively charged β^+ particles (positrons) will be repelled by the nucleus and shifted to higher energies while negatively charged β^- particles (electrons) will be attracted and slowed down. These effects were incorporated by Fermi by using Coulomb-distorted wave functions and are contained in a spectrum distortion expression called the Fermi function, $F\left(Z_D, p_e\right)$, where Z_D is the atomic number of the daughter nucleus. The β spectrum thus has the form:

$$\lambda\left(p_e\right) d_{p_e} = (constants) \, F\left(Z_D, p_e\right) \left(Q - T_e\right)^2 p_e^2 \, d_{p_e} \tag{A.23}$$

The effects of the Coulomb distortion can be seen in the measured spectra from the decay of ^{64}Cu shown in Fig. A.2. This odd-odd nucleus

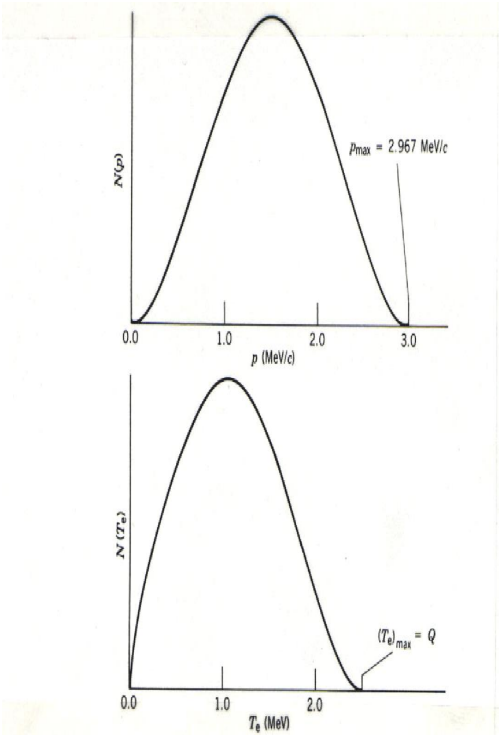

Figure A.1: The shape of the statistical factor for beta decay, which represents the expected shape of the electron momentum distribution before distortion by the Coulomb potential

undergoes both β^- and β^+ decay to its even-even neighbors with very similar Q values.

A.4 Density of States

In this case there are two types of particles (e) and (ν) as a product of the reaction and both can be in continuum of possible states. Then the number of states in a small energy volume $(E + dE)$ is the product of the

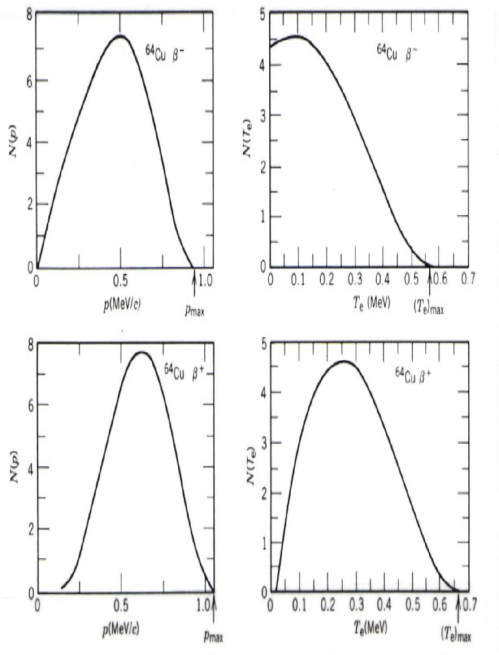

Figure A.2: The momentum and energy spectra from the decay of ^{64}Cu for β^- decay and β^+ decay. The Q values for these decays are 0.5782 and 0.6529 MeV, respectively.

electron and neutrino's states

$$d^2 n_s = dn_e \cdot dn_\nu \tag{A.24}$$

The two particles share the Q energy

$$Q_\beta = T_e - T_\nu \tag{A.25}$$

For simplicity $m_\nu \cong 0$, then we can take relativistic expression as

$$T_\nu = cp_\nu \tag{A.26}$$

While the electron is

$$E^2 = p^2c^2 + m^2c^4 \rightarrow T_e + m_ec^2 \tag{A.27}$$

With $T_e = \sqrt{p^2c^2 + m_e^2c^4} - m_ec^2$ we can write the kinetic energy of the neutrino as a function of the electrons

$$T_\nu = Q_\beta - T_e \tag{A.28}$$

The number of states for the electrons can be calculated from quantized momentum under the assumption that the electron state is a free particle $\psi_e(r) \sim e^{i\vec{k}_e \cdot \vec{r}}$ in a region of Volume $V = L^3$ and

$$dn_e = \frac{4\pi V}{(2\pi\hbar)^3}\ p_e^2\ dp_e \tag{A.29}$$

Similarly, for the neutrino, the number of states of the free neutrino with momentum between p_ν and $p_\nu + dp_\nu$ in a volume V is

$$dn_\nu = \frac{4\pi V}{(2\pi\hbar)^3}\ p_\nu^2\ dp_\nu \tag{A.30}$$

The total number of states is the product of these two factors

$$d^2n_s = dn_e \cdot dn_\nu = \frac{16\pi^2V^2}{(2\pi\hbar)^6}\ p_e^2p_\nu^2\ dp_e\ dp_\nu \tag{A.31}$$

If we assume the neutrino has zero rest Mass

$$p_\nu = \frac{T_\nu}{c} = \frac{Q - T_e}{c} \tag{A.32}$$

$$dp_\nu = \frac{dQ}{c} \tag{A.33}$$

Then, we get

$$dn = \frac{V^2}{4\pi\hbar^6c^3}(Q - T_e)^2\ \ p_e^2\ dp_e dQ \tag{A.34}$$

$$\frac{dn}{dQ} = \frac{V^2}{4\pi\hbar^6c^3}(Q - T_e)^2\ \ p_e^2 dp_e \tag{A.35}$$

(One must understand this equation expresses the variation of the number of final states with changes in the Q value of the decay and does not represent differentiation with respect to a constant Q).

$$\rho\left(E_e\right) = \frac{V^2}{4\pi\hbar^6 c^3}\left(Q - T_e\right)^2 \; p_e^2 \, \frac{dp_e}{dE_e} \tag{A.36}$$

Knowing the density of states, we can calculate how many electrons are emitted in β decay with a given energy, this will be proportional to the rate of emission calculated from the Fermi Golden rule times the density of the state

$$N\left(p\right) = CF\left(Z,Q\right) \mid V_{if} \mid^2 \cdot \frac{p^2}{c^2}\left(Q - T_e\right)^2 \tag{A.37}$$

For the electron

$$N\left(T_e\right) = \frac{C}{c^5} F\left(Z,Q\right) \mid V_{if} \mid^2 \cdot \left(Q - T_e\right)^2 \sqrt{T_e^2 + 2T_e^2 m_e c^2 \left(T_e + m_e c^2\right)} \tag{A.38}$$

This distribution are nothing else than the spectrum of the emitted beta particle e^- or e^+, C is a constant of various parameters deriving from the Fermi Golden rule and density of states calculation. $F(Z,Q)$ is called *Fermi Function*, that takes into account the shape of the nuclear wave function and in particular it describes the Coulomb interaction or repulsion of the electron or positron from the nucleus. Thus $F(Z,Q)$ is different depending on the type of the decay.
There are three terms that describe the spectrum and decay rate of beta decay process

1. $\frac{p^2}{c^2}\left(Q - T_e\right)^2$ is the statistical factor rising from the density of states calculation

2. $F(Z,Q)$ is the Fermi function which is linked with the number of protons of the daughter nucleus and counts for the influence of the nuclear Coulomb field, "the shift affects the low energy electron"

3. $\mid V_{if} \mid^2$ is the translation amplitude from the Fermi Golden rule.

A.5 Kurie Plots

We have seen that the β spectrum has an endpoint at the Q value, but the form of equation for the spectrum does not allow us to easily identify the endpoint. Notice that with a little rearrangement this spectrum can be represented as:

$$\sqrt{\frac{\lambda\left(p_e\right)}{p_e^2 F\left(Z, p_e\right)}} \propto \left(Q - T_e\right) \mid M_{fi} \mid^2 \tag{A.39}$$

If the nuclear matrix element does not depend on the electron kinetic energy, as we have assumed so far, then a plot of the reduced spectral intensity, the left-hand side, versus the electron kinetic energy will be a straight line that intercepts the abscissa at the Q-value. Such a graph is called a *Kurie plot* and an example is shown in Fig. A.3 . This procedure applies to allowed transitions. There are corrections term that need to be taken into account for forbidden transitions.

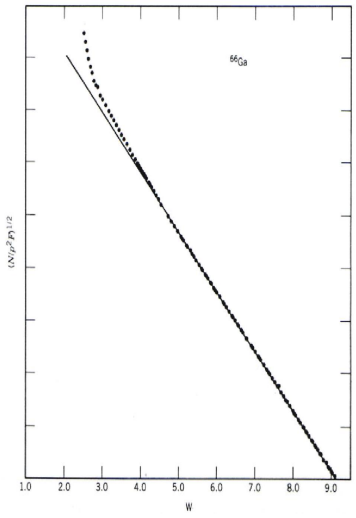

Figure A.3: An example of a Kurie plot.

A.6 Beta Decay Rate Constant

The differential form of the spectrum can be integrated over all electron momenta to obtain the total decay constant. The expression, for a constant nuclear matrix element, to be integrated is

$$\lambda = \frac{g^2 \mid M_{fi} \mid^2}{2\pi^3 \hbar^7 c^3} \int_0^{p_{max}} F\left(Z_D, p_e\right) p_e^2 \left(Q - T_e\right)^2 dp \tag{A.40}$$

Note that an appropriate relativistic substitution for T in terms of the momentum is still needed. This integral has been shown to only depend on the atomic number of the daughter and the maximum electron momentum. The integral, called the *Fermi integral*, $f\left(Z_D, Q\right)$, is complicated but numerical expressions or tables of the solutions are available. Note that the differential Fermi function $F\left(Z_D, p_e\right)$, contains the momentum and the Fermi integral, $f\left(Z_D, Q\right)$, contains the Q value. The Fermi integral is a constant for a given beta decay and has been presented in many forms. The decay constant is now reduced to an expression with the nuclear matrix element, $M\left(\equiv \mid M_{fi} \mid\right)$, and the strength parameter, g, written:

$$\lambda = \frac{g^2 \mid M \mid^2 m_e^5 c^4}{2\pi^3 \hbar^7} f\left(Z_D, Q\right) \tag{A.41}$$

Or in terms of the half-life of the parent, $t_{1/2}$

$$ft_{1/2} = \ln 2 \frac{2\pi^3 \hbar^7}{g^2 \mid M \mid^2 m_e^5 c^4} \propto \frac{1}{g^2 \mid M \mid^2} \tag{A.42}$$

The left-hand side of this equation is called the comparative half-life, or *"ft value"* because this value can be readily measured in experiments and should only depend on the nuclear matrix element and the beta decay strength constant. Recall that β decay half-lives span many orders of magnitude so the ft values will span a similarly large range. It is therefore convenient to use the common logarithm of the ft value (with $t_{1/2}$ in seconds) to characterize observed β decays.

A.7 Selection rule

The quantum mechanical selection rules for beta decay with no relative angular momentum in the exit channel ($l = 0$) are $\Delta I = 0, 1$ and $\Delta\pi = 0$. The two values for the spin change come directly from the two possible couplings of the spins of the electron and neutrino. Some representative "allowed" beta decays are described in the table A.1 along with their ft values and the character of the decay. As mentioned earlier, the decay of the neutron into a proton can take place with no change in angular momentum between the spin $1/2$ particles and the angular momentum coupling rules allow both decay modes.

The decay of the neutron into the proton is an important example of decay between mirror nuclei. In the β decay of mirror nuclei, the transformed nucleons (neutron $\rightarrow$ proton or proton $\rightarrow$ neutron) must be in the same shell and have very similar wave functions. This gives rise to a large matrix element $\mid M_{fi} \mid^2$ and a very small $\log ft$ value. For the beta decay of mirror nuclei to their partners, $\log ft$ values are about 3, which is unusually small. Such transitions are called *super-allowed* transitions. When the initial and final states in beta decay have opposite parties, decay by an *"allowed"* transition cannot occur. However, such decays can occur, albeit with reduced probability compared to the allowed transition. Such transitions are called *"forbidden"* transitions even though they do occur. The forbidden transitions can be classified by the spin and parity changes (and the corresponding observed values of $\log ft$) as in the table A.1.

Table A.1: Classification of β decay transitions

Transition type	$\log ft$	**L**β	$\Delta\pi$	**Fermi**ΔJ	**Gamow- Teller** ΔJ
Super allowed	$2.9 - 3.7$	0	No	0	0
allowed	$4.4 - 6$	0	No	0	$0, 1$
1^{st} **Forbidden**	$6 - 10$	1	Yes	$0, 1$	$0, 1, 2$
2^{nd} **Forbidden**	$10 - 13$	2	No	$1, 2$	$1, 2, 3$
3^{rd} **Forbidden**	> 15	3	Yes	$2, 3$	$2, 3, 4$

Remember that in beta decay

$$\vec{J}_P = \vec{J}_D + \vec{J}_\beta + \vec{S}_\beta \tag{A.43}$$

$$\pi_P = \pi_P \left(-1\right)^{L_\beta} \tag{A.44}$$

Where the subscripts P, D refer to the parent and daughter nuclei, L is the orbital angular momentum carried away by the emitted electron and S_β is the coupled spin of the electron-neutrino pair ($S_\beta = 0$ for a Fermi transition and $S_\beta = 1$ for a Gamow-Teller transition).

A.8 Electron Capture Decay

When the decay energy is less than 1.022 MeV $(2m_e c^2)$ the β decay of a proton rich nucleus to its daughter must take place by electron capture (EC). For decay energies greater than 1.022 MeV, EC and β^+ decay competes. In EC decay, only one particle, the neutrino, is emitted with energy $M_p c^2 - M_D c^2 - E_b$, where E_b is the binding energy of the captured electron. The decay constant for electron capture can be written, assuming a zero neutrino rest mass, as

$$\lambda_{EC} = \frac{g^2 \mid M_{fi} \mid^2 T_\nu^2}{2\pi^2 c^3 \hbar^3} \mid \phi_K \left(0\right) \mid^2 \tag{A.45}$$

Where we have assumed that the capture of a $1s$ (K) electron will occur because the electron density at the nucleus is the greatest for the K electrons. The K electron wave function can be written as

$$\phi_K \left(0\right) = \frac{1}{\sqrt{\pi}} \left(\frac{Z m_e^2 e^2}{4\pi\varepsilon_0 \hbar^2}\right)^{\frac{3}{2}} \tag{A.46}$$

Thus

$$\lambda_{K-EC} = \frac{g^2 Z^3 \mid M_{fi} \mid^2 T_\nu^2}{constant} \tag{A.47}$$

Comparison of the decay constants for EC and β^+ decay show

$$\frac{\lambda_K}{\lambda_{\beta^+}} = constant \, \frac{Z^3 T_\nu^2}{f\left(Z_D, Q\right)} \tag{A.48}$$

Thus EC decay is favored for high Z nuclei. Of course, the decay energy must be greater than 1.022 MeV for β^+ decay, a situation found

mostly in low Z nuclei where the slope of the walls of the valley of β stability is large (see Fig. A.2) and decay energies of > 1.022 MeV occurs. Electron capture decay produces a vacancy in the atomic electron shells and secondary processes that lead to filling that vacancy by the emission of *X*-rays and Auger electrons occur. These *X*-rays permit the detection of EC decays.

Appendix B

Liquid scintillation counting

B.1 Early stage of liquid scintillation counter

Liquid scintillation counting (LSC) was used for relative activity measurements of β-emitters at an early time, and α-emitters later. In this technique the active solution is mixed with a solution of liquid scintillator. As α- or β-particles are emitted, the scintillator emits photons which can be easily detected and counted. In this way the source of self-absorption is avoided. Similarly, effects of wall scattering are eliminated because the detector is effectively of 4π geometry. However, particles emitted near the wall of the scintillator container, traveling towards the wall may not expend all their energy in the scintillator. This will give rise to an excess of low energy pulses and corresponding reduction in the number of high energy pulses the so-called *wall effect*.

When liquid scintillation counting was first introduced in the beginning of 1950, the detection efficiency of liquid scintillation counting was very low with only a few percent for tritium due to the instability of the solutions and low quantum efficiency. The early system consisted of a single phototube. For counting a source with low energy and low activity, the background counting rate in the phototube was a severe limitation. An improvement was made by using a pair of phototubes facing a common scintillation source. Because there are multiple photons emitting in the sample, it is likely that both phototubes will detect the light

and thus the utilization of coincidence technique is possible. The randomly occurring background events (thermal noise) in one phototube are only infrequently coincident with those in the second tube, whereas radiations from the source may generate coincidence events between two tubes. Therefore, a high degree of discrimination against background counts is feasible. Systems operating with two phototubes in the coincidence mode have a reduced efficiency but avoid the effects of thermal noise and after pulsing [268].

A two phototube system does not give enough information to determine the experimental detection efficiency without an additional reference standard or tracer, and therefore is used for indirect activity measurement. The tracer technique relied either upon quench curves or compensating for the quenched state. Various procedures have been employed, such as extrapolation of the integral counting rate versus discrimination level [269, 270, 271] and efficiency tracing [162, 272, 273, 274].

For the measurement of beta radiation three methods are commonly used: gas flow proportional counting, Čerenkov counting and liquid scintillation counting. Liquid scintillation counting has been a very popular technique for the detection and quantitative measurement of radioactivity since the early 1950's. This technique remains one of the most used experimental techniques for the quantitative analysis of radionuclides. These include principally alpha and beta emitters, but may also include weak gamma, *X*-ray and Auger electron emitters. The wide popularity is a consequence of numerous advantages, which are high efficiencies of detection (specially for alpha and high energy beta emissions), improvements in sample preparation techniques, automation including computer data processing and the spectrometer capability of analyzers permitting the simultaneous assay of different nuclides [85]. Due to the low penetrative power of beta radiation, the best quantification of beta emitters is achieved when the sample is dissolved directly in the scintillation solution. The physical information on the amount of radioactivity dissolved in the liquid scintillator is carried out by counting the optical photons produced in the reaction of beta particles with the scintillator. This technique avoids many sources of error associated with counting a solid source, such as self-absorption, backscattering, loss of activity during evaporation because of volatilization, and variable detection efficiency

over a wide beta-energy range. In addition to the improvement in the detection capability offered by LSC over other beta counting techniques, sample preparation time and counting times may be significantly shorter. Sample preparation involves only adding a soluble sample aliquot to the scintillation cocktail to form a liquid test source. The best possible detection efficiency is achieved when the sample is dissolved in the scintillation solution. By counting the optical photons produced in the reaction of beta particles with the scintillator, the quantification of beta emitting isotopes can be easily carried out.

B.2 The scintillation processes

The liquid scintillation technique involves placing the sample containing the radioactivity into a container (plastic or glass), called scintillation vial, and adding a special scintillation cocktail. Basically, the liquid scintillation process is the conversion of the energy of a radioactive decay event into photons of light. The amplification of the scintillator light is done by using a photomultiplier. The photomultiplier tubes (PMTs) are used to detect and convert the photons into electrical pulses [275]. The number of photons released by the scintillator is directly proportional to the energy of the beta particles; this property of the scintillator can be used, not only for counting, but also to record the beta spectrum of the radionuclides dissolved in the liquid scintillator. One of the problems in liquid scintillation counting is that all the scintillation events cannot be detected, so that the counting efficiency is normally less than 100% and the actual efficiency must be determined before the activity of the radioactive material can be calculated [276]. The operation of the scintillation counter can be divided into five distinct, consecutive stages: the absorption of the energy of the incident radiation by the solvent molecules, the transmission of the absorbed energy between the solvent and the fluor molecules, the luminescent conversion of the energy dissipated in the fluor and the emission of photons of light, the transit of the emitted photons to the cathode of the photomultiplier, the absorption of the photons at the cathode and the emission of the photoelectrons and the electron multiplication process [277].

As LSC solvent, aromatic compounds are usually used. When they react with beta particles, a large amount of fluorescence can be produced. To capture the solvent energy and emit light at a wavelength more easily detected by the PMT, fluor is used. Unfortunately, the PMTs are also not sensitive in the region of fluorescence emission of the primary scintillators; therefore a wavelength shifter (secondary scintillator) was introduced. This absorbs energy from the primary scintillator and emits light at a wavelength more suitable to the PMT. Fig. B.1 shows the liquid scintillation process [278]. The PMTs have been developed to convert the minute flashes of light into measurable electrical pulses. The photons of light are collected by the optical reflector system of the scintillation counter to the light sensitive photocathode of the PMT and multiplied. The electrical charge pulse obtained is proportional to the original beta particle energy.

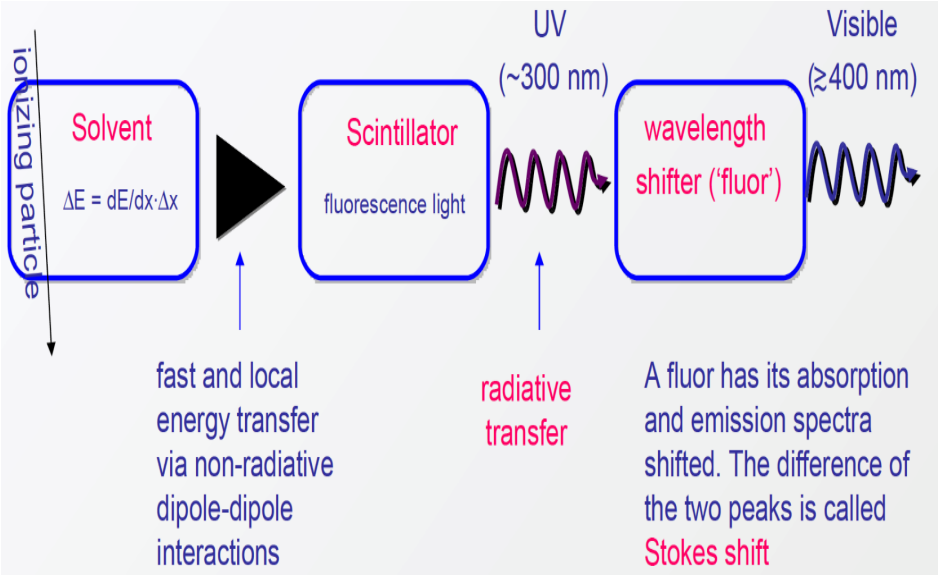

Figure B.1: Liquid scintillation process.

To accomplish the absorption of the emitted energy and its re-emission, the liquid scintillation cocktails contain two basic components, the solvent and the fluor. The solvent must act as an efficient collector of energy and it must conduct that energy to the fluor molecules instead of dissipating the energy by some other mechanism. The solvent must not quench the scintillation of the fluor, and, finally, it must dissolve the fluor to produce a stable, countable solution. The prototypical LSC solvent is toluene. Thus, β-particle passing through a toluene solution leaves in its wake a number of energized toluene molecules. The greater the energy of the beta particle the greater will be the number of solvent molecules that become excimers. The excimers release this energy very quickly in the form of ultraviolet radiation which then excites fluor molecules in the solvent. Dissolved in the solvent, molecules of fluor convert the absorbed energy into light. The incident particle impinges on fluor where it dissipates its energy in the ionization and excitation of the molecules. A fraction of this energy is converted into photons which are radiated in all directions. Some of these photons fall on the photocathode of the photomultiplier tube and eject a number of photoelectrons. The fluor molecules will then release the energy in the UV-Visible light, in a range acceptable for effective conversion into an electronic pulse by the PMT. Each scintillator molecule gives off only one photon on activation, but multiple scintillators are activated by the energized molecules generated by one β-particle. The number of photons generated (pulse event) is directly proportional to the energy of the β-particle and the number of pulse events per second corresponds to the number of radioactive emissions [278]. A schematic representation of the scintillation process is presented in Fig. B.2 [278].

In preparing samples for liquid scintillation counting, the physical and chemical characteristics of the sample determine the type of counting solution required. A wide range of scintillator solutions is available in modern radiochemical laboratories. The choice of suitable cocktail composition for a particular application should be characterized by having low background and high sample loading capacity [276]. Many references are available on the types of solvents and scintillators for a particular application.

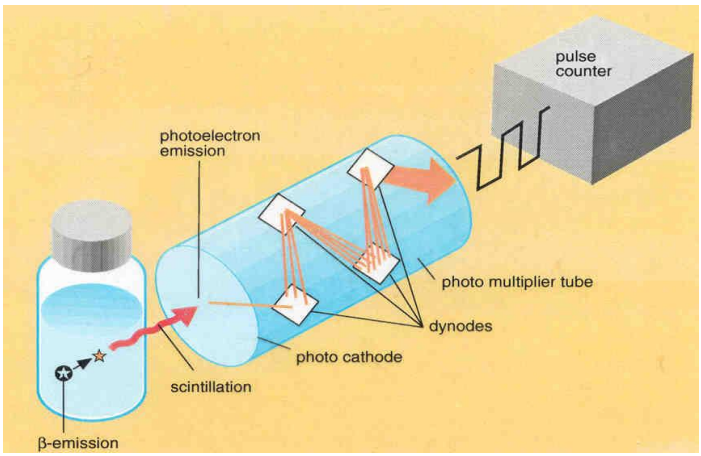

Figure B.2: Schematic representation of LS process.

B.3 Quenching in liquid scintillation counter

As a consequence of the complex processes involved in the energy transfer in the liquid scintillation detector, various disruptions in the energy transfer can occur. These mechanisms are described as quench effects. Quenching is a term used to describe energy losses occurring in the energy transfer process due to sample or cocktail characteristics and may result from a variety of components in a sample. Quenching causes a reduction in the photon yield from each radioactive decay event, resulting in the whole energy distribution being shifted down and counts are reduced. Any factor reduces the efficiency of the energy transfer or causes the absorption of photons, resulting in quenching in the sample. Generally, the more the sample is quenched, the lower it is the counting efficiency capacity [276].

There are three types of quench: physical, chemical and color quench. Physical quench occurs when a barrier impairs contact between the radioactive particle and the scintillator solution, or when the generated

photons of light are absorbed into the vial. Radioactivity adsorbed onto active surfaces or filter disks, and two phase aqueous organic solutions are some of the most common sources of physical quenching. In Fig. B.3, the three types of quench which occur during the scintillation process are presented.

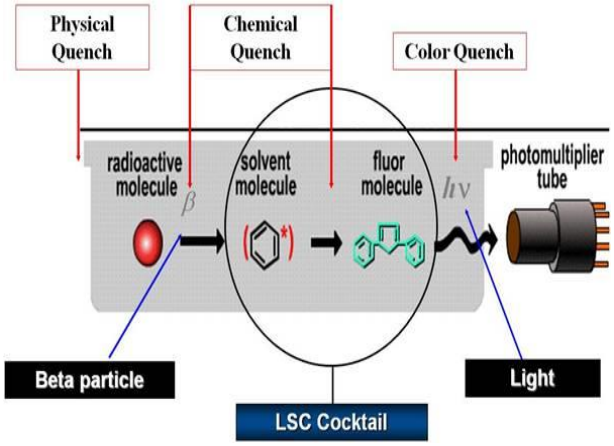

Figure B.3: Three types of quench: physical, chemical, and color quench.

Chemical quench occurs during the transfer of energy from the solvent to the scintillator (fluor molecules) and reduces the number of photons generated by each charged particle. This kind of quench is caused by the presence of added substances acting as chemical scavengers of excited molecules of the solvent, leading to the production of heat instead of light. The scale of chemical quenching depends on the lifetime of the excited states of the solvent and solute molecules, on the chemical structure and on the concentration of the quencher. The most active quenchers are organic acids, amines, aliphatic alkenes, sulfides, ketones, aliphatic hydrocarbons and dissolved oxygen. Color quench is caused by the attenuation of photons emitted by the scintillator, which is due to the presence of colored substances in the radioactive solution or scintillator degradation. Though liquids scintillators are colorless, the addition of certain materials is sufficient to color them and produce quenching [170]. Color quenching

leads to an isotropy of the light emitted, which may cause problems in coincidence counting. In order to take under control the variation on the detection efficiency, it is useful to change the operating conditions of the counter because, if all the contributions to the detection efficiency calculation are correctly evaluated, the measured activity of the source must be equal under different counting conditions. Several methods could be used to decrease detection efficiency, e.g. chemical quenching, use of coaxial grey filters and defocusing of photomultiplier tubes by reducing the focusing electrode potential. The first two processes reduce the mean quantity of light emission. The last reduces the detection probability. The different amount of quenching will be reflected in the counting efficiency and consequently the estimation of the disintegration rate of a sample or sample activity will require information about the counting efficiency [175].

In all three types of quenching, the loss of the pulses is due not only to the pulses below the detectable level, but also to total absorption of the light by the quench agent; the energy of all light pulses is reduced, so the total counting is reduced. This leads to an underestimate of the total counts, and thus of the activity of the radionuclide present in the solution. It also leads to a shift in the energy spectrum of the sample toward the low energy region. These quench effects all contribute to a spectral shift to lower energies and to a decrease in the total count rate. In Fig. B.4, an example of the quench effect on a beta spectrum in a LS counter is shown.

Loss of energy is the result in both cases as quenching shifts the energy spectrum to lower energies (see Fig. B.4). Factors that can influence the degree of quenching include the sample matrix, sample preparation, and choice of scintillation cocktails. Several techniques have been developed to correct the effect of quenching. The traditional method for quench correction is to add an internal standard to each sample to determine the counting efficiency for each sample matrix. This method continues to be one of the most accurate but is labor intensive and expensive [279].

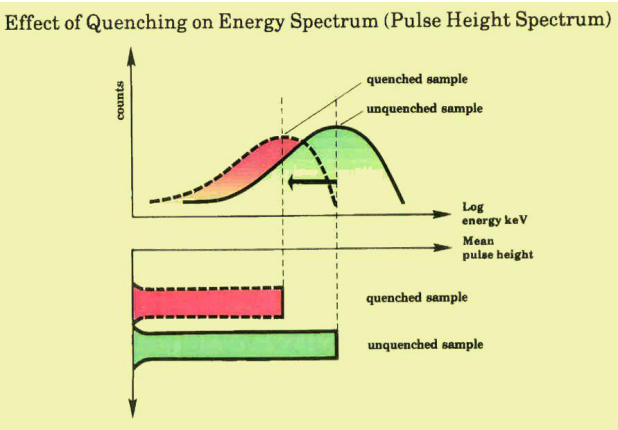

Figure B.4: Quenching effect on beta spectrum in LSC.

Appendix C

Standard uncertainty of the TDCR value

When applying the TDCR method, the detection efficiency is derived from the ratio of the net count rates of triple and double coincidences. For three PMTs named A, B and C, let R_{AB}, R_{BC} and R_{AC} be the double coincidence count rates for the three pairs of PMT, and R_D and R_T be the logical sum of double coincidences and triple coincidence count rates, respectively. The arithmetic relationship between these count rates is: $R_{AB} + R_{BC} + R_{AC} = 2R_T + R_D$. This equation confirms that the count rates are correlated, which is obvious if one considers that triple coincidences are also double coincidences. Thus, for the correct evaluation of the uncertainty of TDCR values, the covariance between the count rates must be considered.

$$\mathrm{u}^2(R_T/R_D) = u^2(R_T) \cdot \left(\frac{\partial(R_T/R_D)}{\partial R_T}\right)^2 + u^2(R_D)$$

$$\cdot \left(\frac{\partial(R_T/R_D)}{\partial R_D}\right)^2 + 2u^2(R_T, R_D) \cdot \frac{\partial(R_T/R_D)}{\partial R_T} \cdot \frac{\partial(R_T/R_D)}{\partial R_D} \qquad \text{(C.1)}$$

The relative variance of R_T/R_D becomes:

$$\frac{u^2(R_T/R_D)}{(R_T/R_D)^2} = \frac{u^2(R_T)}{R_T^2} + \frac{u^2(R_D)}{R_D^2} - \frac{2}{R_T R_D} u^2(R_T, R_D) \qquad \text{(C.2)}$$

And so, the relative standard uncertainty of R_T/R_D is:

$$\frac{u(R_T/R_D)}{R_T/R_D} = \sqrt{\frac{u^2(R_T)}{R_T^2} + \frac{u^2(R_D)}{R_D^2} - \frac{2}{R_T R_D} u^2(R_T, R_D)} \tag{C.3}$$

Experience shows that the covariance term is always positive and thus the relative standard deviation of the TDCR calculated using equation (B.3) is always lower than its simple evaluation neglecting the covariance term. The uncertainty of the TDCR value from equation (B.3) can be propagated to obtain the uncertainty of ε_D. To this end, a function ε_T(TDCR) can be fitted using computed counting efficiencies. Often a 2nd degree polynomial is sufficient to parameterize ε_D(TDCR) in the region of interest.

Appendix D

TDCR parameters as a function of defocusing parameter and KB factor for different radionuclides

Table D.1: ^3H TDCR parameter as a function of defocusing parameter for KB= 0.07 and 0.08 mm/MeV, with uncertainty less than 1%.

KB(mm/MeV)	0.07		0.08	
Defocusing parameter	**CEA**	**G4RDecay**	**CEA**	**G4RDecay**
0.70	0.2912	0.287	0.2834	0.2873
0.72	0.3006	0.3080	0.2892	0.2914
0.74	0.3049	0.3139	0.2933	0.2832
0.76	0.3140	0.3156	0.3179	0.3102
0.78	0.3222	0.3242	0.3279	0.3070
0.80	0.3342	0.3331	0.3199	0.3291
0.82	0.3383	0.3365	0.3204	0.3242
0.84	0.3360	0.3431	0.3346	0.3322
0.86	0.3360	0.3513	0.3367	0.3425
0.88	0.3412	0.3604	0.3465	0.3462
0.90	0.3558	0.3457	0.3576	0.3571
0.92	0.3624	0.3577	0.3690	0.3735
0.94	0.3650	0.3714	0.3636	0.3787
0.96	0.3736	0.3833	0.3822	0.3724
0.98	0.3823	0.3816	0.3788	0.3843
1.0	0.3894	0.3868	0.3985	0.3848

Table D.2: TDCR parameter as a function of defocusing parameter for KB= 0.09 and 0.10 mm/MeV for ^3H, with uncertainty less than 1%.

KB(mm/MeV)	0.09		0.1	
Defocusing parameter	**CEA**	**G4RDecay**	**CEA**	**G4RDecay**
0.70	0.2905	0.2785	0.2865	0.2829
0.72	0.2859	0.2945	0.2772	0.2847
0.74	0.3013	0.3087	0.2861	0.2896
0.76	0.3010	0.3072	0.2893	0.2961
0.78	0.3145	0.3082	0.2876	0.3128
0.80	0.3204	0.3197	0.3165	0.3218
0.82	0.3368	0.3156	0.31351	0.3269
0.84	0.3346	0.3331	0.3200	0.3235
0.86	0.3340	0.3370	0.3378	0.3323
0.88	0.3493	0.3465	0.3274	0.3382
0.90	0.3437	0.3600	0.3375	0.3507
0.92	0.3568	0.3597	0.3500	0.3521
0.94	0.3533	0.3591	0.3721	0.3542
0.96	0.3564	0.3701	0.3616	0.3642
0.98	0.3770	0.3682	0.3770	0.3706
1.0	0.3759	0.3774	0.3695	0.3749

Table D.3: TDCR parameter as a function of defocusing parameter for KB= 0.11 and 0.12 mm/MeV for ^3H, with uncertainty less than 1%.

KB(mm/MeV)	0.11		0.12	
Defocusing parameter	**CEA**	**G4RDecay**	**CEA**	**G4RDecay**
0.70	0.2864	0.2744	0.2657	0.2601
0.72	0.2759	0.2622	0.2686	0.2747
0.74	0.2838	0.2838	0.2858	0.2879
0.76	0.2885	0.2860	0.2973	0.2940
0.78	0.2954	0.3026	0.2896	0.2784
0.80	0.3036	0.3006	0.3037	0.3001
0.82	0.3254	0.3035	0.3092	0.2886
0.84	0.3244	0.3091	0.3003	0.3151
0.86	0.3227	0.3197	0.3033	0.3216
0.88	0.3378	0.3288	0.3159	0.3242
0.90	0.3251	0.3376	0.3177	0.3316
0.92	0.3284	0.3358	0.3338	0.3345
0.94	0.3373	0.3513	0.3424	0.3510
0.96	0.3536	0.3439	0.3391	0.3528
0.98	0.3599	0.3468	0.3490	0.3657
1.0	0.3598	0.3471	0.3349	0.3553

Table D.4: TDCR parameter as a function of defocusing parameter for KB= 0.13 and 0.14 mm/MeV for ^3H, with uncertainty less than 1%.

KB(mm/MeV)	0.13		0.14	
Defocusing parameter	**CEA**	**G4RDecay**	**CEA**	**G4RDecay**
0.70	0.2545	0.2730	0.0642	0.2587
0.72	0.2574	0.2674	0.0688	0.2799
0.74	0.2789	0.2698	0.0716	0.2719
0.76	0.2789	0.2865	0.0785	0.2810
0.78	0.2911	0.2687	0.0816	0.2737
0.80	0.2896	0.2987	0.0842	0.2912
0.82	0.3126	0.2890	0.0851	0.2886
0.84	0.3251	0.3132	0.0907	0.3082
0.86	0.31823	0.3212	0.0927	0.2968
0.88	0.3213	0.3153	0.1003	0.3009
0.90	0.3354	0.3277	0.1025	0.3206
0.92	0.3415	0.3227	0.1046	0.3342
0.94	0.3362	0.3343	0.108	0.3406
0.96	0.3455	0.3271	0.115	0.3296
0.98	0.3535	0.3334	0.1237	0.3277
1.0	0.3581	0.3541	0.1237	0.3467

Table D.5: ^{14}C TDCR parameter as a function of defocusing parameter for KB= 0.07 and 0.08 mm/MeV, with uncertainty less than 1%.

KB(mm/MeV)	0.07		0.08	
Defocusing parameter	**CEA**	**G4RDecay**	**CEA**	**G4RDecay**
0.70	0.8816	0.8759	0.8789	0.8828
0.72	0.885	0.8843	0.8818	0.8825
0.74	0.8882	0.8850	0.8849	0.8902
0.76	0.8892	0.8913	0.8874	0.8865
0.78	0.8908	0.8914	0.8926	0.8940
0.80	0.8908	0.8926	0.9010	0.8940
0.82	0.9010	0.8974	0.8931	0.8914
0.84	0.8967	0.9017	0.8939	0.8989
0.86	0.9102	0.9074	0.8961	0.9030
0.88	0.9056	0.9117	0.9059	0.9063
0.90	0.9046	0.9085	0.9014	0.9047
0.92	0.9110	0.9117	0.9079	0.9049
0.94	0.9050	0.9173	0.9116	0.9121
0.96	0.9171	0.9115	0.9119	0.9153
0.98	0.9148	0.9153	0.9134	0.9158
1.0	0.9193	0.9178	0.9119	0.9140

Table D.6: ^{14}C TDCR parameter as a function of defocusing parameter for KB= 0.09 and 0.10 mm/MeV, with uncertainty less than 1%.

KB(mm/MeV)	0.09		0.10	
Defocusing parameter	**CEA**	**G4RDecay**	**CEA**	**G4RDecay**
0.70	0.8785	0.8768	0.8764	0.8737
0.72	0.8798	0.8796	0.8727	0.8808
0.74	0.8864	0.8830	0.8819	0.8808
0.76	0.8859	0.8899	0.8899	0.8919
0.78	0.8940	0.8850	0.8843	0.8916
0.80	0.895	0.8930	0.8933	0.8930
0.82	0.8972	0.8987	0.8971	0.8917
0.84	0.8915	0.8979	0.8950	0.8947
0.86	0.9039	0.8979	0.8996	0.8979
0.88	0.9018	0.8980	0.8974	0.9002
0.90	0.9046	0.9068	0.9078	0.9038
0.92	0.9078	0.9066	0.9056	0.9035
0.94	0.9076	0.9110	0.9041	0.9095
0.96	0.9073	0.9055	0.9061	0.9153
0.98	0.9150	0.9185	0.9121	0.9113
1.0	0.9158	0.9135	0.9142	0.9139

Table D.7: ^{14}C TDCR parameter as a function of defocusing parameter for KB= 0.11 and 0.12 mm/MeV, with uncertainty less than 1%.

KB(mm/MeV)	0.11		0.12	
Defocusing parameter	**CEA**	**G4RDecay**	**CEA**	**G4RDecay**
0.70	0.8714	0.8687	0.8667	0.8756
0.72	0.8747	0.8777	0.8794	0.8759
0.74	0.8852	0.8760	0.8780	0.8737
0.76	0.8871	0.8813	0.8730	0.8847
0.78	0.8928	0.8886	0.8854	0.8842
0.80	0.8866	0.8892	0.8894	0.8920
0.82	0.8888	0.8922	0.8971	0.8917
0.84	0.8961	0.8889	0.8950	0.8947
0.86	0.8966	0.8904	0.8996	0.8979
0.88	0.8932	0.9044	0.8974	0.9002
0.90	0.8999	0.9028	0.9078	0.9038
0.92	0.9006	0.9074	0.9056	0.9035
0.94	0.9082	0.9025	0.9041	0.9095
0.96	0.9074	0.9108	0.9061	0.9153
0.98	0.9120	0.9101	0.9121	0.9113
1.0	0.9120	0.9113	0.9142	0.9139

Table D.8: ^{14}C TDCR parameter as a function of defocusing parameter for KB= 0.13 and 0.14 mm/MeV, with uncertainty less than 1%.

KB(mm/MeV)	0.13		0.14	
Defocusing parameter	**CEA**	**G4RDecay**	**CEA**	**G4RDecay**
0.70	0.8729	0.8720	0.8720	0.8699
0.72	0.8751	0.8770	0.8797	0.8667
0.74	0.8750	0.8744	0.8752	0.8746
0.76	0.8849	0.8784	0.8829	0.8833
0.78	0.8853	0.8870	0.8919	0.8765
0.80	0.8876	0.8852	0.8861	0.8875
0.82	0.8886	0.8905	0.8881	0.8933
0.84	0.8917	0.8955	0.8898	0.8889
0.86	0.8933	0.8957	0.8991	0.8896
0.88	0.8999	0.8959	0.9011	0.8933
0.90	0.8970	0.8967	0.8993	0.9008
0.92	0.9012	0.8979	0.8989	0.8946
0.94	0.8997	0.9030	0.9013	0.9052
0.96	0.9032	0.9008	0.9024	0.9036
0.98	0.9114	0.9022	0.9073	0.9130
1.0	0.9093	0.9132	0.9049	0.9099

Table D.9: ^{90}Y TDCR parameter as a function of defocusing parameter for KB= 0.07 and 0.08 mm/MeV, with uncertainty less than 1%.

KB(mm/MeV)	0.07		0.08	
Defocusing parameter	**CEA**	**G4RDecay**	**CEA**	**G4RDecay**
0.70	0.9969	0.9992	0.9962	0.9993
0.72	0.9960	0.9995	0.9960	0.9992
0.74	0.9948	0.9987	0.9963	0.9991
0.76	0.9961	0.9985	0.9974	0.9995
0.78	0.9961	0.9993	0.9967	0.9991
0.80	0.9956	0.9989	0.9966	0.9996
0.82	0.9963	0.999	0.9962	0.9998
0.84	0.9961	0.9988	0.9974	0.9994
0.86	0.9976	0.9988	0.9968	0.9993
0.88	0.9971	0.9997	0.9971	0.9995
0.90	0.9983	0.9997	0.997	0.9993
0.92	0.9975	0.9992	0.996	0.9989
0.94	0.9976	0.9994	0.9954	0.9994
0.96	0.9976	0.9994	0.9984	0.9997
0.98	0.9972	0.9992	0.997	0.9997
1.0	0.9978	0.9991	0.9973	0.9991

Table D.10: ^{90}Y TDCR parameter as a function of defocusing parameter for KB= 0.09 and 0.1 mm/MeV, with uncertainty less than 1%.

KB(mm/MeV)	0.09		0.1	
Defocusing parameter	**CEA**	**G4RDecay**	**CEA**	**G4RDecay**
0.70	0.9957	0.9996	0.996	0.999
0.72	0.9956	0.9994	0.9965	0.9991
0.74	0.9964	0.999	0.9965	0.9993
0.76	0.9963	0.9989	0.9961	0.9991
0.78	0.9963	0.999	0.9965	0.9991
0.80	0.9972	0.9991	0.9961	0.9995
0.82	0.996	0.9988	0.9973	0.9989
0.84	0.9965	0.999	0.9972	0.999
0.86	0.9963	0.9986	0.9964	0.9993
0.88	0.9967	0.9995	0.9969	0.999
0.90	0.9975	0.9991	0.9981	0.9988
0.92	0.9973	0.9992	0.9978	0.9995
0.94	0.9964	0.9995	0.9972	0.9995
0.96	0.9972	0.9995	0.9965	0.9991
0.98	0.9973	0.9993	0.9972	0.9996
1.0	0.9977	0.9994	0.9972	0.9991

Table D.11: ^{90}Y TDCR parameter as a function of defocusing parameter for KB= 0.11 and 0.12 mm/MeV, with uncertainty less than 1%.

KB(mm/MeV)	0.11		0.12	
Defocusing parameter	**CEA**	**G4RDecay**	**CEA**	**G4RDecay**
0.70	0.9955	0.9993	0.996	0.9983
0.72	0.9971	0.9991	0.9961	0.9988
0.74	0.9965	0.9994	0.9962	0.9995
0.76	0.9969	0.9992	0.9954	0.9987
0.78	0.9966	0.999	0.9964	0.9987
0.80	0.9962	0.9993	0.997	0.9995
0.82	0.9968	0.999	0.9961	0.9994
0.84	0.9962	0.9991	0.99789	0.9994
0.86	0.9971	0.9994	0.9968	0.9995
0.88	0.9971	0.9992	0.9964	0.9994
0.90	0.9969	0.9994	0.9979	0.9993
0.92	0.9968	0.9991	0.9967	0.999
0.94	0.9971	0.9994	0.9974	0.9994
0.96	0.9964	0.9996	0.9969	0.9989
0.98	0.9966	0.9997	0.9969	0.9996
1.0	0.9971	0.9995	0.9973	0.9997

Table D.12: ^{90}Y TDCR parameter as a function of defocusing parameter for KB= 0.13 and 0.14 mm/MeV, with uncertainty less than 1%.

KB(mm/MeV)	0.13		0.14	
Defocusing parameter	**CEA**	**G4RDecay**	**CEA**	**G4RDecay**
0.70	0.9963	0.9994	0.9955	0.9988
0.72	0.9947	0.9988	0.9964	0.9987
0.74	0.9961	0.9994	0.9961	0.9993
0.76	0.9954	0.9988	0.9966	0.9994
0.78	0.9952	0.9992	0.9963	0.9992
0.80	0.9973	0.999	0.9965	0.9992
0.82	0.9974	0.9993	0.9966	0.9994
0.84	0.9965	0.9985	0.996	0.9993
0.86	0.9962	0.9996	0.996	0.9991
0.88	0.9978	0.999	0.9969	0.999
0.90	0.9967	0.9994	0.9969	0.9988
0.92	0.9976	0.9992	0.9972	0.9992
0.94	0.9971	0.999	0.9972	0.9994
0.96	0.9972	0.9994	0.9968	0.9992
0.98	0.9984	0.9989	0.9963	0.9988
1.0	0.9965	0.9992	0.9975	0.9996

La borsa di dottorato è stata cofinanziata con risorse del
Programma Operativo Nazionale Ricerca e Innovazione 2014-2020 (CCI 2014IT16M2OP005),
Fondo Sociale Europeo, Azione I.1 “Dottorati Innovativi con caratterizzazione Industriale”

UNIONE EUROPEA
Fondo Sociale Europeo